Bulk hetero-junction hybrid solar cells prepared from n-ZnO precursor

GRADUATE SCHOOL OF LIFE SCIENCE AND SYSTEM ENGINEERING
KYUSHU INSTITUTE OF TECHNOLOGY

DISSERTATION
FOR THE DEGREE OF
DOCTOR OF PHILOSOPHY

SANDEEP KUMAR DAS

JULY 2013

PHD. SUPERVISOR

PROFESSOR. SHUZI HAYASE

Abstract

Dye-sensitized solar cells (DSSCs) have emerged as one of the low-cost solar cells, due to the ease of their fabrication by printing processes under ambient conditions. Recently, all-solid DSSCs having solid hole-transport layers (HTL) instead of the liquid electrolyte have been studied to avoid the complicated encapsulation of DSSCs to protect the evaporation of the liquid electrolyte. Solid state DSSCs consisting of the inorganic Electron transport layer (ETL)/dye/HTL are generally fabricated multiple step process namely, fabrication of a nano porous TiO_2 layer, sintering, dye adsorption, and fabrication of a HTL. Although, this step-by-step process is a convenient way to control photo-conversion interfaces, but it's costly and time consuming.

Dye-sensitized polymeric bulk hetero-junction solar cells (DSPSC) are another class of low cost, easily processable solar cells that can be prepared by a single step coating process. In the DSPSC solar cells a mixture of dye, donor and acceptor materials are mixed in common solvent and then coated on to the substrate in single step process. The working principal and structure of DSPSC and solid-state DSPSC are much similar. However, the only difference between them is the class of acceptors used. DSPSC generally uses organic acceptors (like fullerene derivatives), whereas all solid DSSC have inorganic metal oxides such as TiO_2, ZnO as electron acceptors.

For single step fabrication of all solid-DSSC using DSPSC fabrication method, first there is need for solution processable inorganic oxide, which along with dye and polymeric HTL is soluble in a common solvent. First step for fabrication would be successfully fabricating binary polymeric hybrid bulk hetero-junction (PHSC) solution processable inorganic oxide and polymeric. Thereafter this fabrication approach would be extended for fabricating dye sensitized PHSC, which has same material components as that of all solid DSSC.

This thesis explores and demonstrates the way for single-pot fabrication process of all-solid DSSCs using a DSPHSC fabrication method.

Table of contents

Chapter 1. Introduction

1.1 Utilization of solar energy

With the rapid expansion of world's economy and population, there is also ever increasing demand for energy. However, the intrinsic properties of the fossil fuels (also called traditional nonrenewable energy resources), such as coal, oil and nature gas, prevent them from fulfilling the energy requirements of the future. Burning the fossil fuels generates carbon dioxide and other detrimental pollutants which are major constituent contributing to global warming through the greenhouse effect. The need to contain global warming is extremely crucial for maintaining our fragile ecosystem. Reports shows that the global temperature has risen by about 0.6°C during the entire 20th century; while this number is predicted to be 1.4 - 5.8°C during the following century [1]. Apart from global warming there are also other pollutants such as nitrogen oxides, sulfur dioxide and respiratory suspended particles which are generated due to fossil fuel combustion and adversely affects the human health. Additionally reliance on fossils fuels for future energy demands is also non sustainable as the formation process of the fossil fuels is very complicated and usually takes millions of years.

With the advent of the Industrial Revolution in 18th century, consumption of the energy resources has sky rocketed, leading to a rapid depletion of the nonrenewable fossil fuels. The shortage of the energy resources in the future will definitely de accelerate the economic development and may degrade the living standard of human being. Hence, to ensure a sustainable society and an environment-friendly place for future generations, great efforts must be taken to explore the renewable and clean energy resources. There is no accepted definition of the renewable energy resources (also called green energy) which typically include wind, solar energy, ocean waves, geothermal, and hydroelectric power. As the name suggests, renewable energies are abundant, inexhaustible, sustainable, and usually environment-friendly. Exploration and utilization of the renewable energy resources can reduce the reliance on the fossil fuels currently and they are also expected to substitute the traditional energy resources in the future. According to the Renewables 2011 Global Status Report, the renewable energy accounts for about 16% of

total global energy consumption. This share continues increasing year by year. For instance, the renewable energy accounts for about 20% of global electricity supply in 2010, and this share increases to 25% in early 2011.

It is no doubt that the renewable energy resources will dominate the energy market in the future. Among several typical renewable and environmental-friendly energy sources, such as wind and biogas, solar energy stands out due to its distinct properties. First and foremost, solar energy is very abundant. Estimation shows that global power consumption would be up to 30 TW by the year 2050, while the energy on the surface of earth provided by the sun is 89000 TW [2]. Secondly, solar energy is also very clean and does not pollute environment. Besides, solar energy has other merits such as noiseless, negligible negative effect on the beautifulness of scenery, requiring much less maintenance compared with wind turbines and much less arable land compared with biofuels. Thus, it is straightforward to consider the utilization of solar energy as one possible energy alternative among the four typical ways of harnessing solar energy (photovoltaic, heating, concentrating solar power and lighting), photovoltaic technology has received extensive attention in the past decades. Photovoltaic cells (also called solar cells) are devices that can convert solar energy to electrical energies to power the electrical equipment. Alexandre-Edmond Becquerel first observed the photovoltaic effect in an electrolyte solution in 1839 [3], and the modern era of solid-state solar cells was ushered in with developments at Bell Labs in 1954 [4]. Since then there is ever increasing photovoltaic market, especially during recent years.

1.2 Current solar cell technologies

Many solar technologies exist with varying degrees of development, and organic solar cells are one of the newer classes of these technologies. This section will briefly discuss the main solar cell technologies at present to help put the role of organics in context. The most commercially available solar cell technologies can be divided into two main groups: crystalline and multi crystalline silicon and inorganic thin films. After these two main groups, there are several emerging technologies that have not yet seen broad commercial availability but are still being

heavily investigated in the laboratory for future application, including GaAs, concentrator, dye-sensitized, and organic thin-film solar cells.

1.2.1 Crystalline and multi-crystalline silicon solar cell

Solar cells based on crystalline and multi-crystalline silicon are by far the most developed and produced of all the solar cell technologies and currently account for ~80% of the solar cell market. The development of silicon solar cells greatly benefited from the large-scale effort to understand and process silicon as a semiconductor for electronics and integrated circuits. In silicon solar cells, a photon is absorbed to generate a free hole and electron that are separated and collected to generate current [3]. Recombination of the carriers before collection, which leads to losses, can be reduced by using high-purity silicon and by applying processing techniques and device structures made possible by the deep understanding of the physics in silicon. Furthermore, the optical absorption spectrum of silicon is well matched to the solar spectrum for solar cells based on a single material [4]. While there are concerns about the supply of silicon wafers going into the future [5], the widespread availability of silicon from the integrate circuit industry has also contributed to the success of silicon solar cells. Power conversion efficiencies, which define the percent of incoming light power converted into electrical power, up to 25% and 20.4% have been demonstrated in crystalline and multi-crystalline silicon solar cells, respectively [6]. While silicon is by far the leading solar cell technology, there are still many areas for improvement either with advances in silicon or with other material systems. First, high-purity silicon is generally expensive and slow to grow. Because silicon is an indirect band-gap semiconductor and has a weaker absorption compared to other semiconductors, thicker layers of silicon are generally required compared to other materials [4]. For these and other reasons, the silicon alone accounts for nearly 50% of the cost of a completed solar module [5]. To circumvent some of these limitations and potentially achieve lower costs per produced power, technologies are also being developed that can use less material either by having thinner active layers based on thin films or smaller active layers with light from a large area concentrated onto the small cell.

1.2.2 Inorganic thin film solar cell

Inorganic thin-film solar cells are the basis for nearly all of the presently available commercial solar cells that are not based on crystalline and multi-crystalline silicon. Thin film solar cells attempt to reduce the expensive cost of wafers in silicon cells by using thin films of semiconductors that are usually deposited onto a supporting substrate. The active layers are only a few microns thick but can still absorb significant amounts of light because of strong absorption in the materials. More impurities in the semiconductors can be tolerated since charges have a shorter distance to travel through the thin films [4]. Deposition and processing of thin-film materials also uses lower temperatures compared to silicon. Lower active material volume, purity, and processing temperatures can all lead to lower cost per area for thin-film solar cells, though it generally comes with a tradeoff of efficiency relative to crystalline and mono-crystalline silicon. The net effect is a cost per Watt that is competitive with silicon. The leading material platforms for inorganic thin-film cells are amorphous silicon (a-Si), $Cu(InGa)Se_2$ (CIGS), and CdTe with highest efficiencies of 10.1%, 19.4%, and 16.7%, respectively [6]. While the production of inorganic thin-film cells is rapidly growing, barriers still exist. Whereas silicon purification, wafer production, cell processing, and encapsulation have already developed as separate operations, all of these functions are often grouped into one facility for thin-film cells, leading to high capital costs [5]. The toxicity of cadmium itself is a major concern for CdTe solar cells, and the limited amount of indium reserves poses a long-term issue for CIGS, which requires the metal in the semiconductor [5]. Novel solutions to each of these challenges might be found with continued development.

1.2.3 Emerging technologies

Numerous other solar cell technologies exist that are still not widely available commercially. The highest efficiencies have been demonstrated in cells based on GaAs for both single and multi-junction devices. Multi-junction solar cells use multiple layers that are tailored to more efficiently convert different portions of the solar spectrum based on the band gap of the layers. However, GaAs solar cells have generally been limited to space applications because of their higher cost [4]. The high cost of high efficiency cells can potentially be offset by concentrating a large area of sunlight onto a solar cell with a small area. Concentration can produce a large amount of power

with only a small amount of semiconductor. Furthermore, higher efficiencies can be obtained under concentrated light compared to the standard one sun illumination [7]. Efficiencies of 41.6% have been obtained in multi-junction solar cells under concentrated sunlight [6]. However, concentrator systems are more complex because of the additional hardware for focusing light, tracking of the sun, and cooling the cell. Two other technologies that have been garnering significant attention are based on organic materials. Dye-sensitized solar cells use an organic dye coating a porous electrode with high surface area to absorb light. Efficiencies of up to 11% have been achieved for dye-sensitized solar cells [6]; however, the use of a liquid electrolyte in the cells is presently a source of reliability issues. Another organic technology is thin-film solar cells based on solid-state organic semiconductors. Organic semiconductors can have their chemical and electrical properties tailored in numerous ways by modifying the chemical structures and can allow for new processing methods. Organics have great potential for light-weight, flexible devices fabricated with high-throughput processes from low-cost materials in a variety of colors. However, organic semiconductors are still a relatively young field, and the highest efficiencies are only around 11% for the very best organic thin-film cells [6, 8].

1.2.4 State of the art

Solar cells performances have been continuously increasing over the last few decades. At present, commercially available solar cells have, sometimes drastically, lower efficiencies compared to the records because of additional complexities when manufacturing cells on a large scale. While multi-junction concentrators and GaAs cells have the highest record efficiencies, crystalline and multi-crystalline silicon are still the market leaders. Even with their lower efficiencies, thin-film solar cells are making significant market penetration because of tradeoffs between efficiency and cost. However, it is clear that there are many different approaches to reach the same goal of converting sunlight to electricity, and each technology may be able to fill an appropriate role based on its individual advantages and tradeoffs.

1.3 Polymeric bulk hetero-junction solar cells

Polymeric bulk hetero-junction solar cells (PSC) based on organic semiconductors are interesting for several reasons. For one, the electrical and chemical properties of organic semiconductors can be tailored by modifying the chemical structure of the compounds in endless combinations. Though specific design rules are still under investigation, the potential for tailoring molecules to different applications is great. Furthermore, the polymeric organic materials have the potential to be cheaply synthesized without significant concern on the limit of raw materials. Next, polymeric organic semiconductors can be deposited in a number of low temperature and high-throughput ways, such as evaporation and solution processing that can lower manufacturing costs. Because polymeric organic materials can have high absorption coefficients, a layer of only a few hundred nanometers is often enough to absorb a large fraction of light in the material's absorption spectrum. The use of such thin layers reduces the amount of active material needed and also makes light-weight and flexible devices possible. For these and other reasons, polymeric organic solar cells have gained significant attention. The first modern solid-state solar cell based on organic materials with an efficiency close to or higher than 1% was developed by C. W. Tang during his time at Eastman Kodak [9]. Tang stacked an organic material that donates electrons, or a donor, and an organic material that accepts electrons, or an acceptor, between the electrodes. When a photon is absorbed in an organic material, a bound electron-hole pair, called an exciton, is created and must be dissociated to contribute to the current. Stacking an acceptor material on top of a donor material (Figure 1.1), in this case 3,4,9,10-perylenetetracarboxylic-bis-benzimidazole (PTCBI) on copper phthalocyanine (CuPc),creates an interface that drives the dissociation of light-generated excitons and preferentially separates the electrons into the acceptor layer and the holes into the donor layer. This architecture yielded larger fill factors than those seen in previous single-layer devices [10] and current-voltage (J-V) characteristics similar in shape to their high-efficiency inorganic counterparts. The architecture is commonly referred to as a planar hetero-junction because the deposited layers can be idealized as stacked planes of different materials. Vacuum thermal evaporation is the most common method of depositing the organic layers for these devices. However the planar architecture limits the performance of organic solar cells owing to low exciton diffusion length of organic materials.

The exciton diffusion length is the average distance that an exciton travels before recombining and is critical in planar-hetero-junction devices because a photo generated exciton must travel a distance to the donor / acceptor interface to be separated into a hole and electron. Short exciton diffusion lengths in most polymeric organic materials (on the order of tens of nanometers) limit the thickness of the polymeric organic layers. While thick layers are desired for high absorption, layers must also be sufficiently thin to prevent excessive recombination because of the short exciton diffusion lengths. To overcome some of the limitations of the small exciton diffusion length, the donor and acceptor layers can be blended together to minimize the distance an exciton must travel to reach a donor / acceptor interface. This structure is called a bulk hetero-junction since the hetero-junction is dispersed throughout the bulk of the layer. A comparison of the two hetero-junction designs is displayed in Figure 1.1. A device with a large dispersion of interfaces throughout the photoactive layer requires smaller exciton diffusion distances, and thus, a larger exciton dissociation yield is achieved. There exists a trade-off between increasing interfacial area via the intimate dispersion of phases and the creation of efficient conductive pathways through which free electrons and holes may be transported. The arrangement of donor and acceptor phase is thus crucial to device performance.

Hiramoto et al. first demonstrated the bulk hetero-junction structure with a co-deposited layer of metal-free phthalocyanine (as donor) and a perylene tetracarboxylic derivative (as acceptor) between neat layers of the donor and acceptor [13]. Bulk hetero-junctions also helped facilitate the transition to solution processing of the organic layers. Solution processing is attractive because it might be more easily applied to large-scale, high-speed manufacturing processes such as printing compared to vacuum processing. While a single layer of a semiconductor can easily be spin-coated from solution with the subsequent layers vacuum deposited [11, 12, 18], solution processing of both layers for a planar hetero-junction is challenging because the deposition of the second layer must not dissolve and remove the first layer. Application of bulk hetero-junctions would simplify solution processing by depositing a single layer that is a blend of donor and acceptor.

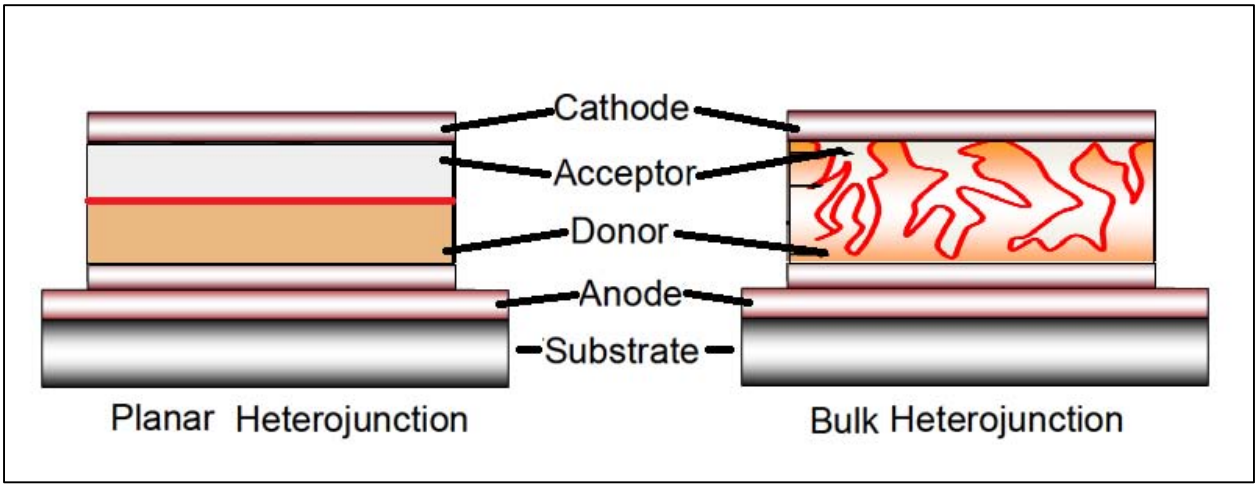

Figure 1.1 Schematics of the basic structures for solar cells based on a planar hetero-junction and on a bulk hetero-junction.

This structure led to higher photocurrent compared to devices without the mixed layer. Since then, bulk hetero-junctions formed with other vacuum-deposited small molecules have also been demonstrated, primarily with CuPc and C60 or PTCBI [14-17]. The main challenge would be creating percolation pathways for the holes and electrons to be efficiently transported to and collected at the electrodes. The first solution-processed organic solar cells incorporating a blend for the active layer were demonstrated by blending the polymers MEH-PPV and cyano-PPV (CN-PPV) as donor and acceptor and reached external quantum efficiencies up to 6% [21, 22]. The natural phase segregation of polymer blends was expected to create pathways to enhance carrier transport [19], and the work functions of the electrodes are thought to determine the extracted carrier type [20]. Yu et al. showed that the acceptor polymer could be replaced with a soluble derivative of C60, [6, 6]-phenyl C61 butyric acid methyl ester (PCBM), to yield devices with power conversion efficiencies up to ~1.5% under low-intensity broadband illumination [21]. The combination of polymer and small molecule has become the most common approach to solution-processed bulk hetero-junction. Much effort has been spent exploring new polymers and acceptors for bulk hetero-junction solar cells to increase absorption and carrier transport. One of the most researched combinations to date is region regular poly(3-hexylthiophene) (P3HT) blended with PCBM, which reaches power conversion efficiencies close to 5% [22,23]. Recently, new polymers (PCPDTBT, PTB1, and PCDTBT) with absorption spectra that extend farther into the red part of the spectrum have been reported in blends with PC71BM yielding efficiencies greater than 5% [24-26]. The phase segregation in the films has become apparent as a major factor influencing

overall device efficiency. Annealing of devices [22, 23], changing the solvent and the drying speed of the film [23], and adding chemicals with selective solubility of the fullerene component to affect crystallization [24] have been found to affect the phase segregation and improve performance. However, finding the optimum conditions can be very tedious and time consuming. Solution-processed cells based on blends of small molecules are now starting to be reported with efficiencies above 3%. Researchers are taking advantage of the ability to solution process by demonstrating cells fabricated by screen printing [27], inkjet printing [28], gravure printing [29], brush painting [30], and even roll-to-roll printing [31].

1.4 Polymeric hybrid bulk hetero-junction solar cells

Polymeric hybrid bulk hetero-junction solar cells (PHSC) combine organic (normally conjugated polymers) and inorganic nanoparticles, with the intent of incorporating the advantages associated with both material groups [32, 33]. The inorganic electron acceptor material can provide further advantages to the system, whilst still maintaining low cost processability. First, inorganic acceptor materials are more environmentally stable than organic materials [34]. Adding these materials to PSC devices could assist in overcoming one of the major downfalls of the technology, which is the photo induced degradation of the conjugated organic semiconductors. Second, photo generation of charge carriers can be achieved by excitons absorbed in the inorganic material [35, 36]. The contribution of light absorption by an inorganic acceptor has the potential to be greater than the absorption contribution of PCBM in PSC devices [37, 38]. Additionally, quantum confinement, as a result of modification of the size and shape of the inorganic nanoparticle, alters the band gap and thus absorption profile of the nanoparticle [39]. This provides the possibility of choosing the spectral window of the complementary absorption profile [40]. Third, inorganic quantum dots are known for ultrafast photo induced charge carrier transfer to organic semiconductors. This transfer rate has been observed in the order of picoseconds [41]. As this transfer rate is faster than the competing recombination mechanisms, efficient charge transfer between the donor and acceptor can be established. Lastly, the physical dimensions of some inorganic semiconductors, namely oxides, can be tailored via synthesis methods to produce

vertically well-aligned nanostructures [42]. This can lead to device architectures which allow simultaneously efficient excitonic dissociation and electron transporting pathways. These advantages could be obtained, whilst maintaining the solution processability and thus high throughput, low cost device production. Although there are multiple theoretical advantages associated with using an inorganic electron acceptor, the currently achieved device efficiencies of hybrid solar cells are significantly lower than polymer: fullerene PSC devices. Here exist multiple factors responsible for this discrepancy. Seemingly, the most important issues are related to the nanoparticle surface chemistry and the nano morphology of the photoactive layer.

1.5 Dye sensitized polymeric bulk hetero-junction solar cells

One of the crucial parameters limiting the theoretically efficiency of PSC and PHSC is narrow photon harvesting spectrum window of conjugated organic polymer. The high band gap of polymers limit the numbers of photons that could be harvested for conversion of it into electrical energy. Figure 1.2 shows the large unused spectrum in case of typical P3HT/PCBM PSC compared to conventional Si based solar cells. Practically, most of the solar cells cannot efficiently use the photon having wavelength below 350–400 nm due to absorption at the substrate and front electrodes (i.e. glass, ITO). However, this part of the spectrum contains very little spectral intensity. The range of wavelengths from 280 to 400 nm amounts to only 1.4% of the total possible current or 1 mA/cm^2 in current density [43]. Table 1.1 shows that there will be large increase in current density by increasing the λ max from 650 to 1000 nm, i.e. decreasing the band gap. Poly (3-hexylthiophene) has a band gap of 650 nm (1.9 eV) and thus only has the possibility to harvest up to 22.4% of the available photons giving a maximum theoretical current density of 14.3 mA/cm^2.

Panchromatic photon harvesting in wide wavelength region is highly desired to further increase the efficiency. One possible solution for this problem came with the development of low band gap polymers. Low band gap polymers are loosely defined as a polymer with a band gap below 2 eV, i.e. absorbing light with wavelengths longer than 620 nm. During the last decade several research groups have reported the synthesis and use of materials which absorb light with wavelengths above 600 nm in PSC, leading to the development of low band gap (LBG) conducting

polymers. LBG conducting polymers surpassing the efficiency of robust P3HT/PCBM system are only few [44,45] and require tedious multistep synthesis. Controlling the molecular weight and poly dispersity index of such LBG conducting polymers is also quite cumbersome.

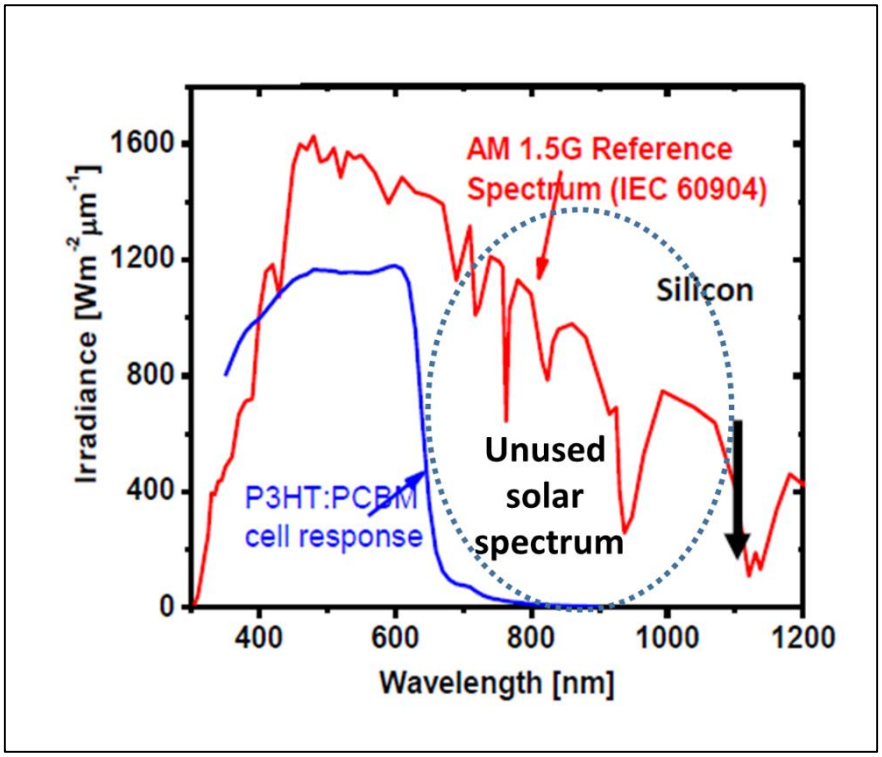

Figure 1.2 Large unused solar spectra of typical P3HT/PCBM PSC compared to Si based solar cell.

Another possible route to bypass the lower performance often observed with such systems is the fabrication of dye-sensitized bulk-heterojunction using P3HT and PCBM [46-48]. Fabrication of the dye-sensitized bulk heterojunction solar is based on the utilization of small molecule sensitizers having sharp and intense light absorption in high wavelength region. In this system high band gap conjugated polymer absorbs photons mainly in visible region, and additional photons are absorbed by small molecule dyes in NIR region. However, these system can only work, if there is suitable maintenance of the energetic cascade in terms of the energy of their highest occupied molecular orbital (HOMO) and lowest unoccupied molecular orbital (LUMO) with respect to the donor conjugated polymer and acceptor molecule, along with the solution processability. There are several families of solution processable small molecules that have been used as donor materials in BHJ solar cells. Small molecular dyes often have high mobility, are

easily purified, and are more prone to long range order than low band gap polymers. Small molecules in solution, however, may lack the viscosity necessary for film casting via most solution processing techniques and are often prone to unfavorable phase separation in a BHJ structure due to their tendency to crystallize [46]. There are three major kinds of NIR sensitizers to date, squaraine, porphyrin, and phthalocyanine. These dyes have gained recognition as one of the most versatile building blocks for designing sensitizers mainly in dye sensetized solar cells (DSCs) owing to their unique optical as well as electrochemical properties and their excellent photochemical stability.

Wavelength	**Max. % harvested (280 nm)**	**Current density (mA/cm^2)**
500	8.0	5.1
600	17.3	11.1
650	22.4	14.3
700	27.6	17.6
750	35.6	20.8
800	37.3	23.8
900	46.7	29.8
1000	53.0	33.9
1250	68.7	43.9
1500	75.0	47.9

Table 1.1 The integrated photon flux and maximum current density available for a PV that harvest light from 280 nm up to the wavelength quoted assuming that every photon is converted into one electron in the external circuit

1.6 Working of bulk hetero-junction solar cells

1.6.1 Device architecture and general operating principles

The device architecture (Figure 1.3) and operation of PSC and PHSC is very similar, the only difference being that the organic electron accepting material like PCBM (or other fullerene derivatives) in PSC is replaced by an inorganic nanoparticle in PHSC. This could be in the form of quantum dots dispersed in a polymer matrix, or a more complex shaped nanoparticle like nano rods, nanowires or tetra pods, mixed with a polymer.

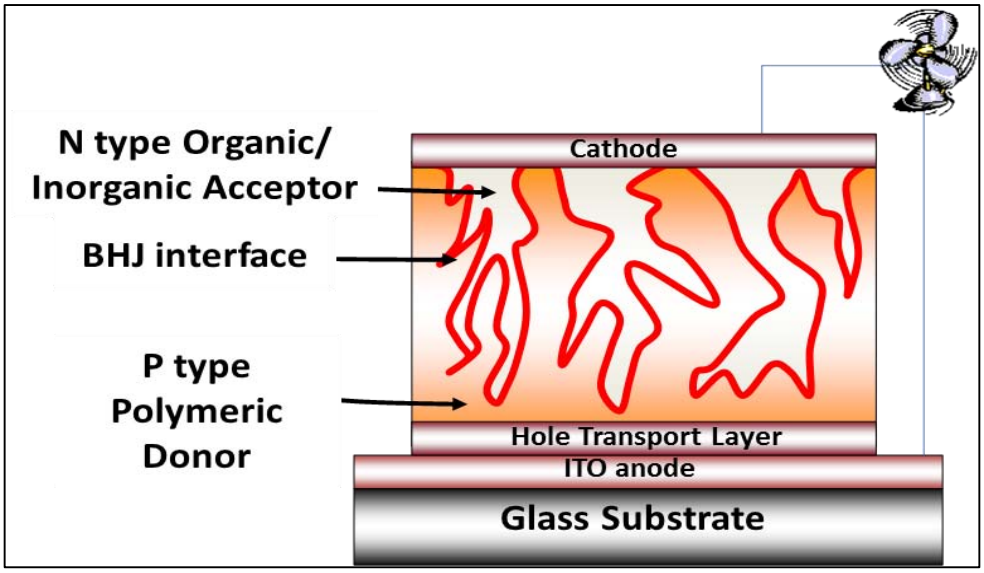

Figure 1.3: Device architecture of PSC and PHSC solar cells.

The device is built on a transparent substrate, usually glass or PET. This substrate may be flexible. The anode consists of a semitransparent oxide layer, usually indium tin oxide (ITO). Its role is to allow light to pass through, and to collect holes from the device. A layer of the conductive polymer mixture (PEDOT–PSS) may be applied between the anode and the photoactive layer. This thin layer is spin coated on top of the ITO surface. The PEDOT–PSS layer serves several functions. As well as a hole transporting layer and exciton blocker, it smoothens the ITO surface, seals the active layer from oxygen, and prevents the cathode material from diffusing into the active layer, which can lead to unwanted trap sites [49]. The light absorbing photoactive layer containing the donor and acceptor material is sandwiched between two electrodes. For lab devices, this layer is

spin coated from a common solution which contains the polymer donor and inorganic nanoparticles suspended in an appropriate solvent or mixture of solvents. The cathode is usually aluminum, although calcium or magnesium is sometimes used. The function of the cathode is to collect electrons from the device. This layer is deposited via thermal evaporation. With this device structure, the light is illuminated through the glass substrate.

1.6.2 Structure of photoactive layer

In bulk hetero-junction solar cells, excitons formed in the donor material are dissociated at the donor–acceptor (D–A) interface. The force required to overcome the exciton binding energy is provided by the energy level offset of the lowest unoccupied molecular orbital (LUMO) of the donor and the conduction band edge of the acceptor materials. Figure 1.3 displays a simplified energy band diagram. This energy offset used to dissociate excitons is denoted as Δ_{EES} in Figure 1.4, which is the excited state energy offset. For dissociation of excitons formed in the acceptor material, the energy offset of the highest occupied molecular orbital (HOMO) of the donor and the valence band edge of the acceptor materials is required. This energy offset used to dissociate excitons is denoted as Δ_{EGS} in Figure 1.3. This is the ground state energy offset. Excitonic dissociation due to this energy offset occurs at the interface between the donor and acceptor phase, and thus, the arrangement of the two materials in the active layer is crucial for the successful operation of the device.

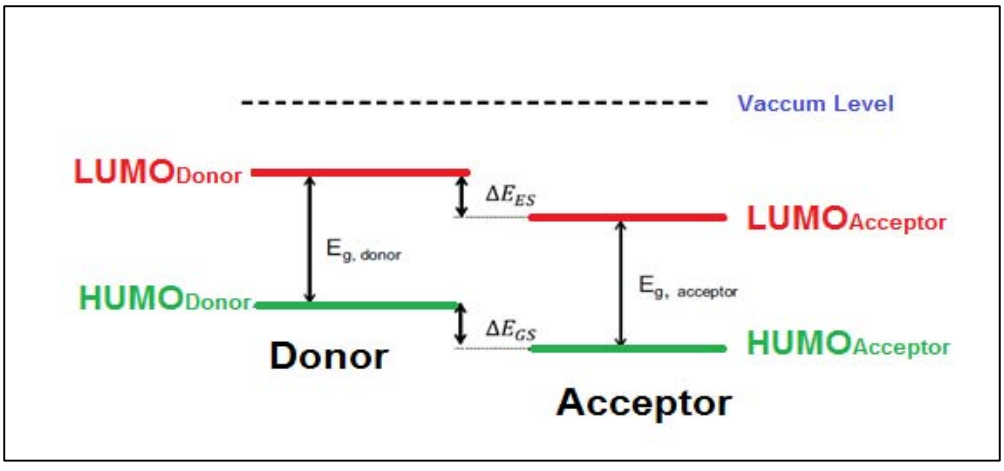

Figure 1.4 General energy band diagram of the hetero-junction formed in a bulk hetero-junction solar cell.

Due to the small excitonic diffusion length in conjugated polymers (~10 nm) [50–52], bi layer structures are severely limited in excitonic dissociation, as there exists only one interface. The only place where dissociation can occur is at the single interface between the materials, implying that only photoexcitation which occurs within an excitonic diffusion length of the interface can produce free charge carriers. In order to increase the interfacial area and thus excitonic dissociation, the donor and acceptor material can be intimately mixed, forming what is called a bulk hetero-junction

1.6.3 Performance characteristics

The power conversion efficiency (PCE) of a solar cell is defined as:

$$\mathbf{PCE} = \frac{\boldsymbol{Jsc} \times \boldsymbol{Voc} \times \boldsymbol{FF}}{\boldsymbol{Pin}}$$

Where Jsc is short circuit current density, Voc is open circuit voltage, FF is fill factor and Pin is incident input power. To allow for valid comparison of device performance, an international standard for input power is used. This standard is an incident spectrum of AM 1.5 G with an intensity of 1000 W/m^2 (100 mW/cm^2), whilst the cell is at a temperature of 25^{0}C. The air mass (AM) is the ratio of the path length of incoming sunlight through the atmosphere when the Sun is at an angle Θ to the zenith, to the path length when the Sun is at the zenith. AM1.5 corresponds to the spectral power distribution of light coming in with an angle Θ of 48° to the zenith. Therefore, there are three major device characteristics which completely determine the efficiency of the device.

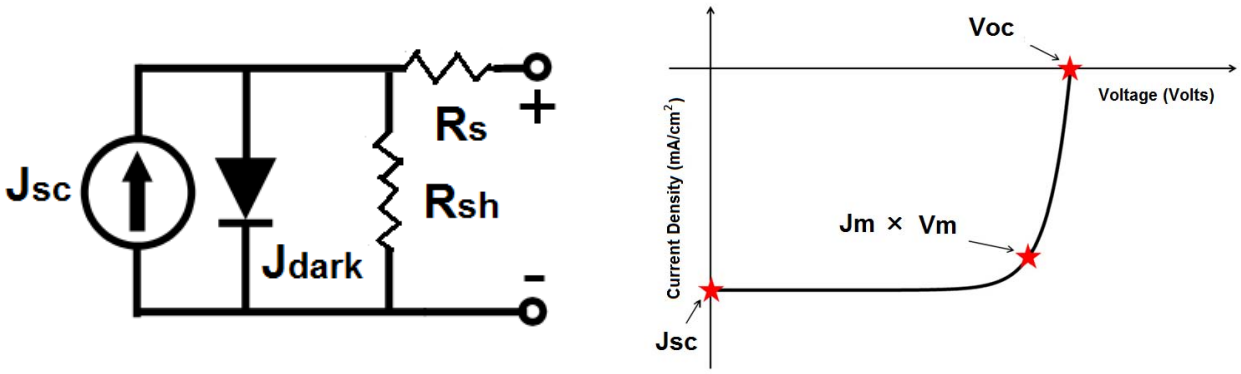

Figure 1.5 (a) Equivalent circuit (b) Current density–voltage (J–V) characteristics for a generic illuminated solar cell.

Figure 1.5 (a) describes the typical electrical equivalent circuit of a solar cell. Figure 1.5 (b) displays a typical illuminated J–V characteristic curve which illustrates these three characteristics. The following describes the factors which influence these device characteristics for organic–inorganic hybrid solar cells.

1.6.3.1 Short circuit current density

The short circuit current density (Jsc) is the maximum photocurrent density which can be extracted from the device at short circuit conditions. The Jsc is directly related to the external quantum efficiency (EQE). This relationship can be expressed as:

$$\mathbf{Jsc} = \frac{q}{hc}\int_{\lambda min}^{\lambda max} \boldsymbol{EQE} \times \boldsymbol{Pin}\,(\boldsymbol{\lambda})\boldsymbol{\lambda} \times \boldsymbol{d\lambda}$$

The EQE is the ratio of photo generated electrons collected to the number of incident photons at a specific wavelength. For the operation of a hybrid solar cell, this quantity is dependent on five major steps, each of which has some associated efficiency. Thus, EQE can be expressed as:

$$\mathrm{EQE} = \eta_A \times \eta_{ED} \times \eta_{CT} \times \eta_{CC}$$

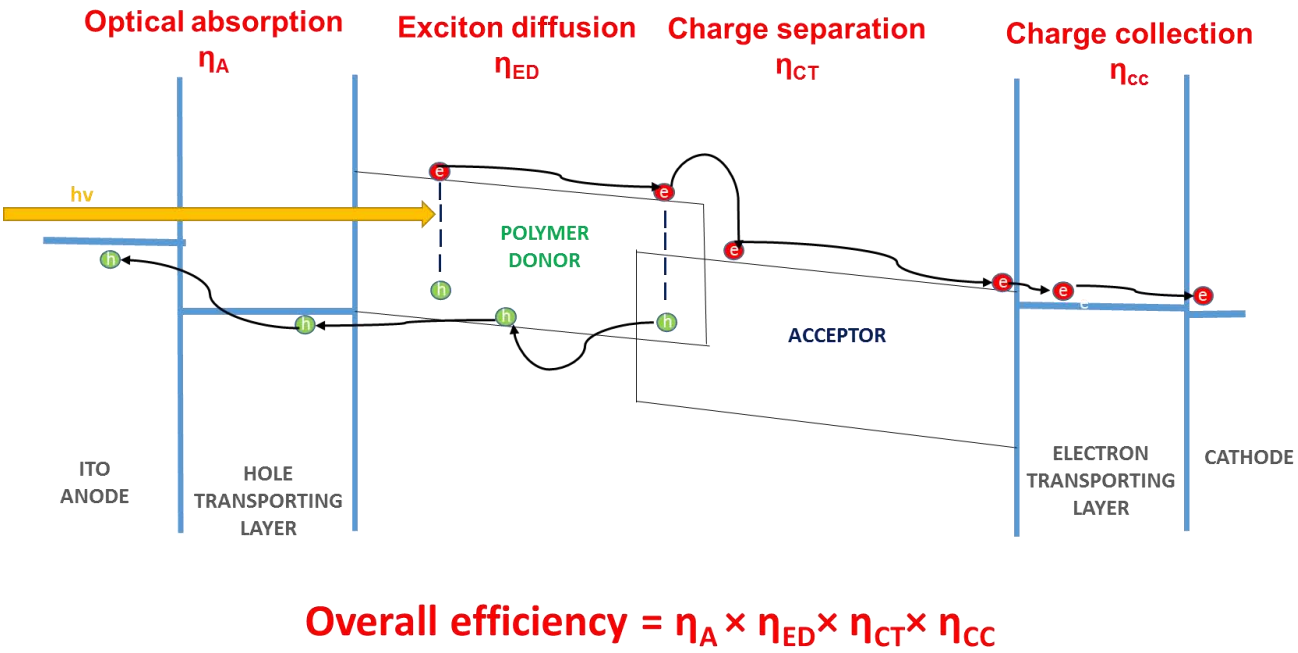

Figure 1.6 Energy band diagram illustrating the four key steps in the charge transfer process. The efficiency of these steps determines the EQE of the bulk hetero-junction device.

The parameter η_A describes the absorption yield of the device, which is displayed as (1) in Figure 1.6 This represents the most effective way of increasing the Jsc of a hybrid device [32, 53]. The absorption spectrum of the material is determined by both the band gap and absorption coefficient of the material, whilst the thickness of the active layer will also affect the absorption yield [54]. Additionally, thin film interference will affect the absorbance of the bulk hetero-junction photoactive layer. In hybrid solar cells, significant useful absorption may be provided by the inorganic acceptor material. This implies that the electronic composition of the inorganic material will impact the Jsc of the device.

The parameter η_{ED} (Figure 1.6), describes the ability of an exciton to diffuse to a D–A interface. This is dependent on both the excitonic diffusion length, which is a material property, and the distance between excitation and the nearest interface, which is related to the nano scale design of the photoactive layer. As the excitonic diffusion length in conjugated polymers is very low [50-52], control over the D–A arrangement is crucial for successful exciton diffusion. This factor is inversely related to the rate of recombination within the photoactive material.

The parameter η_{CT} (Figure 1.6), is the exciton dissociation yield. As the electron is still

bound within the exciton, the energy offset formed at the D–A interfaces is required to provide a driving force which releases the electron and allows conduction to occur. This energy offset must be larger than the excitonic binding energy in the material to facilitate charge transfer. This energy is typically in the range of 0.1–0.5 eV [50, 55]. This occurs only at the boundaries between the two materials and therefore, the distribution of the interface throughout the active layer is vitally important for the efficiency of the solar cell.

The parameter η_{CC} describes the efficiency of charge collection at the electrodes. This represents the ability of the charge carriers to be injected into the electrodes from the photoactive layer. The success of this step is greatly dependent on the electronic composition of the device. For successful injection of electrons into the cathode, the magnitude of the conduction band edge energy level of the acceptor material, with respect to the vacuum level, must be lower than the work function of the metal. For successful injection of holes into the anode, the magnitude of the HOMO level of donor material must be higher than the work function of the transparent anode. This is displayed schematically in Figure 1.4. The material used for the electrodes must be carefully selected. A discrepancy between the work function of the anode and cathode material is required to provide a direction for the photocurrent. Often intermediate layers between the photoactive layer and electrodes are introduced to make the injection of charge carriers more energetically favorable [56, 57]. The quality of the ohmic contact with the cathode, which is determined by the nature of the interface with the aluminum, also influences the charge collection efficiency.

1.6.3.2. Fill factor

The fill factor describes the ‘square-ness’ of the J–V curve. It is defined as:

$$\text{Fill Factor (FF)} = \frac{Jm \times Vm}{Jsc \times Voc}$$

Where Jm and Vm are the maximum power point current density and voltage, respectively. This ratio is illustrated in Figure 1.4. Due to physical constraints on diode quality, the practical limit to fill factor is less than the ideal value of 1. The behavior of a real diode will deviate from the ideal, primarily as a result of recombination occurring at the junction. For OPV and organic–inorganic hybrid solar cells, the ‘junction’ is the D–A interface, which is distributed throughout the entire

photoactive layer. Deviations from the ideal case, and thus the shape of the J–V curve, can be quantitatively characterized by the parasitic loss mechanisms of series and shunt resistance. Zero series resistance (Rs=0) is ideal, however, poor conductivity through the active layer and reduced charge carrier injection to the electrodes represents increased series resistance. Conversely, the ideal diode case demands infinite shunt resistance. Reduction in Rsh is caused by imperfections within the photoactive film or current leaks at the interface between layers in the device [58].

1.6.3.3 Open circuit voltage

In contrast to silicon p–n junction solar cells, the origin of open circuit voltage in bulk hetero-junction devices is still not well understood. Multiple reports have investigated this property for PSC devices, using PCBM as the electron acceptor. In 2001, Brabec et al. proposed an effective band gap model for bulk hetero-junction cells, whereby the maximal value of Voc is related directly to the energy difference between the HOMO level of the donor and the LUMO level of the acceptor [32, 59]. This proposition was verified by an empirical investigation of the effect of fullerene acceptor strength (electron affinity) on open circuit voltage. A linear relationship between acceptor strength and open circuit voltage was discovered. This study also showed that Voc is weakly dependent on the type of metal used as the cathode. In 2006, a breakthrough communication on the matter was published by Scharber et al. This report studied the relationship between the energy levels of the D–A blend and the open circuit voltage for 26 different bulk hetero-junction devices. For each device, the acceptor material used was kept constant (PCBM), whilst the donor material was varied. It was found that there exists a linear relationship between the HOMO position, which is related to the diagonal band gap of the hetero-junction, and the open circuit voltage [60]. From this analysis, a simple relationship between the HOMO of the donor material and the Voc of the device was derived. This was reported as [32, 60]:

$$\mathbf{Voc} = \left(\frac{\mathbf{1}}{\boldsymbol{e}}\right)\left(\left|\boldsymbol{E^{Donor}\,HOMO}\right| - \left|\boldsymbol{E^{PCBM}LUMO}\right|\right) - \mathbf{0.3}\,\boldsymbol{V}$$

This suggests that Voc is directly proportional to the diagonal band gap of the hetero-junction; however, there exists an empirical loss factor related to the bulk hetero-junction design. The systematic nature of this study made the proposition of the effective band gap model convincing, however, these results are derived purely from empirical evidence, rather than theoretical understanding. Vandewal et al. discovered a similar relationship by analyzing charge transfer absorption using Fourier-transform photocurrent spectroscopy. The EQE spectra of polymer: PCBM solar cells was analyzed for photon energies which do not overlap with the absorption bands of either the polymer or PCBM. Photocurrent response at these energies is attributed to charge transfer complexes created at the polymer: PCBM interface. It was suggested that the spectral position of this charge transfer band correlates to the diagonal band gap of the hetero-junction [61].

This effective band gap can be extracted from the onset of photocurrent generated by the charge transfer band. The authors thus conclude that the Voc is, in fact, related to this effective band gap. They obtained the following linear fit to describe Voc [32, 61]:

$$\text{Voc} \cong \frac{E_g}{e} - 0.43\,V$$

Where Eg is the charge transfer complex band gap, which is considered as the effective band gap of the hetero-junction. Detailed balance theory suggests that maximal Voc will be obtained when recombination is exclusively radiative. Large luminescence quenching in bulk hetero-junction blend films implies that radiative recombination is only a small fraction of total recombination, and thus, practically achieved values of Voc are far removed from the optimum value [62]. The Voc in PSC devices is thus hindered primarily by non-radiative recombination at the D–A interface. However, a recent, contradictory report found no linear relationship between the diagonal band gap of the hetero-junction and Voc [63]. It was shown; however, that diagonal band gap serves as an upper bound for Voc. Such reports highlight the remaining ambiguity regarding the origin of Voc in bulk hetero-junction OPV devices.

The origin of Voc in PHSC remains thus far largely unexplored. Few reports have shown a link between the diagonal band gap and Voc. One report investigating hybrid polymer/TiO_2 solar cells suggests that the Voc is dependent on the ionization potential, or HOMO energy level, of the polymer [64]. This presents the view that the effective band gap model is transferrable to hybrid

solar cells. The Voc may be optimized by tuning the position of the conduction band edge in the inorganic material by molecular modification. Brandenburg et al. recently showed that the Voc of P3HT: CdSe hybrid solar cells depended heavily upon the size of the CdSe nanocrystals [65]. This dependence was attributed to the size-related shift of the conduction band edge of the CdSe nano crystals. These findings are in line with the effective band gap model suggested for OPV devices, however, much uncertainty remains regarding the exact mechanisms governing this fundamental property in hybrid solar cells. Current understanding, at the very least, suggests the maximal theoretical Voc of a PHSC is determined by the diagonal band gap of the hetero-junction. The requirement to maximize diagonal band gap for Voc is in conflict with the desire to minimize the band gap of the individual isolated materials, such that light absorption can be maximized. Understanding this trade-off is necessary for the design and optimization of materials used in hybrid solar cells [32].

1.7 Challenges

While the primary factor preventing the commercial application of PSC and PHSC is their limited efficiency and stability, other major challenges that must be addressed scaling and processiablity. Still large part of research of organic solar cells are limited to laboratories. Apart from achieving high efficiencies research are underway for looking for low cost, high speed, low material wastage fully scalable rolls to rolls compatible fabrication processes. With all the coating techniques, there are additional associated factors of processing speed, wet film thickness, ease of preparation of solution, solution viscosity, and maximum solution usage. Along with these pre and post annealing of prepared thin films is also crucial factor know to affect the nano morphology of the bulk hetero-junction blends.

For the PHSC, processing is still the key issue before potential of this technology can be realized. First, it is imperative to find the most optimal combination of organic and inorganic materials for hybrid solar cells. This requires careful consideration of the size of the individual material band gaps, which affects the range of absorption and thus maximum obtainable Jsc, and the diagonal band gap of the hetero-junction, which determines the maximum obtainable Voc. Advances in the synthetic processes used to form the inorganic material are required. Reproducible,

well ordered structures are vital for the optimization of the photoactive layer; however, these structures must be fabricated using techniques which are easily scalable. A precise control over the physical geometry of the nanoparticle is needed to tailor and optimize the electronic structure. Additionally nano morphology of the photoactive layer is very important factor that plays a balance between interfacial area and continuous conducting pathways is maintained within the photoactive layer.

1.8 Organization of the present thesis

This thesis explores and demonstrates the way for single-pot fabrication process of all-solid DSSCs using a DSPHSC fabrication method.

First chapter describes the basic background about solar cells particularly focusing on working and performance characteristics of PSC and PHSC.

Second chapter describes the details of materials and their properties used for present investigation. Addition to this it also explores the fabrication and characterization method for the polymeric and polymeric hybrid BHJ solar cells,

Third chapter describes the basic fabrication process for the PSCs. Additionally it also explores the performance characteristics of P3HT/PCBM polymeric BHJ device fabricated using new and efficient spray system, and its comparison with device fabricated using spin coating process.

Fourth chapter describes the use of solution processable ZnO precursor for the single step fabrication of P3HT/ZnO PHSC solar cells. The aim of using solution processsable precursor is to do in situ generation of ZnO nanoparticle inside the polymer matrix, and thus fabricating polymeric hybrid BHJ in single step. For further improving performance of solution processed P3HT/ZnO polymeric hybrid BHJ efforts are also done for improvement of P3HT interface by modifying it with ester functionality.

Fifth chapter describes the extension of concept of single step fabrication of P3HT/ZnO

PHSC for fabrication of DSPHSC. Here dye is used as additional sensitizer along with ester modified P3HT for photon harvesting in near infra-red region of solar spectrum. Considering the analogous structure of DSPHSC and solid state DSSC, a perspective for single step fabrication for all solid state dye sensitized solar cells is also given with using solution processable precursor.

Finally the sixth and last part of this work will summarize the main result and provide guidelines for future investigation.

References

[1] Trevor Letcher, Climate Change: Observed impacts on Planet Earth, Elsevier Science (2009).

[2] K. Sukhatme, Suhas P. Sukhatme, Solar Energy: Principles of Thermal Collection and Storage, Tata McGraw Hill (2008).

[3] Green M. A, Solar cells: Operating principles, technology and system applications. Kensington: The University of New South Wales (1998).

[4] Hegedus S. S. and Luque A., Handbook of Photovoltaic Science and Engineering, Hoboken, NJ: John Wiley & Sons (2003).

[5] Green M. A., Journal of Materials Science: Materials in Electronics, 18, S15-S19 (2007).

[6] Green M. A., Emery K., Hishikawa Y. and Warta W., Solar cell efficiency tables (version 36). Progress in Photovoltaics: Research and Applications, 18, 346-352(2010).

[7] Kurtz S. and Geisz J., Optics Express, 18, A73-A78 (2010).

[8] Heliatek. http://www.heliatek.com/news-19 (2010).

[9] Tang C. W., Applied Physics Letters, 48, 183-185 (1986).

[10] Chamberlain G. A., Solar Cells, 8, 47-83(1983).

[11] Wei G., Wang S., Renshaw K., Thompson M. E., and Forrest S. R., ACS Nano, 4, 1927-1934(2010).

[12] Lloyd M. T., Mayer, A. C., Tayi A. S., Bowen A. M., Kasen, T. G. Herman, D. J. Mourey, D. A. Anthony, J. E., and Malliaras G. G., Organic Electronics, 7, 243-248 (2006).

[13] Hiramoto M., Fujiwara H., and Yokoyama M., Applied Physics Letters, 58, 1062-1064 (1991).

[14] Peumans P., Uchida S. and Forrest S. R., Nature, 425,158-162 (2003).

[15] Heutz S., Sullivan P., Sanderson B. M., Schultes S. M., and Jones, T. S., Solar Energy Materials & Solar Cells, 83, 229-245 (2004).

[17] Xue J. G., Rand B. P., Uchida S. and Forrest, S. R., Advanced Materials, 17, 66-71 (2005).

[16] Yang F., Shtein M. and Forrest, S. R., Nature Materials, 4, 37-41 (2005).

[17] Pfuetzner S., Meiss J., Petrich A., Riede M., and Leo K. Applied Physics Letters, 94, 223307 (2009).

[18] Sariciftci N. S., Braun D., Zhang C., Srdanov V. I., Heeger A. J., Stucky G. and Wudl, Applied Physics Letters, 62, 585-587 (1993).

[19] Halls J. J. M., Walsh C. A., Greenham N. C., Marseglia E. A., Friend R. H., Moratti S. C. and Holmes, A. B., Nature, 376, 498-500 (1995).

[20] Yu G., and Heeger, A. J., Journal of Applied Physics, 78, 4510-4515(1995).

[21] Yu G., Gao J., Hummelen J. C., Wudl F. and Heeger A. J. Science, 270, 1789-1791(1995).

[22] Ma W., Yang C., Gong X., Lee K., and Heeger, A. J., Advanced Functional Materials, 15, 1617-1622 (2005).

[23] Li G., Shrotriya V., Huang J., Yao Y., Moriarty T., Emery K. and Yang Y., Nature Materials, 4, 864-868 (2005).

[26] Peet, J., Kim, J. Y., Coates, N. E., Ma, W. L., Moses, D., Heeger, A. J., and Bazan, G. C., Nature Materials, 6, 497-500 (2007).

[27] Shaheen, S. E., Radspinner, R., Peyghambarian, N., and Jabbour, G. E., Applied Physics Letters, 79, 2996-2998(2001).

[28] Hoth, C. N., Choulis, S. A., Schilinsky, P., and Brabec, C. J., Advanced Materials, 19, 3973-3978(2007).

[29] Kopola, P., Aernouts, T., Guillerez, S., Jin, H., Tuomikoski, M., Maaninen, A., and Hast, J, Solar Energy Materials & Solar Cells, 94, 1673-1680 (2010).

[30] Kim, S.-S., Na, S.-I., Jo, J., Tae, G., and Kim, D.-Y., Advanced Materials, 19, 4410-4415(2007).

[31] Krebs, F. C., Tromholt, T. and Jørgensen, M., Nanoscale, 2, 873-886 (2010).

[32] Matthew Wright n, Ashraf Uddin, Solar Energy Materials & Solar Cells, 107, 87–111 (2012)

[33] Y. Zhou, M. Eck and M. Kruger, Energy & Environmental Science, 3, 1851–1864 (2010).

[34] S. Ren, L.-Y. Chang, S.-K. Lim, J. Zhao, M. Smith, N. Zhao, V. Bulovic,M. Bawendi, and S. Gradecˇak, Nano Letters 11,3998–4002(2011).

[35] Y. Zhou, M. Eck, C. Veit, B. Zimmermann, F. Rauscher, P. Niyamakom,S. Yilmaz, I. Dumsch, S. Allard, U. Scherf, M. Kr ¨ uger, Solar Energy Materialsand Solar Cells 95,1232–1237(2011).

[36] D. Celik, M. Krueger, C. Veit, H.F. Schleiermacher, B. Zimmermann, S. Allard,I. Dumsch, U. Scherf, F. Rauscher, P. Niyamakom, Solar Energy Materials and Solar Cells 98,433–440(2012).

[37] S. Dayal, N. Kopidakis, D.C. Olson, D.S. Ginley, G. Rumbles,Nano Letters 10,239–242(2009).

[38] N.C. Nicolaidis, B.S. Routley, J.L. Holdsworth, W.J. Belcher, X. Zhou, P.C. Dastoor, The Journal of Physical Chemistry C 115, 7801–7805(2011).

[39] T. Takagahara, K. Takeda, Physical Review B 46, 15578–15581(1992).

[40] A. Guchhait, A.K. Rath, A.J. Pal, Solar EnergyMaterials and Solar Cells 95, 651–656(2011).

[41] J. Huang, Z. Huang, Y. Yang, H. Zhu, T. Lian, Journal of the American Chemical Society 132, 4858–4864(2010).

[42] I. Gonzalez-Valls, M. Lira-Cantu, Energy & Environmental Science 2, 19–34 (2009).

[43] E. Bundgaard, F. C. Krebs, Solar Energy Materials & Solar Cells 91, 954–985 (2007).

[44] J. Hou, H.-Y. Chen, S. Zhang, R.I. Chen, Y. Yang, Y. Wu, G. Li, J. Am. Chem. Soc. 131 15586 (2009)

[45] Y. Liang, Z. Xu, J. Xia, S.-T. Tsai, Y. Wu, G. Li, C. Ray, L. Yu, Adv. Mater. 22 1(2010).

[46] J. Peet, A.B. Tamayo, X.D. Dang, J.H. Seo, T.Q. Nguyen, Appl. Phys. Lett. 93 163306 (2008).

[47] W.J. Belcher, K.I. Wagner, P.C. Dastoor, Sol. Energy Mater. Sol. Cells 91 447 (2007).

[48] S. Honda, T. Nogami, H. Ohkita, H. Benten, S. Ito, Appl. Mater. Interfaces 1 804 (2009).

[49] S. Brian R, Science 369, 1–15(2012).

[50] C.J. Brabec, S. Gowrisanker, J.J.M. Halls, D. Laird, S. Jia, S.P. Williams, Advanced Materials 22 3839–3856 (2010).

[51] N.S. Sariciftci, L. Smilowitz, A.J. Heeger, F. Wudl, Science 258, 1474–1476 (1992).

[52] S.H. Park, A. Roy, S. Beaupre, S. Cho, N. Coates, J.S. Moon, D. Moses, M. Leclerc, K. Lee, A.J. Heeger, Nature Photonics 3,297–302 (2009).

[53] E. Bundgaard, F.C. Krebs, Solar Energy Materials and Solar Cells, 91, 954–985(2007).

[54] E. Bundgaard, S.E. Shaheen, F.C. Krebs, D.S. Ginley, Solar Energy Materials and Solar Cells, 91, 1631–1637 (2007).

[55] B.A. Gregg, M.C. Hanna, Journal of Applied Physics, 93, 3605–3614(2003).

[56] H.-L. Yip, A.K.Y. Jen, Energy & Environmental Science, 5, 5994–6011(2012)

[57] L. Zuo, X. Jiang, M. Xu, L. Yang, Y. Nan, Q. Yan, H. Chen, Solar Energy Materials and Solar Cells, 95, 2664–2669(2011).

[58] W.J. Potscavage, A. Sharma, B. Kippelen, Accounts of Chemical Research 42, 1758–1767 (2009).

[59] C.J. Brabec, A. Cravino, D. Meissner, N.S. Sariciftci, T. Fromherz, M.T. Rispens,L. Sanchez, J.C. Hummelen, Advanced Functional Materials, 11, 374–380, (2001).

[60] M.C. Scharber, D. M¨ uhlbacher, M. Koppe, P. Denk, C. Waldauf, A.J. Heeger,C.J. Brabec, Advanced Materials, 18, 789–794 (2006).

[61] K. Vandewal, A. Gadisa, W.D. Oosterbaan, S. Bertho, F. Banishoeib, I. VanSeveren, L. Lutsen, T.J. Cleij, D. Vanderzande, J.V. Manca, Advanced Functional Materials, 18, 2064–2070 (2008).

[62] K. Vandewal, K. Tvingstedt, A. Gadisa, O. Inganas, J.V. Manca, Nature Materials, 8, 904–909(2009).

[63] T. Yamanari, T. Taima, J. Sakai, K. Saito, Solar Energy Materials and Solar Cells, 93, 759–761 (2009).

[64] T. Ishwara, D.D. Bradley, J. Nelson, P. Ravirajan, I. Vanseveren, T. Cleij, D. Vanderzandee, L. Lusten, S. Tierney, M. Heeney, I McCulloch, Applied Physics Letters, 92, 053308 (2008).

[65] J.E. Brandenburg, X. Jin, M. Kruszynska, J. Ohland, J. Kolny-Olesiak, I. Riedel,H. Borchert, J. Parisi, Journal of AppliedPhysics, 110, 064509–064509 (2011).

Chapter 2: Materials, instrumentation and methods

2.1 Materials

The following section provides the brief preview about the major materials used in active layer and blocking layer for the various solution processable polymeric bulk hetero-junction (PSC), polymeric hybrid bulk hetero-junction (PHSC) and dyes sensitized polymeric hybrid bulk hetero-junction (DSPHSC) solar cells fabricated for present thesis.

2.1.1 Poly (3-hexyl thiophene)

Polythiophenes are to date one of the most extensively investigated class of conjugated materials. They are long chain molecules made up of multiple (several thousands in some cases) thiophene molecules (Figure 2.1). Their chemical stability in various redox states and excellent electronic and charge transport properties make them good candidates for application in molecular electronic devices. Hexyl [CH_3 $(CH_2)_4$ CH_2] substitution of the thiophene monomer at the 3-position greatly enhances the solubility of the resulting polymer (P3HT).

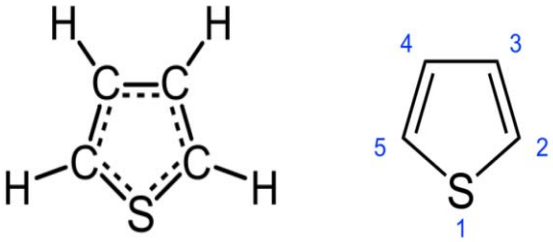

Figure 2.1 Schematic 2-D representation of the ring structure of thiophene, the image on the left represents the actual structure of the molecule, while the skeletal image on the right indicates the types of bonds and the numbering convention for the atoms in the ring.

However, substitution also introduces an additional level of complexity arising from the polymerization of an asymmetric monomer. The asymmetry of 3-substituted thiophenes results in three possible couplings when two monomers are linked between the 2- and the 5-positions.

3- Substituted thiophene monomer, can be joined at the 2-5 (head to tail), 2-2 (head –head) or 5-5 (tail-tail) positions. These three diads can be combined into four distinct triads. The triads are distinguishable by NMR spectroscopy, and the degree of regioregularity can be estimated by integration [1, 2].

If the ratio of head to tail bonds is greater than other bonds (>2:1) the molecule has what is known as a regioregular structure and has better electrical properties than P3HT without this structure (known as regiorandom) [3, 4]. The higher the ratio of head to tail bonds to other bond types the more photoconductive the material will be. Regioregular, or head-to-tail coupled, P3HTs exhibit enhanced coplanarity, conductivity, and mechanical properties compared to their regiorandom counterparts. The effect of regioregularity on the optical, electronic, and physical properties of P3HTs is ascribed to the supramolecular assembly of the polymer chains in highly-ordered solid-state structures [5].

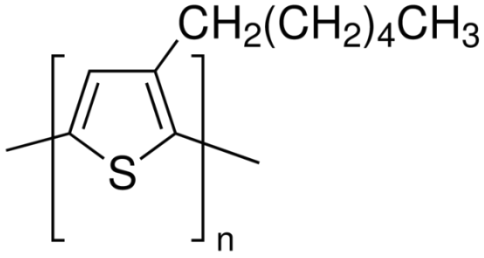

Figure 2.2 Schematic 2-D structure of Poly (3-hexyl thiophene)

P3HT could be synthesized by both chemical and electrochemical synthesis method, and could be p-type doped during both in-situ and after polymerization process. P3HT is typically soluble in aromatic and halogenated aromatic solvents. Most common used solvent for processing are trichlorobenzene, chlorobenzene, toluene, xylenes, chloroform and to a lesser degree tetrahydrofuran (THF). Regioregular P3HT (Rieke Metals, Mn = 45-50 kg/mol) used for present work was purchased from the Sigma-Aldrich USA and used as received without further purification.

P3HTis a commonly used polymer in organic solar cells and acts as the light absorbing and hole transporting material. The hole mobility in P3HT depends on different factors and lies between 10^{-5} and 10^{-2} cm^2/V-sec [6, 7]. The electron mobility is negligible small [8] .It has a band gap of around 1.9eV and is generally classed as a low band gap polymer i.e. has a band gap less

than 2eV and absorbs light with wavelengths longer than 620nm [9,10].

In present thesis P3HT has been used as photo-active electron donor material in all PSC, PHSC and DSPHSC devices.

2.1.2 [6, 6]-Phenyl-C_{61}-butyric acid methyl ester (PCBM)

PCBM is a fullerene derivative of the C_{60} buckyball that was first synthesized in the 1990s [11] Fullerenes are isotopes of carbon that form regular ball shaped structures from a combination of hexagonal and pentagonal structures known as a truncated icosahedron [12], with alternating double and single bonds they typically have diameters greater than 1nm. They come in a variety of different allotropes including; C_{20}, C_{26}, C_{60}, C_{70}, C_{84} and C_{100}, of which C_{60} and C_{70} are the most common. C_{60} has been found to form spontaneously in condensing carbon vapor [13]. Buckminsterfullerene (C_{60}) is a strong electron acceptor as it has a three layer LUMO capable of taking up to 6 extra electrons they are often combined with materials such as pentacene which are strong π-conjugated electron donors [14].

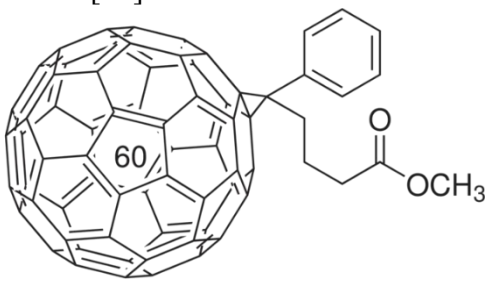

Figure 2.3 Schematic 2-D structure of [6, 6]-phenyl-C_{61}-butyric acid methyl ester

Fullerenes are often prepared with ligands to enable them to more evenly distribute through the bulk polymer and to prevent clumping. The most common ligand attached fullerenes is [6, 6]-phenyl-C_{61}-butyric acid methyl ester (PCBM) (Figure 2.3) and is widely used organic nanoparticle electron acceptor for all organic-polymer solar cells [15]. Its wide usage is mainly due to ease of processablity owing to its solubility in many aromatic solvents (like chlorobenzebne). They form either discrete layers or can be distributed into a photoconductive polymer matrix to form a bulk hetero-junction. The mobility in PCBM is between $2*10^{-3}$ and $2*\ 10^{-2}$ cm^2/V s [16]. The hole mobility is negligible small. The HOMO level is 6.1 eV and the LUMO level is 4.4 eV [17] PCBM used in present work is supplied by Sigma Aldrich. In present thesis PCBM has been used as n

type electron acceptor material in PSC devices.

2.1.3 Diethyl zinc

Zinc oxide is a wide band semiconductor, having tunable structural properties. Because of ZnO's non-toxicity, relatively low temperature and low cost fabrication process for crystalline ZnO, there is growing interest in its use as an electron acceptor material in polymer inorganic hybrid solar cells [18-23].

Two different approaches have been developed to reap the benefits of ZnO nanostructures in hybrid solar cells. In first approach, p type conjugated polymer is deposited on ZnO nanostructures, allowing enhanced hybrid interface while controlling active layer morphology [24-25]. However, it's difficult to attain complete infiltration of polymer within ZnO nanostructures for realizing efficient charge transport [26]. In second approach, blends are made by mixing polymer and ZnO nanoparticles by adopting the solution processable fabrication techniques realizing an architecture closed to PHSC. However, it's difficult to realize interpenetrating structures of ZnO in the polymers. These drawbacks could be overcome via in-situ generation of ZnO nanoparticles in the polymer matrix using organometallic precursor like diethyl zinc.

DEZ is a highly pyrophoric organozinc compound consisting of a zinc center bound to two ethyl groups. Despite its highly pyrophoric nature, diethylzinc is an important chemical reagent. For DEZ use in PHSC, it is coated together with semiconducting polymer from solution in controlled humid conditions [27]. During and after deposition, DEZ is converted to $Zn(OH)_2$ by reacting with ambient moisture and after annealing, interpenetrating ZnO nanoparticles are formed in polymer matrix leaving no residual byproduct. DEZ (0.4 M solution in toluene-tetrahydrofuran) used in this thesis was supplied by Tosho Fine Chemicals, Japan.

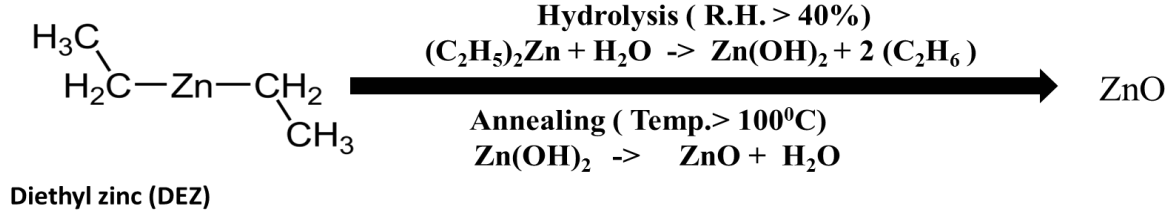

Figure 2.4 Structure of Diethyl Zinc (left), and its conversion reaction to ZnO after controlled hydrolysis and annealing.

In present thesis, DEZ is used as solution precursor for obtaining ZnO nanoparticles. DEZ is used for fabrication of all PHSC and DSPHSC devices in present thesis.

2.1.4 Squaraine dye

Squaraine-based (SQ) sensitizers are the soluble small molecule sensitizers having sharp intense electronic absorption spectrum from visible to near infra-red region, good stability, solution processability and synthetic versatility. They find their potential applications in the area of non-linear optics [28], imaging [29], photodynamic therapy [30], ion sensing [31], chromo/fluorogenic probes [32] and solar cells. In the area of solar cells, there are a good deal of reports about the use of squaraine dyes as sensitizers for dye sensitized solar cells (DSSCs) [33, 34]. Silvestri et al. reported the fabrication of solution processable bulk heterojunction solar cells using a blend of squaraine dye as p-type donor with PCBM acceptor having power conversion efficiency of 0.1–1.2% [35]. Bagnis et al. [36], have experimentally verified the p-type behavior of their squaraine dyes by field effect transistor mobility measurement. They emphasized the marked influence of molecular design of squaraine dyes upon their photon harvesting behavior also. A planer heterojunction solar cell based on soluble squaraine dyes using thermal evaporation of C_{60} as electron acceptor with the p-type thermally evaporated [37] as well as solution processed squaraine dyes [38] has also been reported recently. Pandey et al. [39] has shown that energy level of the SQ-dyes can be systematically tuned only by alkyl chain substitution. Further they also shown that SQ-dyes behave like p-type donors forming a p–n heterojunction with soluble fullerene derivative phenyl-C_{61}-butyric acid methyl ester (PCBM) as n-type organic electron acceptor.

Generally, symmetrical squaraine dyes are synthesized by condensation of squaric acid with two equivalents of a quaternized methylene base such as an aniline derivative or 1,2,3,3-tetramethyl-3H-indolium iodide (Figure 2.5) in the mixture of high boiling solvents like butanol:toluene or butanol:benzene at reflux condition.. Structural variation are simply achieved by using different precursors. For the present thesis far-red sensitizing symmetrical SQ-dyes bearing varying alkyl chain lengths have been synthesized as per the method reported by Pandey et al [40]. The symmetrical SQ-dye is used as additional sensitizing molecule for the fabrication of DSPHSC.

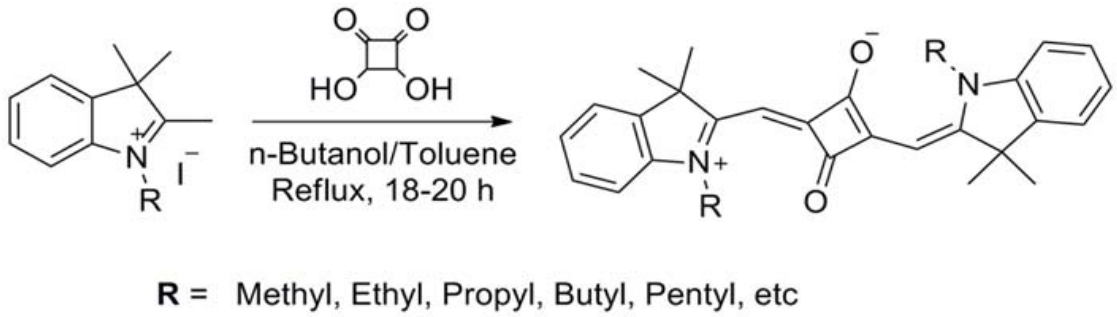

Figure 2.5 General scheme for synthesis of indole based symmetrical SQ-dyes.

2.1.5 Poly (3, 4-ethylenedioxythiophene) poly (styrenesulfonate) (PEDOT: PSS)

Poly(3,4-ethylenedioxythiophene) (PEDOT) is a highly transparent electrically conductive ionomer based on the 3,4-ethylenedioxythiophene (EDOT) monomer being developed by German company (Bayer AG) in late 80's. An ionomer is a polymer with repeating electrically neutral units of which a fraction, generally no more than ~15%, are ionized [41]. PEDOT is generally used to modify the electrical characteristics of ITO layers in transparent electrodes and other opto electrical devices.

Electrical characteristics of PEDOT is because of conjugated polymer backbone like of P3HT. However its usability is limited due to its poor solubility in many commonly used thin films processing solvents. This fault is overcome by the addition of a sulfonated polystyrene (poly (styrenesulfonate) (PSS)) chain which carries negative charges and enhances solubility. This emulsion is known for its ability to form transparent, stable and conductive film. Its conductivity depends on size of the particles, on PEDOT: PSS ratio, on suspension concentration, on the solvent used and on the curing temperature. PEDOT: PSS is usually sold as a dispersion in water, but this does not form high quality films when spin coated because water is quite slow to evaporate in comparison with alcohol based or similar solvents. By adding ethanol or methanol in a 1:1 ratio with the PEDOT: PSS suspension the evaporation rate and ability to bond to surfaces is enhanced and good quality films can be fabricated [42]. This layer is water soluble and can be surface modified by RF plasma treatment. PEDOT: PSS is a very transparent material that has a virtually

flat absorption spectrum in the visible region and typically reduces the amount of photons passing through to the active layer by less than 5% [43]. However, advantage of the enhanced performance due to increase in the work function of ITO from ~4.7eV to ~5.2eV offsets these minimal losses [44].

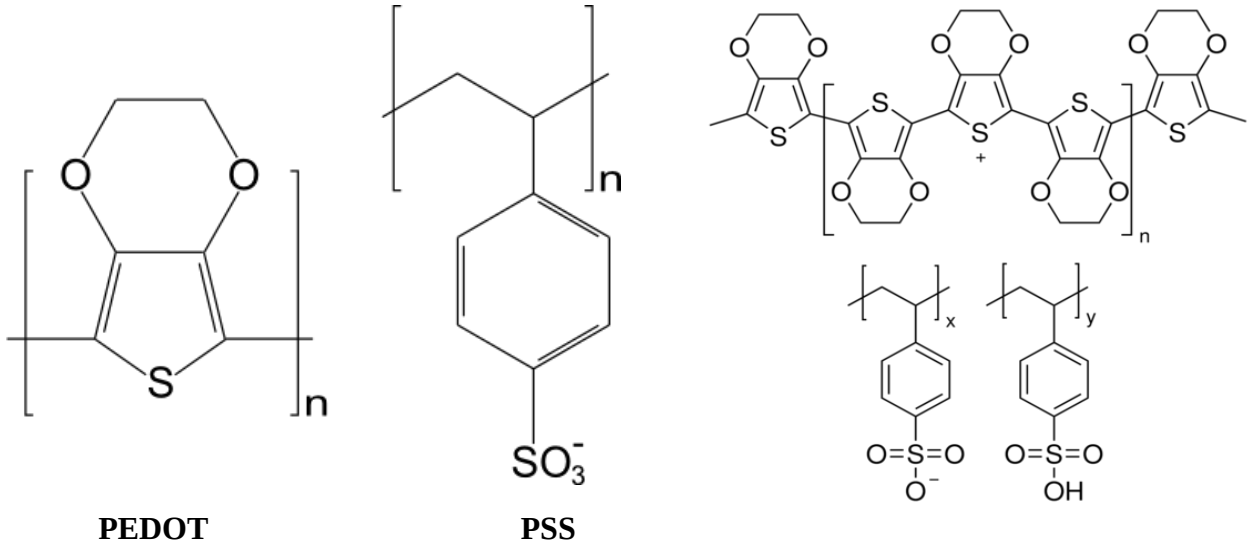

Figure 2.6 Chemical structure of PEDOT: PSS and its constituent ionomers.

The PEDOT: PSS used in this thesis was Clevios PVP Al 4083, which was purchased from H.C.Starck. Purchased aqueous solution was blue in color and was kept in refrigerator at Temperature 5^0C. The PEDOT: PSS ratio was 1:6 by weight, its solid content was between 1.3 to 1.7%, and its viscosity was 5 to 12 $mPas^{-1}$

2.2 Methods for thin film fabrication

The following section provides the brief preview about the major instrumentation used for active layer and metal thin film fabrication in the various PSC,PHSC and DSPHSC solar cells fabricated for present thesis.

2.2.1 Spin coating

Spin coating is one of main technique for the deposition of thin films in laboratories. For the deposition of different materials to be fabricated as thin film, first a solution of desired materials are prepared in a common solvent. In a typical spin coating process an excess amount of solution is placed onto the substrate which is then spun at high speeds (up to 10,000 rpm) for certain duration. The solution will then spread by centrifugal force and excess will be ejected from edges, leaving a thin film on surface of substrate. Usually spinning time is optimized according to the used solvent's viscosity and boiling point. The final thickness depend both on spin coater's parameters (acceleration, rotation speed, time, exhaust etc.) and on the solution (viscosity, concentration, solvent used, etc.). Typically more concentrated or viscous solutions will produce thicker layers at a given spin speed. This has implications for the fabrication of the BHJ solar cells, as pure polymer is mixed with other materials such as fullerenes and/or other nano-materials for active layer fabrication, which thus affects the viscosity and hence the thickness of thin film in solar cell.

For spin coating, the substrate is generally held onto a rotating chuck by means of a vacuum pump, to prevent substrate from being thrown in the air .The spin speed ramps up to the required spin speed, stays at that speed for a specified length of time and then ramps back to a stationary position at which point the substrate can be removed from the spin coater.

Modelling the spin coating process is difficult due to the many different factors involved such as; viscosity of the solution, rate of evaporation, spin speed and exhaust. It is therefore necessary to optimize the process by spin coating a range of samples with the desired viscosity at different spin speeds to determine the optimum speed and viscosity for the required film thickness. This process is known for its good reproducibility but it is important to note that subtle variation in the parameters can result in drastic variations on the coated film. Also, this is very sensitive to the ambient atmosphere, like presence of dust particle which prevent the desired spreading of the solution. Thus, spin coating usually requires clean rooms or glove box. Another drawback is that it can't be used for large scale production since it's difficult to coat large areas, also wastage of solution is too much. In this thesis most of the work was done on an ACTIVE spin coater which was placed in glove box that can be manually filled with nitrogen. Spin coater was always used

with the open lid.

In present thesis spin coater have been used for deposition of active layer (donor/acceptor BHJ) and hole transporting layer (PEDOT-PSS) in all PSC, PHSC and DSPHSC devices.

Figure 2.7 Spin coater machine used for present thesis

2.2.2 Circular nano spray deposition

Spray deposition is the roll to roll compatible technique that involves forcing the printing ink through a nozzle whereby a fine aerosol is formed. Electrostatic charging or a neutral carrier gas may be involved to aid in directing the aerosol at the surface that is to be coated. Aerosol formation and solvent evaporation is complex process thus need to be controlled for preparation of smooth thin film surface. The formation of film quality is very much dependent on solvent's viscosity used for making ink, The ease with which inks are prepared ranges from simple to complex and the range of viscosities that will work is wide. With the spray coating technique it is possible to obtain wide range of film thickness.

Figure 2.8 Circular Spray coating system used for this thesis

There are different kind of spray techniques available for thin film fabrication. For this thesis we have used the circular nano vapor deposition spray system (NVD). NVD offers many benefits in terms material usage, thin film uniformity and reproducibility over conventional spray systems. Details of various spray techniques, and NVD advantages are discussed in section 3.1 of this thesis.

2.2.3 Vacuum thermal evaporation

Vacuum thermal evaporation is one of the common technique used for thin film deposition. It is a technique that is suitable for a wide range of materials including; metals, metallic oxides and some organic materials. In present thesis this technique is being used for top electrode (Aluminum) deposition in polymeric BHJ solar cells. The material that has to be deposited is heated until its evaporation starts and then atoms are ejected. Evaporation involves two basic processes: a hot source material evaporates and condenses on to the substrate. This technique is done in vacuum, as it allows vapor particles to travel directly to the target object (substrate), where

they condense back to a solid state. Because of vacuum, vapors other than the source material are almost entirely removed before the process begins. However, hot objects in the evaporation chamber, such as heating filaments may produce unwanted vapors that can limit the quality of the vacuum. Evaporated atoms that collide with those foreign particles may react with them; for instance, if aluminum is deposited in the presence of oxygen, it will form aluminum oxide. They also reduce the amount of vapor that reaches the substrate, which makes the thickness difficult to control. In high vacuum (with a long mean free path), evaporated particles can travel directly to the deposition target without colliding with the background gas. For a typical pressure of 10^{-4} Pa, a 0.4-nm particle has a mean free path of 60 m.

Figure 2.9 Vacuum thermal evaporation machine used for present thesis

The general appearance of the used vacuum thermal evaporator is shown in Figure 2.9. For Aluminum deposition tungsten was used as heating filament, because of their high melting point (3695 K) in comparison with aluminum (934 K). Vacuum were achieved in the chamber with help of rotary and diffusion pump. A crystal thickness monitor was used to determine the thickness of the films. Sample holders was used to hold the masked substrate.

In present thesis vacuum thermal evaporation have been used for deposition of top electrode (Al)

in both PSC, PHSC and DSPHSC devices.

2.3 Instrumentation for material and device characterization

The following section provides the brief preview about the major instrumentation used in material and device characterization of various PSC, PHSC and DSPHSC for present thesis.

2.3.1 Film thickness measurement

Measurement for all the polymeric- nanomaterial BHJ thin films in present thesis was performed using Dektak 6M stylus profiler (Veeco instruments inc.). The Dektak 6M takes the measurement electromechanically by moving sample beneath a diamond-tipped stylus. The stylus is mechanically coupled with the core of linear variable differential transformer (LVDT). According to the user –programmed scan length, scan time, speed and stylus force, the fine stylus is moved across the sample. Due to surface variation of thin film stylus movement is translated vertically thus changing the core position of LVDT and producing the corresponding electrical signal. The LVDT scales an AC reference signal proportional to the positional change, which in turn is conditioned and converted to a digital format through high precision integrated analog to digital converter.

The digitized signals from printing a single scan are stored in computer memory for display, manipulation, measurement and printing (Figure 2.10). A useful secondary function of step profilometry is the ability to carry out surface roughness measurements. By having the stylus travel across the surface of the film, irregularities in the film surface can also be measured and maximum, minimum and average heights of the peaks and troughs can be recorded

However, this technique also has two main limitations; firstly it requires a reasonably sharp face to the film i.e. the slope of the face of the film from top to bottom is less than the length the stylus travels, secondly the film should be sufficiently dense that the stylus does not become

embedded in the film, which can occur with some polymeric materials.

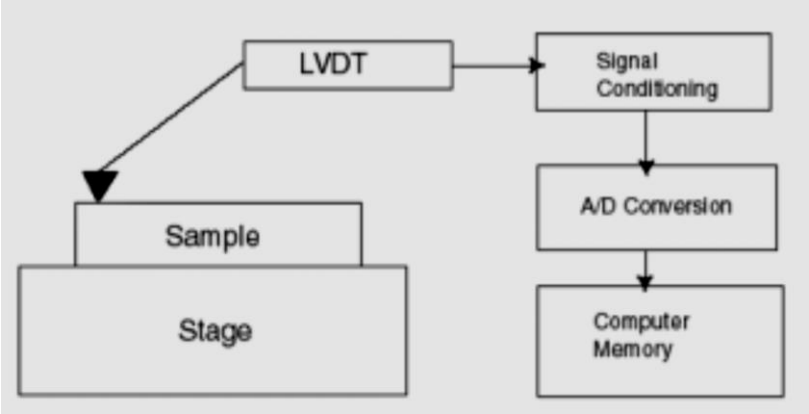

Figure 2.10 Block diagram of DEKTAK 6M profiler

2.3.2 Photovoltaic device characterization

In this thesis, photovoltaic performance of PSC and PHSC were monitored with a solar simulator (Bunko-Keiki Co., Ltd., KHP-1) equipped with a xenon lamp (XLS-150A). The exposure of light was adjusted to be AM1.5 (100 mW/cm^2). The two widely used techniques for photovoltaic characterizations are, current to voltage measurements under simulated sunlight and monochromatic light generated current measurements of also knows as incident photon current conversion efficiency (IPCE).

2.3.2.1 Solar simulator and spectro-radiometer

For the measurement of solar cell efficiency, the spectral response of the solar simulator under investigation is first calibrated by LS-100 grating spectro-radiometer. It was specially designed from use in measuring the spectral irradiance of solar simulators that are used for the measurement of photovoltaic cells. Moreover, it is calibrated against a National Institute of Standards and Technology (NIST) traceable standard lamp. Its size is compact and it is very easy to operate. This spectro-radiometer must be connected to a PC (or laptop computer) via a RS232C cable, and data are obtained using the furnished (included) software. The measurement/analysis software is used to process the obtained data as follows;

a. Compare with the data obtained in the standard test conditions

b. Calculate the integrated irradiance in the specified spectral range

c. Calculate the spectral coincidence (JIS C 8912)

d. Calculate the difference and ratio compared to the standard data

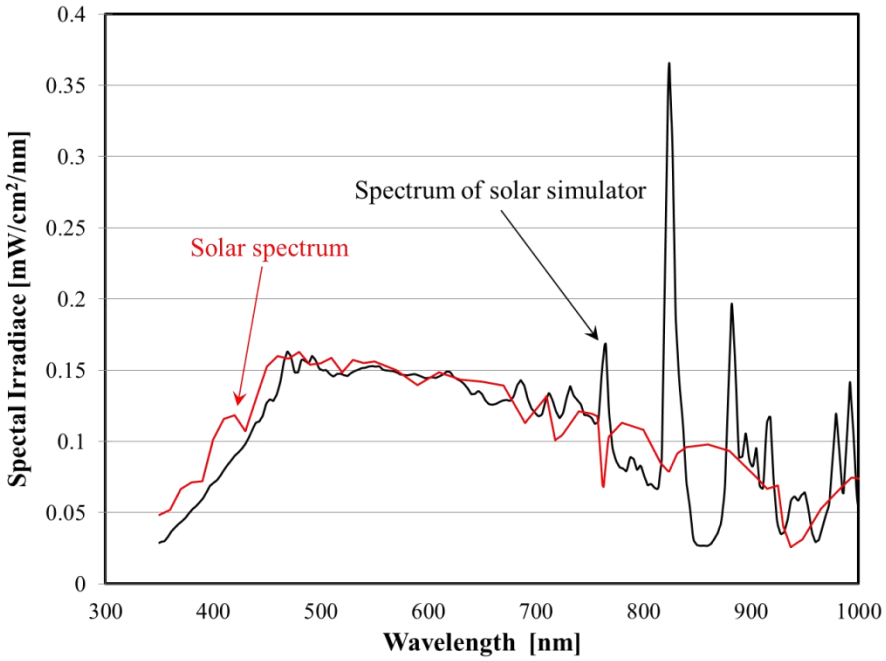

Figure 2.11 The calibrated solar simulator spectrum based on solar spectrum of AM1.5 by LS-100 grating spectro-radiometer.

2.3.2.2 Current-voltage measurements

Current voltage (I-V) measurements are the basis of many of the electrical measurements used in present thesis, while they are basically a simple process, the results can be interpreted in a variety of ways to obtain a number of useful parameters. In this work I-V measurements under AM 1.5 illumination were used to calculate basic parameters of polymer BHJ solar cells (Jsc, Voc, FF, Efficiency), whereas the dark I-V measurements were used to obtain leakage current and mobility of devices. The details about the solar cells parameters are discussed in section 1.6.3 of chapter 1

in this thesis.

2.3.2.3 Incident photon to current conversion efficiency (IPCE)

The photosensitization behavior of a solar cell varies with the wavelength of the incoming light. IPCE is being measured under irradiation of monochromatic light and is basically defined by the ratio of the number of electrons generated by the solar cell to the number of incident photons on the active surface:

$$\mathbf{IPCE}(\boldsymbol{\lambda}) = \frac{\boldsymbol{n_{electrons}}(\boldsymbol{\lambda})}{\boldsymbol{n_{photons}}(\boldsymbol{\lambda})} = \frac{\boldsymbol{I}(\boldsymbol{\lambda})/\boldsymbol{e}}{\boldsymbol{P_{in}}(\boldsymbol{\lambda})/\boldsymbol{h}\cdot\boldsymbol{\nu}} = \frac{\boldsymbol{I}(\boldsymbol{\lambda})}{\boldsymbol{\lambda}\cdot\boldsymbol{P_{in}}(\boldsymbol{\lambda})}\cdot\frac{\boldsymbol{hc}}{\boldsymbol{\nu}}$$

Where, $I(\lambda)$ and $P_{in}(\lambda)$ is the current given by the cell at wavelength λ the incoming power at wavelength λ, respectively. The spectral sensitivity $S(\lambda)$ is the product of the $IPCE(\lambda)$ and the wavelength (λ). If one knows the spectral irradiance $E(\lambda)$, It is possible to estimate the short-circuit I_{sc} using the relation:

$$\boldsymbol{I_{sc}} = \int \boldsymbol{S}(\boldsymbol{\lambda})\cdot\boldsymbol{E}(\boldsymbol{\lambda})\cdot\boldsymbol{d\lambda}$$

This method is useful for an indirect determination of the short-circuit current of the solar cell.

2.3.3 UV-visible-NIR spectroscopy

Ultraviolet–visible spectroscopy or ultraviolet-visible spectrophotometry (UV-Vis or UV/Vis) refers to absorption spectroscopy or reflectance spectroscopy in the ultraviolet-visible spectral region. This spectroscopy uses the light in the visible and adjacent (near-UV and near-infrared (NIR)) ranges. The absorption or reflectance in the visible range directly affects the perceived color of the chemicals involved. In this region of the electromagnetic spectrum, molecules undergo electronic transitions. Molecules containing π-electrons or non-bonding electrons (n-electrons) can absorb the energy in the form of ultraviolet or visible light to excite these electrons to higher anti-bonding molecular orbitals. The more easily excited the electrons (i.e. lower energy gap between the HOMO and the LUMO), the longer the wavelength

of light it can absorb.

The instrument used in ultraviolet-visible spectroscopy is called a UV/Vis spectrophotometer. It measures the intensity of light passing through a sample **I**, and compares it to the intensity of light before it passes through the sample $\mathbf{I_0}$. The ratio $\mathbf{I/I_0}$ is called the transmittance, and is usually expressed as a percentage **(%T).** The absorbance A, is based on the transmittance:

$$\mathbf{A = -\log (\% T/100 \%)}$$

The UV-visible spectrophotometer can also be configured to measure reflectance. In this case, the spectrophotometer measures the intensity of light reflected from a sample **I**, and compares it to the intensity of light reflected from a reference material $\mathbf{I_0}$ (such as a white tile). The ratio $\mathbf{I/I_0}$ is called the reflectance, and is usually expressed as a percentage **(%R).**

For present thesis, UV-visible absorption spectra of thin films were measured via UV-vis.-NIR double beam spectrophotometer (JASCO, model V-530, Nihon Bunko, Japan). For measuring absorbance, first thin films of different materials were coated on to glass substrate using spin coater. The incident beam was then transmitted from the glass sides of the reference and sample. All the measurements done are in absorbance mode.

2.3.4 Atomic Force Microscopy

Atomic Force Microscopy (AFM) is a type of high resolution Scanning probe microscopy (SPM). In SPM a sharp probe is passed back and forth across a sample surface to obtain a two or three dimensional raster image built up in a similar way to the picture on a television screen. AFM is widely used to determine surface topography of thin films. An AFM consist of a cantilever with a sharp tip (a few nanometers) at its end which is used to scan sample point to point. Depending upon the type of measurements, an AFM has three main modes: contact mode, non-contact mode and tapping mode. In contact mode the tip is dragged across the surface to be scanned, although this gives precise topographical impression of the surface, but may result in damage of both the sample and the tip due to forces between the surface and the tip. In non-contact mode, AFM measures the van der Waal forces between the tip and surface thus obtaining an image of the surface. As these forces are much weaker than those encountered in either of the contact or tapping

modes and it is supplemented by oscillating the tip and applying an AC voltage. In tapping mode the tip makes brief contact with the surface before being lifted up, this is repeated over the surface of the sample. In the present thesis tapping mode is used for scanning surface of polymeric thin films.

In tapping mode cantilever oscillates near the resonant frequency of piezzo attached to it. As the tip comes close to the thin film surface, oscillation gets reduced due to interactions of forces. This modification is measured via a laser spot which is reflected from top surface of cantilever, just above the tip, into the array of photodiodes. Thereafter, a servo system adjusts the height to maintain a set cantilever oscillation amplitude. The image obtained by tapping mode is intermittent contact of tip with the thin film surface.

2.4 Fabrication of PSC, PHSC and DSPHSC solar cells

2.4.1 Substrate preparation

In this thesis, Indium tin oxide (ITO) coated glass having nominal sheet resistance of 8Ω/□ were used as base substrate for polymeric BHJ solar cells. Along with good transparent and conduction properties, ITO also energetically favorable Fermi level for polymeric and polymeric hybrid BHJ. Commercially available ITO coated glass sheets usually comes in dimension of 10cm × 10cm. For ease of fabrication, ITO sheet was cut into the samples of dimension 2.5cm × 2.5cm. For avoiding scratches during this step, ITO coated face was held on tissue paper. The freshly cut glass square samples were then cleaned respectively in distilled water, acetone, and isopropanol ultrasonic baths for about 10 min each, so as to remove the reminiscent impurities and glass fragments from the ITO surface. After the bathes substrate samples were dried with blower. Followed by drying, substrate were patterned using tape for ITO etching. Figure 2.12 shows the typical patterned substrate used in thesis.

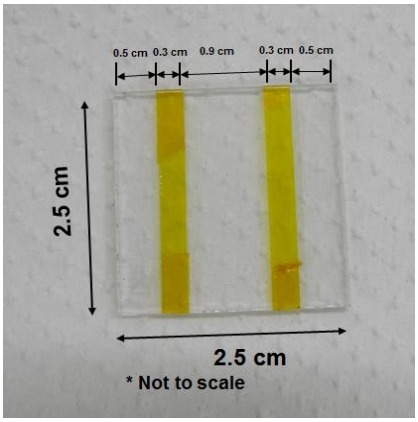

Figure 2.12 Patterned ITO glass plate (with dimensions)

After patterning substrate were etched in aqua regia solution (mixture of concentrated HNO_3 and HCl, in a volumetric ratio of 1:3 respectively) heated up to 70^0C for 3 minutes. The substrates were than rinsed in distilled water and the patterning tape was removed with plastic tweezers to avoid any scratches. The quality of etching was checked with the help of optical microscope. For device fabrication there should be no traces of left ITO on the glass surface, otherwise it leads to short circuiting thus produces high leakage current. Also edge of ITO surface should be iso-tropically etched, as an-isotropic etching along the edges reduces the performance of device. (Figure 2.13)

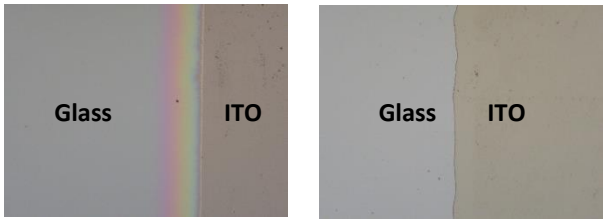

Figure 2.13 ITO etching along the edges: anisotropic etching (left), isotropic etching (right)

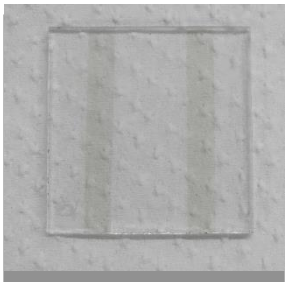

Figure 2.14 Patterned ITO glass substrate after etching

After etching ITO patterned glass substrate were cleaned respectively in distilled water,

acetone and isopropanol ultrasonic baths for 15 minutes each at ambient temperature to get rid of any impurities left on the surface. Finally the ITO patterned glass surface was dried with blowers.

2.4.2 Deposition of PEDOT: PSS

In this thesis PEDOT: PSS was used as electron blocking layer in both polymeric and polymeric hybrid BHJ solar cells. Before coating of PEDOT: PSS, ITO surface was UV ozone treated for 30 minutes to improve surface wettability. As ITO being ceramic, thus it possess a high cohesion strength due to strong iono-covalent bonds between atoms. Therefore this type of solid has strong surface energy and low wettability, so it has to be treated for increasing wettability before any further coating on it.

For all the solar cells in this thesis, an aqueous solution of PEDOT: PSS (Clevios PVP Al 4083) was used as purchased from H.C. Strack. Before using PEDOT: PSS, it was first filtered through 0.45 μm PVDE filters for avoiding any lump clusters, which usually forms due to long storage of PEDOT: PSS in refrigeration.

For coating, ITO patterned glass substrate was first blown N_2 gas to get rid of any dust particles, and then placed on to the chuck of spin coater. PEDOT: PSS was dropped onto the substrate using glass pipette and then spin coated at 4000 rpm for 30 seconds. All the deposition of PEDOT: PSS was done at ambient room temperature condition. Thereafter layer was annealed for 10 minute at 150^0C for removal any residual water. The average thickness of PEDOT: PSS coated on to the substrate was 40 nm (measured using DEKTAK 6M Profilometer).

2.4.3 Deposition of active layer

The respective composition and concentration of active layer solutions for polymeric BHJ and polymeric hybrid BHJ solar cells are discussed in relevant chapters of this thesis. After the PEDOT: PSS coating active layer were deposited on the substrate either using spin coater or NVD systems. The experimental conditions and post annealing conditions are also discussed in detail in relevant chapter of this thesis.

2.4.4 Metal electrode deposition

After the curing/annealing of the active layer coated substrates, Aluminum (Al) was deposited as cathode using the thermal evaporation system. The deposition was done in vacuum conditions of 10^{-4} torr. Rate of deposition was usually between 2-3 kÅ/ sec, which was monitored with the help of quartz crystal monitor. The average thickness for deposited Al in devices were 100 nm.

References

[1] G. Barbarella, A. Bongini, M. Zambianchi, Macromolecules 27, 11, (1994).

[2] G. A. Diaz-Quijada, B. M. Pinto, S. Holdcroft Macromolecules 29, 5416–5421, (1996).

[3] Y. Kim, S. A. Choulis, J. Nelson, D. D. C. Bradley, S. Cook, and J. R. DurrantKim , Appl. Phys. Lett. 86, 063502 (2005).

[4] Chen, T.-A., X. Wu, and R.D. Rieke, Journal of the American Chemical Society 117, 233-244 (1995).

[5] McCullough, R. D. Adv. Mater. 10, 93 (1998).

[6] A. Mozer, N. Sariciftci, A. Pivrikas, R. Oesterbacka, G. Juska, L. Brassat, and H. B"assler, Physical Review B, 71, 352141-352149, (2005).

[7] H. Hoppe and N. Sariciftci, J. Mater. Res., 19, 1924-1945, (2004).

[8] J. Nakamura, K. Murata, and K. Takahashi, Appl.Phys. Lett. 87, 132105, (2005).

[9] E. Bundgaard, F.C. Krebs, Solar Energy Materials and Solar Cells, 91, 954-985 (2007).

[10] S. Sensfuss, M. Al-Ibrahim, Optoelectronic Properties of Conjugated Polymer/Fullerene Binary Pairs with Variety of LUMO Level Differences, in Organic Photovoltaics: Mechanisms, Materials and Devices, S.-S. Sun and N.S. Sariciftci, Editors, Taylor and Francis: Boca Raton (2005).

[12] J. C. Hummelen, B. W. Knight, F. Lepeq, F. Wudl, J. Yao; C. L Wilkins,., Journal of Organic Chemistry 60, 532–538 (1995).

[13] P.A. Lane, Z.H. Kafafi, Solid-State Organic Photovoltaics: A Review of Molecular and Polymeric Devices, in Organic Photovoltaics: Mechanisms, Materials and Devices, S.S. Sun and N.S. Sariciftci, Editors. Taylor and Francis: Boca Raton. p. 217-237 (2005).

[14] S. Yoo, W. J. Potscavage Jr., B. Domercq, S.H. Han, T.D. Li, S. C. Jones, R. Szoszkiewicz, D. Levi, E. Riedo, S. R. Marder, B. Kippelen, Solid-State Electronics 51, 1367-1375 (2007).

[15] Tang, C.W., Applied Physics Letters, 48, 183 (1986).

[16] J. Nakamura, K. Murata, K. Takahashi, Appl.Phys. Lett. 87, 132105, (2005).

[17] D. Veldman, S. Meskers, R. Janssen, Adv.Funct.Material, 19, 1939-1948, (2009).

[18] P. Schilinsky, C. Waldauf, C. J. Brabec, Appl. Phys. Lett. 81, 3885 (2002).

[19] P. A. Van Hal, M. P. T. Christiaans, M. M. Wienk, J. M. Kroon, R. A. J. Janssen, Phys. Chem. B 103, 4352 (1999).

[20] M. Shim, P.J. Guyot-Sionnest, Am. Chem. Soc. 123, 11651(2001)

[21] F. C. Spano, J. Chem. Phys. 122, 234701 (2005).

[22] J. F. Chang, J. Clark, N. Zhao, H. Sirringhaus, D. W. Breiby, J. W. Andreasen, M. M. Nielsen, M. Giles, M. Heeney, and I. McCullochet, Phys. Rev.B. 74, 115318 (2006).

[23] J. K. J. vanDuren, X. Yang, J. Loos, C. W. T. Bulle-Lieuwma, A. B. Sieval, J. C. Hummelen, R. A. J.

Janssen, Adv. Funct. Mater. 14, 425 (2004).

[24] D. C. Olson, S. E. Shaheen, R. T. Collins, D. S. Ginley, J. Phys. Chem C 111, 16670 (2007).

[25] J. Boucle, H. J. Snaith, N. C. Greenham, J. Phys. Chem. C. 114, 3664 (2010).

[26] B. Kannan, K. Castelino, A. Majumdar, Nano Lett. 3, 1729 (2003).

[27] J. D. Moet, L. J. A. Koster, B. de Boer, P. W. M. Blom, Chem. Mater 19 5856 (2007).

[28] C.-T. Chen, S.R. Marder, L.-T. Cheng, J. Am. Chem. Soc. 116 3117 (1994).

[29] K.-Y. Law, F.C. Bailey, J. Org. Chem. 57 3278 (1992).

[30] L. Beverina, M. Crippa, M. Landenna, R. Ruffo, P. Salice, F. Silvestri, S. Versari, A.Villa, L. Ciafoni, E. Collini, C. Ferrante, S. Bradamante, C.M. Mari, R. Bozio, G.A. Pagani, J. Am. Chem. Soc. 130 1894 (2008).

[31] P.T. Snee, R.C. Somers, G. Nair, J.P. Zimmer, M.G. Bawendi, D.G. Nocera, J. Am. Chem. Soc. 128 13320 (2006).

[32] A. Ajayghosh, Acc. Chem. Res. 38 449 (2005).

[33] J.H. Yum, P. Walter, S. Huber, D. Rentsch, T. Geiger, F. Nuesch, F.D. Angelis, M. Grätzel, M.K. Nazeeruddin, J. Am. Chem. Soc. 129 10320 (2007).

[34] S.S. Pandey, T. Inoue, N. Fujikawa, Y. Yamaguchi, S. Hayase, Thin Solid Films 519 1066 (2010).

[35] F. Silvestri, M.D. Irwin, L. Beverina, A. Facchetti, G.A. Pagani, T.J. Marks, J. Am. Chem. Soc. 130 17640 (2008).

[36] D. Bagnis, L. Beverina, H. Huang, F. Silvestri, Y. Yao, H. Yan, G.A. Pagani, T.J. Marks, A. Facchetti, J. Am. Chem. Soc. 132 4074 (2010).

[37] S. Wang, E.I. Mayo, M.D. Perez, L. Griffe, G. Wei, P.I. Djurovich, S.R. Forest, M.E. Thompson, Appl. Phys. Lett. 94 233304 (2009).

[38] G. Wei, R.R. Lunt, K. Sun, S. Wang, M.E. Thompson, S.R. Forest, Nano Lett. 10 3555 (2010).

[39] S. S. Pandey, T. Mizuno, S. K. Das, Y.Ogomi, S. Hayase Thin Solid Films 522 401–406 (2012).

[40] S.S. Pandey, T. Inoue, N. Fujikawa, Y. Yamaguchi, S. Hayase, J. Photochem. Photobiol. A 214 269 (2010).

[41] H. Yan, S. Arima, Y. Mori, T. Kagata, H. Sato, H. Okuzaki, Thin Solid Films 517, 3299-3303 (2009).

[42] J. Yan, C. Sun, F.Tan, X. Hu, P. Chen, S. Qu, S. Zhou, J. Xu, Solar Energy Materials and Solar Cells 94, 390-394 (2010).

[43] W. T. Chiang, S. H. Su, Y. F. Lin, M. Yokoyama, Japanese Journal of Applied Physics, 49, 4 (2010).

[44] F. Zhang, O. Inganas, Conducting and Transparent Polymer Electrodes, in Organic Photovoltaics: Mechanisms, Materials and Devices, S.-S. Sun and N.S. Sariciftci, Editors. Taylor and Francis: Boca Raton (2005)

Chapter 3:

Study of fabrication techniques for polymeric bulk hetero-junction solar cells

This chapter describes the basic fabrication process for the polymeric bulk hetero-junction (PSC) solar cells. Additionally it also explores the performance characteristics of P3HT/PCBM PSC device fabricated using new and efficient spray system, and its comparison with device fabricated using spin coating process.

3.1 Introduction

PSC devices have been attracting extensive research attention over the last decade as they can significantly decrease the fabrication cost of solar energy conversion. Low production cost is attributed to solution processing at low temperatures and possibility of PSC manufacturing by high-speed coating or printing techniques i.e. roll-to-roll (R2R) manufacturing on flexible substrate [1–5]. A model solution processed polymeric-organic nanoparticle system, which has been widely studied is poly (3-hexylthiophene) (P3HT) as electron donor and [6, 6]-phehyl-C61 butyric acid methyl ester (PCBM) as an electron acceptor. Optimization of the P3HT/PCBM device structure and post treatment have continuously increased the power conversion efficiency [6, 7]. For solution processing, mostly PSC active layers are fabricated by spin-coating method, but this process has large material losses, usage of high solution concentration, low throughput and also its scalability for roll-to-roll (R2R) fabrication is difficult [1].

For overcoming the problem of low throughput and scalability, several groups have explored various coating techniques such as screen printing [8], doctor blading [9], inkjet printing [10, 11] and spray-coating [12–16]. But with all these coating techniques, there are additional associated factors of processing speed, wet film thickness, ease of preparation of solution, solution viscosity, and maximum solution usage. Table 3.1[1] gives a brief comparison of above mentioned fabrication techniques in terms of these crucial parameters.

Parameters / Techniques	Solution Wastage	Processing Speed	Solution preparation	Solution Viscosity(cP)	Wet film thickness (µM)	R2R Compatibility
Spin coating	5	N/A	1	1	0-100	No
Doctor blade	2	N/A	1	1	0-100	No
Spray coating	3	1-4	2	2-3	1-500	Yes
Inkjet	1	1-3	2	1	1-500	Yes
Screen printing	1	1-4	3	3-5	10-500	Yes

Table 3.1 Comparative analysis of various fabrication techniques.

Solution wastage: 1 (none), 2 (little), 3 (some), 4 (considerable), 5 (significant).
Processing Speed: 1 (very slow), 2 (slow 1mmin^{-1}), 3 (medium 1–10mmin^{-1}), 4 (fast 10–100mmin^{-1}), 5 (very fast 100–1000mmin^{-1}).
Solution preparation: 1 (simple), 2 (moderate), 3 (demanding), 4 (difficult), 5 (critical).
Solution viscosity: 1 (very low 10 cP) 2 (low 10–100 cP), 3 (medium 100–1000 cP), 4 (high 1000–10,000 cP), 5 (very high 10,000–100,000 cP)

Table 3.1 shows that among the different fabrication techniques suitable for R2R compatibility, spray coating offers wider processing speeds, ease of solution preparation and larger wet film thickness window. However table 3.1 also shows that conventional spray coating system still has large material wastage in comparison to other competitive R2R coating techniques (Inkjet, Screen printing etc.). In most commonly used spray systems, solution are poured on to the substrate directly with varying shooting angles, which causes material losses.

Circular nano vapor spray deposition system (NVD) is a spray system which controls the material losses by pouring material in circular shooting way on to the substrate. NVD is basically a state of art high accuracy and low material consumption spray coater equipped with unique liquid control system and tornado nozzle. Apart from low material wastage NVD system also offers high reproducibility in terms of thin film thickness with each subsequent coating [20]. Spray coating began to gain attention when Vak et al. in 2007 [13] showed they could easily fabricate the active layer with a commercially available hand-held airbrush. After this various groups have studied the P3HT/PCBM PSCs with different type of spray coating systems. Throughput of spray coating system is highly dependent on used solvent's viscosity, an ideal solvent will be such that it has enough viscosity so the solution can easily come out of nozzle and disperse uniformly on to the

substrate. However, annealing conditions of active layer blend is another crucial factor that affects the performance of fabricated PSC. Annealing conditions determine the extent of phase separation which is needed for better charge transport properties. For better phase separation slow annealing is needed, that means solvent should have relatively higher boiling point. So, the choice of solvent system for any spray coater is dependent on its viscosity and boiling point. Table 3.2 gives a brief comparison between different kinds of spray coating system used for fabrication of P3HT/PCBM PSCs with their fabrication conditions.

Deposition Method	**Solvent System**	**Concentration, Annealing conditions**	**Power conversion efficiency (%)**
Airbrush Spray Coating	Chlorobenzene	1.5 mg/ml, 110^{o}C for 7 min	2.83 % [13]
Ultrasonic Spray Coating	Chlorobenzene; Xylene	2 mg/ml, 110^{o}C for 10 min	3.0 %; 1.2 % [15]
Airbrush Spray Coating	Chlorobenzene; Dichlorobezene - Mesitylene mixture	15 mg/ml, 140^{o}C for 10 min	1.7 %; 2.7 % [16]
Evaporative Spray Coating	Tetrahydrofuran	10 mg/L, 150^{o}C for 10 min	2.15 % [17]
Airbrush Spray Coating	Chloroform; Toluene; Xylene; Chlorobenzene	2 mg/ml, 120^{o}C for 10 min	2.35 % [18]
Multi-source Air Brush Spray Coating	Chlorobenzene; Alternating/Blend	5 mg/ml, 170^{o}C/ 150^{o}C	2.8 % ,2.9 % [19]

Table 3.2 Comparison of different spray coating system used for fabricating of P3HT/PCBM PSCs with the fabrication conditions.

This chapter presents the experiment and results, related to the parametric optimization of NVD system for fabrication of PSC using well studied P3HT/PCBM PSC. Experiments are done for comparative performance analysis of NVD fabricated devices with that of spin coated one

under similar experimental conditions. PSC devices are basically heterojunction of two different semiconductors, so the performance of device is dependent on mobility of charge carriers of major charge generating species (in BHJ case p type conjugated polymer). Therefore, we measured the hole mobility in different devices fabricated using spin-coating and NVD spray by space charge limited current (SCLC) method.

3.2 Experimental section

Different solutions of P3HT/PCBM were prepared for NVD and spin coating systems. For optimization of NVD system P3HT/PCBM mixtures of 1:1 weight ratio were mixed in different 5ml solvents of 1, 2 dichlorobenzene (ODCB), chlorobenzene (CB) and mixture of 70 %/ 30 % of CB/ODCB solvents. For spin coating devices, P3HT/PCBM mixture of 1:1 weight ratio were mixed in different 1ml solvents of ODCB and CB. All the solutions were stirred overnight on a hot plate (temperature ~ 40^0C) in glove box with an inert nitrogen atmosphere (<1 ppm H_2O and <1ppm O_2). Before the use, P3HT/PCBM solutions were filtered using 0.20 µm PVDE filters for avoiding any lump clusters.

For P3HT/PCBM device preparation (Figure 3.1), ITO patterned glass plates were cleaned through sonication in distilled water, acetone, and isopropanol respectively. After ultraviolet ozone treatment, poly(3,4-ethylenedioxythiophene) poly(styrenesulfonate) (PEDOT:PSS) (BAYTRON P, HC Starck, GMBH, Germany) having thickness of about 40 nm was spin coated followed by heating at 150^0C for 10 min on a hot plate .Thereafter photoactive layer (~210 ± 10 nm for all devices) were deposited via NVD system and spin coating process with their respective solutions, and then all the devices were annealed (120^0C for 15 min.) in the glove box with. After depositing hole blocking layer of LiF (1nm), devices were then finally completed by thermal evaporation of Aluminum (100 nm).

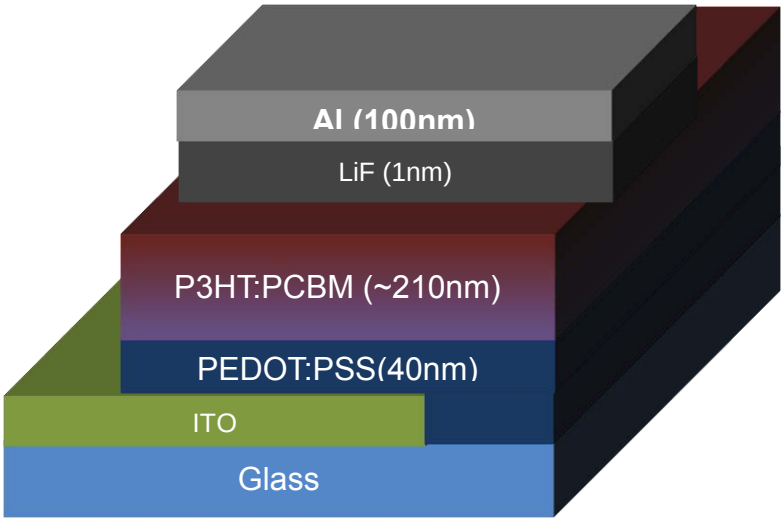

Figure 3.1 Device architecture of P3HT/PCBM BHJ PSC

Thickness of the PEDOT: PSS and active layer were measured using DEKTAK Stylus Profiler (6M, ULVAC Inc.). Atomic Force Microscopy (AFM) studies were carried out in tapping mode. Electronic absorption spectroscopic investigations for thin films of P3HT/PCBM on glass substrate were conducted using JASCO V 530 spectrophotometer. Photovoltaic measurements of the devices were performed under irradiation of 100 mW/cm^2 simulated solar light at global AM 1.5 condition using a solar simulator (Bunko Keiki, KHP-1). Irradiated active area of (0.06 cm^2) was precisely controlled using a black metal mask. Photocurrent action spectrum also known as incident photon-to-current conversion efficiencies (IPCE) as a function of wavelength was measured with a constant photon flux of 1x10^{16} photon/cm^2 at each wavelength in DC mode using an action spectrum measurement system connected to a solar simulator (model CEP- 2000, Bunko-Keiki, Japan).

3.3 Result and discussion

3.3.1 Optimization of NVD fabricated P3HT/PCBM device

For high efficient BHJ solar cells, it's very important to control the morphology which affects the extent of phase separation of donor-acceptor interfaces in order to ensure maximum

exciton dissociation at the interface. Better phase separation depends on the annealing conditions and choice of solvent system. Until now two best-suited solvents for P3HT/PCBM blend are CB and ODCB [21-24]. For the comparison, P3HT/PCBM blends were prepared in two separate solutions of pure CB and pure ODCB. Thin film could not be prepared from pure ODCB solvent, as for any spray system to be effective it should have low viscosity so that solution may come easily out of nozzle of the spray. Pure ODCB due its high surface tension and viscosity in comparison with CB (Figure 3.2) is not suitable for spray. But ODCB solvent, owing to its higher boiling point in comparison to CB (Table 3.3) is better solvent for phase separation during post annealing treatment of thin film. For harnessing the benefit out of both CB (Low viscosity and surface tension) and ODCB (for high boiling point) for NVD system, different blends of CB and ODCB were tried for fabrication of thin films. Best suited blend was found to be CB/ODCB in ratio of 7:3 (As higher proportion of CB significantly decreases the overall viscosity of blend, and presence of smaller proportion of ODCB slightly increases the boiling point, which will be helpful in slow annealing process).

Solvent properties / **Solvent**	**Boiling Point (^{0}C)**	**Surface Tension(dynes cm $^{-1}$)**	**Viscosity at 25^{0}C (mPa)**
Chlorobenzene (CB)	132	33.0	0.76
Ortho- Dicholrobenzene (ODCB)	180	37.0	1.32

Table 3.3 Physical properties of CB and ODCB solvent

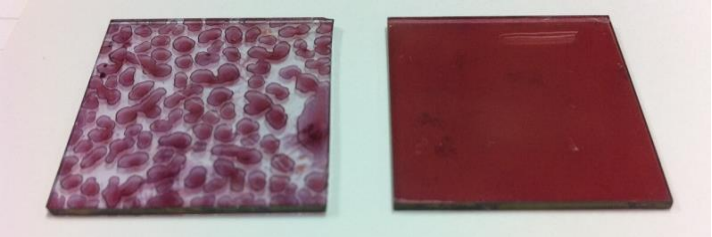

Figure 3.2 Thin film formation via NVD system using pure ODCB and pure CB solvents.

Figure 3.3 shows the AFM image for surface morphology of post annealed thin films (a) Spin (ODCB) (b) Spin (CB) (c) NVD spray (CB/ODCB) (d) NVD spray (CB). Better phase separation and high percolation of donor and acceptor is more prominent in case of NVD spray (CB/ODCB) blend and is as equivalent to the spin (ODCB) thin film. Relatively poor phase separation may be the cause of low charge generation in CB solvent in P3HT/PCBM devices, thus affecting their short circuit current density and efficiency as we will see later.

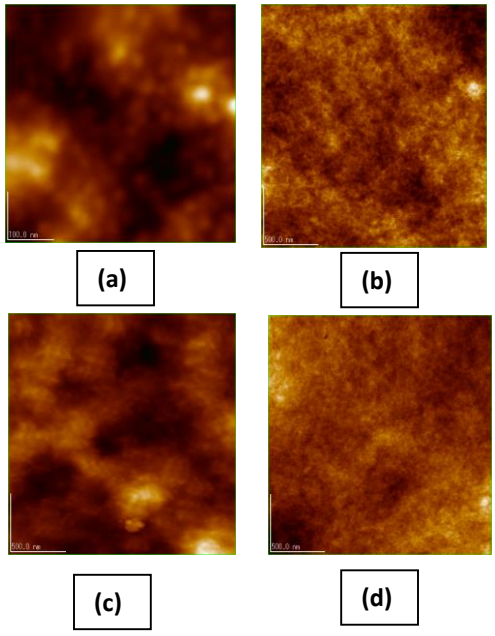

Figure 3.3 AFM images in tapping mode of P3HT: PCBM active layers deposited from (a) Spin (ODCB) (b) Spin (CB) (c) NVD spray (CB/ODCB) (d) NVD spray (CB)

3.3.2 Electronic absorption spectra of thin film BHJ

Normalized absorption spectra of thin films of P3HT/PCBM BHJ prepared using either NVD spray or spin coating system using different solvents are shown in the Figure 3.4. As the main absorption comes from the P3HT component, the absorption spectra of P3HT:PCBM blend films were normalized to the maximum of P3HT absorption region The absorption spectrum shows absorption maximum at 520 nm, which is due to P3HT and is associated with π-π^* electronic transition along with the appearance of vibronic shoulders at 550 nm and 610 nm. These clear

vibronic shoulders are associated with polymer crystallization [25, 26]. As the higher order of the P3HT phase attributes the high performance of BHJ PSC [27], these peaks are more prominent in case of spin (ODCB) and NVD spray (CB/ODCB), showing effect of higher control on nano morphology in comparison to pure CB spin or NVD spray thin films. The more intense vibronic feature in the case of samples prepared from ODCB might be due to the better aggregation and thus leading to better phase separation of the donor P3HT. This is also causing relatively higher P3HT to PCBM absorbance ratio. These observations are in accordance with AFM analysis discussed previously.

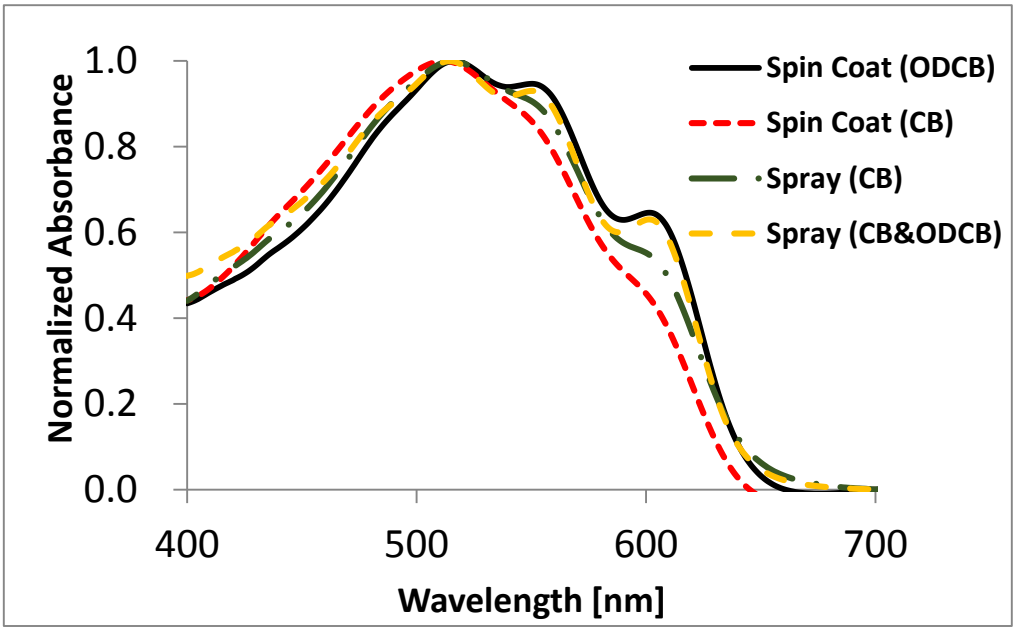

Figure 3.4 Electronic absorption spectra of thin films PSCs.

3.3.3 Electrical characteristics of thin film BHJ devices.

The current density–voltage (J–V) characteristics under illumination at AM1.5G (100 mW/cm^2) are presented in Figure 3.5. The NVD spray (CB/ODCB) device has comparable performance with spin (ODCB) device. In fact NVD spray (CB/ODCB) device shows better short circuit current density (Jsc =9.03) and open circuit voltage (Voc = 0.59) than spin (ODCB) device. However relatively lower efficiency in NVD spray (CB/ODCB) device is due to poor Fill factor

(FF = 0.51) in comparison to spin coated device. The effect of low FF could also be seen in NVD spray (CB) device. The low FF could be due to high series resistance in case of NVD spray devices.

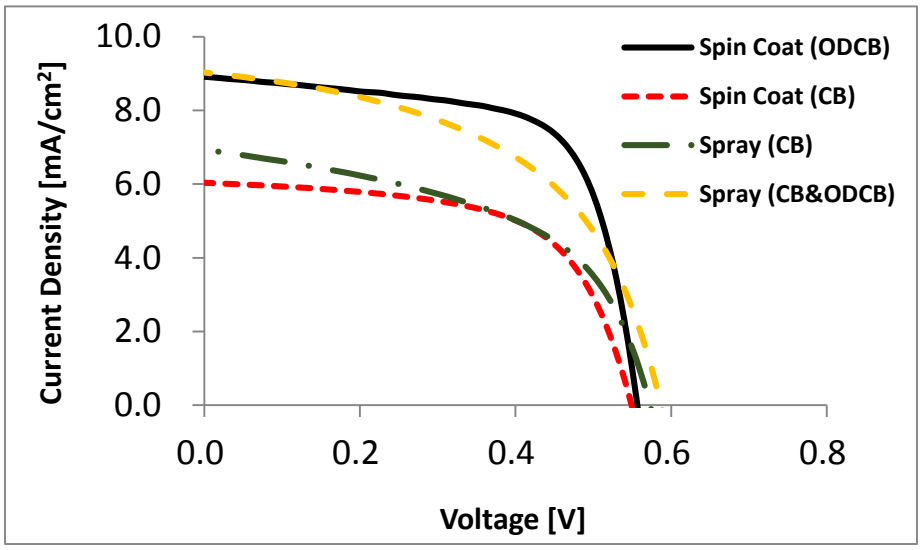

Figure 3.5 Photovoltaic characteristic (I-V) of P3HT/PCBM PSC devices

	Efficiency [%]	FF	Voc [Volts]	Jsc [mA/cm^2]
Spin Coat (ODCB)	3.32	0.67	0.56	8.92
Spin Coat (CB)	2.02	0.61	0.55	6.03
Spray (CB)	2.03	0.51	0.57	6.94
Spray (CB&ODCB)	2.71	0.51	0.59	9.03

Table 3.4 Photovoltaic characteristic (I-V) of P3HT/PCBM PSC devices

The relatively lower FF in case of NVD spray devices could be attributed to possibility of high number of trap sites. Fabrication of thin films via NVD spray is done in multiple coating steps process unlike spin coating fabrication where thin film is coated in single step coating. For example, for coating the thin film of 200nm (as in case of our devices), the NVD spray process is repeated 4 times, in each step thin film of approximately 50nm is fabricated. As no annealing was done after each successive coating of thin films, so, there might be possibility, presence of high number of trapping sites, which increases the recombination thus increasing the series resistance.

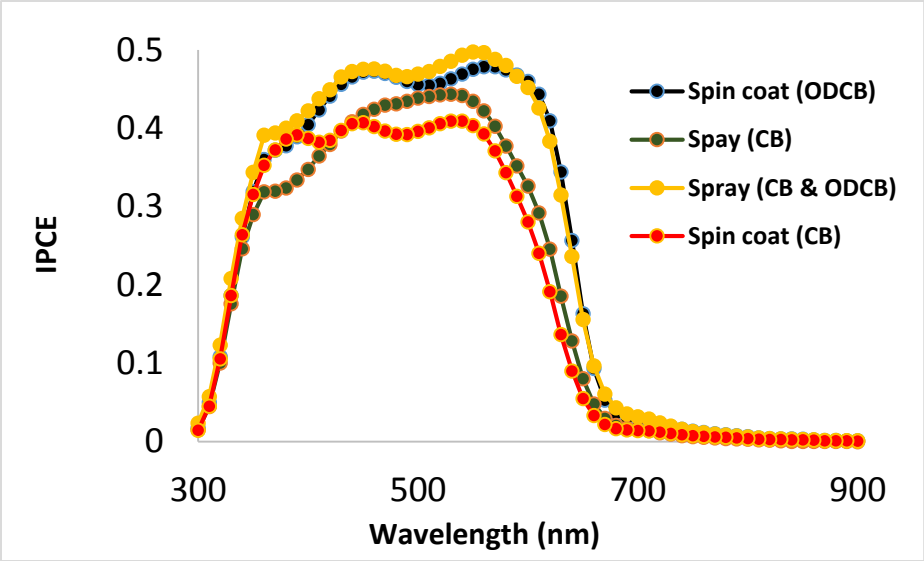

Figure 3.6 Photocurrent action spectra of P3HT/PCBM PSC devices

However NVD spray (CB/ODCB) device has high Jsc, suggesting better phase separation and improved percolation pathways in comparison to all the devices. The results is also supported by AFM and UV studies as discussed earlier.

The photo current action spectra (IPCE) of all the devices are shown in Figure 3.6. IPCE shows relatively higher and broader peaks at 520nm for both ODCB/CB NVD spray device, suggesting relatively higher charge generation than all the other devices.

3.3.4 Calculation of mobility by space charge limited current method

With the SCLC method, mobility of organic semiconductors could be calculated with a simple IV curve. SCLC region dominates the IV characteristics when the charge carrier concentration is larger than the doping level or the free carriers in a semiconductor. This current is dominated by the applied electric field, thus major contribution in SCLC is of drift current. However, the high charge carrier concentration re-affects the electric field distribution, thus making a feedback loop between the field and the current. This feedback mechanism is described by the relation called the Mott-Gurney law.

$$J = \frac{9}{8}\varepsilon_s \mu \frac{V^2}{L^3}$$ **(Equation 3.1)**

Where, V is the applied voltage, J the SCLC, L is the thickness of the thin film, μ is the mobility and ε_s is the permittivity of the semiconductor. It has been shown that SCLC can be used for mobility measurement of organic diodes [28-30]. With increase of applied electric field, the J–V characteristics switch to the SCLC region. As it was shown by Stefan et al that there is no considerable difference in calculated mobility of organic BHJ under illumination and dark [31], so, we have used J-V characteristics under dark conditions for device mobility estimations (Figure 3.7).

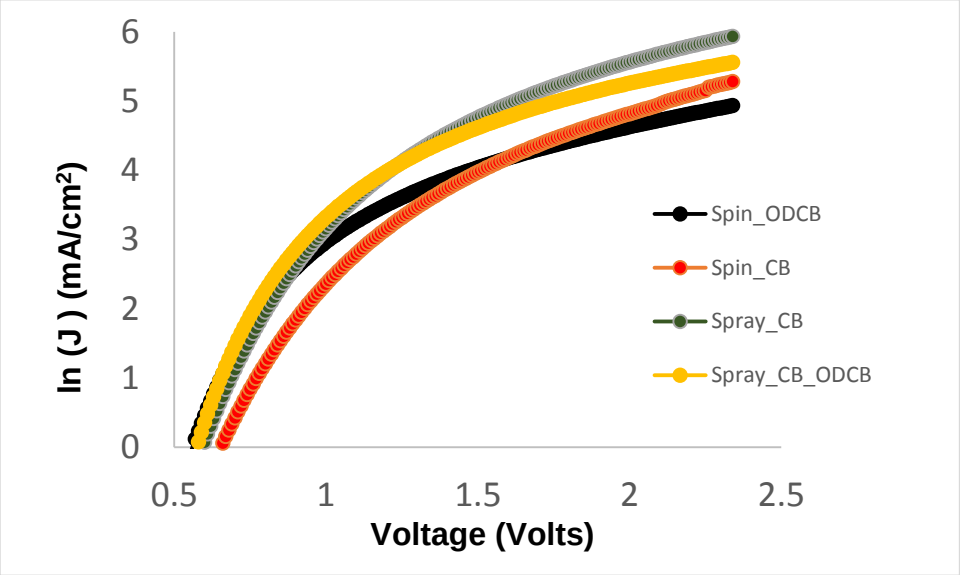

Figure 3.7 J–V characteristics under dark condition of P3HT/PCBM PSC devices

As the charge carrier mobility μ in organic thin films, is affected by the energetic disorder due to the interaction of each hopping charge with randomly located and randomly oriented dipole [30]. Therefore, the mobility is dependent on the electric field and can be expressed by a Poole–Frenkel equation

$$\mu(E) = \mu_0 \exp(\beta/\sqrt{E})$$ **Equation 3.2**

Where μ_0 is the zero-field mobility and β is the Poole–Frenkel factor. From the combination of Equations 3.1 and 3.2, the field dependent SCLC can be easily expressed by equation 3.3.

$$J = \frac{9}{8}\varepsilon_s \mu_0 \exp(\beta/\sqrt{E})\frac{V^2}{L^3}$$ **Equation 3.3**

Figure 3.8 shows the logarithm of J/E^2 versus the square root of the mean electric field. The fitted lines are in good agreement with the experimental data and the current in this region follows a field-dependent SCLC behavior. The slope and the intercept gives β and zero-field mobility (μ_0), respectively. The relative dielectric constant is assumed to be 2.7 and the permittivity of the free space ε_0 is 8.85×10^{-14} C/V cm.

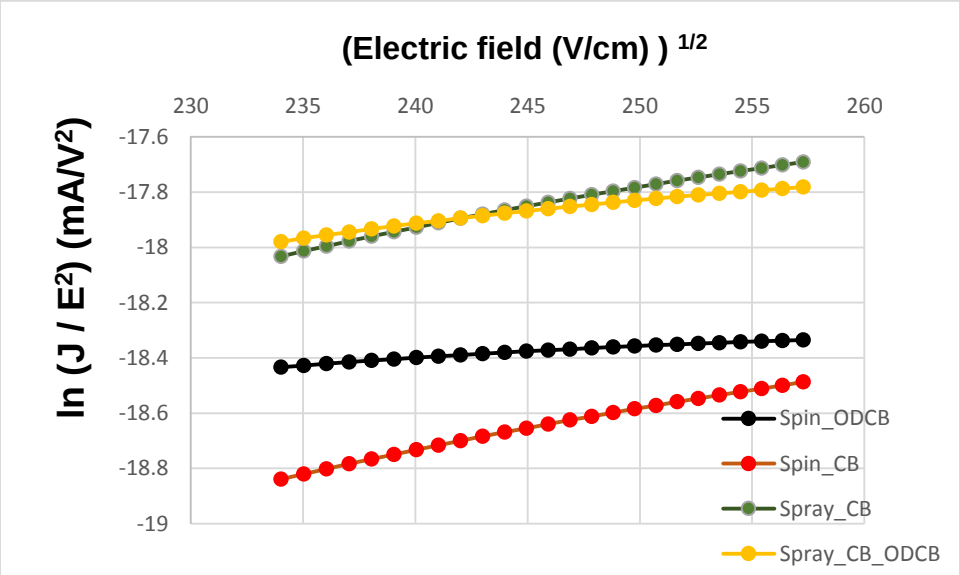

Figure 3.8 Space charge limited current for P3HT/PCBM PSC devices

	Mobility (V/cm-sec)
Spray (CB/ODCB)	2.34526×10^{-4}
Spin (ODCB)	1.22551×10^{-4}
Spray (CB/ODCB)	2.57546×10^{-5}
Spin (CB)	1.07375×10^{-5}

Table 3.5 Mobility's of P3HT/PCBM PSC devices calculated using SCLC method.

The calculated hole mobility's for different devices are given in table 3.5. The table shows high mobility in case of ODCB NVD spray coated and ODCB spin coated devices, and that is almost one order of magnitude greater than NVD spray and spin coat fabricated devices using CB. The high mobility could be attributed to good percolation pathways and phase separation attained in case of ODCB blend devices. These hole mobility enhancement is supported by high π-π stacking and chain ordering as supported by UV data. The calculated mobility's are in accordance with the high extent of phase separation attained, as was visible in AFM images.

3.4 Conclusion

In conclusion, present experiments successfully demonstrates that NVD spray deposition technique is a promising deposition process for the fabrication of active layers in solution processed organic solar cells. Strong solvent effect was observed with 40 % increase in efficiency when using chlorobenzene/dichlorobenzene/ solvent of 7/3 ratio is used in comparison to pure chlorobenzene solution, which is due to better phase separation of donor /acceptor interfaces. The study also shows that performance of NVD spray coated system is at par with the spin coating technique, which is widely used laboratory technique. NVD fabricated devices could attain higher performance by reducing the series resistance thus increasing the Fill factor. Another asset of the present method is the use of low concentration solutions, allowing a wide range of polymers with low solubility to be candidates for future device applications.

References

[1] F.C. Krebs, Solar Energy Materials and Solar Cells 93, 394–412 (2009).

[2] H.-L. Yip, S.K. Hau, N.S. Baek, A.K.-Y. Jen, Applied Physics Letters 92, 193313-1–193313-3 (2008).

[3] M. Manceau, D. Angmo, M. Jorgensen, F.C. Krebs, Organic Electronics, 12, 566–574 (2008).

[4] F. Huang, K.-S. Chen, H.-L. Yip, S.K. Hau, O. Acton, Y. Zhang, J. Luo, A.K.-Y. Jen, Journal of the American Chemical Society 131, 13886–13887 (2009).

[5] G. Dennler, M.C. Scharber, C.J. Brabec, Advanced Materials 21, 1323–1338 (2009).

[6, 7] W. Ma, C. Yang, X. Gong, K. Lee, A.J. Heeger, Adv. Funct. Mater. 15 1617 (2005).

[8] F.C. Krebs, M. Jorgensen, Kion Norrman, Ole Hagemann, Jan Alstrup, Torben D. Nielsen, Jan Fyenbo, Kaj Larsen, Jette Kristensen, , Solar Energy Materials and Solar Cells 93, 422–441 (2009).

[9] P. Schilinsky, C. Waldauf, C.J. Brabec, , Advanced Functional Materials 16,1669–1672 (2006).

[10] T. Aernouts, T. Aleksandrov, C. Girotto, J. Genoe, J. Poortmans, Applied Physics Letters 92, 033306 (2008).

[11] C.N. Hoth, S.A. Ch oulis, P. Schilinsky, C.J. Brabec, Advanced Materials 19, 3973–3978 (2007).

[12] L.-M. Chen, Z. Hong, W.L. Kwan, C.-H. Lu, Y.-F. Lai, B. Lei, C.-P. Liu, Y. Yang, ACS NANO 4, 4744–4752 (2011).

[13] D Vak, S.-S. Kim, J. Jo, S.-H. Oh, S.-I. Na, J. Kim, D.-Y. Kim, Applied Physics Letters 91, 081102 (2007).

[14] C. Girotto, D. Moia, B.P. Rand, P. Heremans, Advanced Functional Materials 21, 64–72 (2011).

[15] K.X. Steirer, M.O. Reese, B.L. Rupert, N. Kopidakis, D.C Olson, R.T. Collins, D.S. Ginley, Solar Energy Materials and Solar Cells 93, 447–453 (2009).

[16] C.N. Hoth, R. Steim, P. Schilinsky, S.A. Choulis, S.F. Tedde, O. Hayden, C.J. Brabec, Organic Electronics 10,587–593 (2009).

[17] M. Shakutsui1, T. Iwamoto1, K. Fujita, Jpn. J. Appl. Phys. 49 060207 (2010).

[18] R. Green, A. Morfa, A. J. Ferguson, N. Kopidakis, G. Rumbles, and S. E. Shaheen, Appl. Phys. Lett. 92, 033301, (2008).

[19] Yang Yang, Nano Lett.; 7, 4744, (2010).

[20] http://www.mechasol.co.jp/english/meka_detail01.html.

[21] J. Y. Kim, S. H. Kim, H.-Ho. Lee, K. Lee, W. Ma, X. Gong, A. J. Heeger, Adv.Mater., 18, 572 (2006).

[22] M. D. Irwin, D. B. Buchholz, A. W. Hains, R. P. H. Chang, T. J. Marks, PNAS, 105, 2783 (2008).

[23] G. Li, V. Shrotriya, J. Huang, T. Mariarty, K. Emery, Y. Yang, Nat. Mater., 4, 864 (2005).

[24] W.Ma, C. Yang, X. Gong, K. Lee, A. J.Heeger, Adv. Funct. Mater. 15, 1617 (2005).

[25] S. S. Pandey, W. Takashima, S. Nagamatsu, T. Endo, M. Rikukawa, K. Kaneto, Jpn. J. Appl. Phys. 39, 94 (2000).

[26] M. Ahlskog, J. Paloheimo, H. Stubb, P. Dyrklev, M. Fahlman, O. Inganäs, M. R. Anderson, J. Appl. Phys. 76, 893 (1994).

[27] S. Berson, R. De Bettignies, S. Bailly, S. Guillerez, Adv. Funct. Mater. 17, 1377 (2007).

[28] A. Campbell, D. Bradley, and H. Antoniadis, Synth. Met., 122, 161. (1955).

[29] P.W.M. Blom, M.J.M. de Jong, J.J.M. Vleggaar, Appl. Phys. Lett. 68, 3308 (1996).

[30] L. Bozano, S.A. Carter, J.C. Scott, G.G. Malliaras, P.J. Brock, Appl. Phys. Lett. 74, 1132 (1999).

[31] G.G. Malliaras, J.R. Salem, P.J. Brock, C. Scott, Phys. Rev. B 58, R13411 (1998).

Chapter 4:

Controlling the processable ZnO and Polythiophene interface for polymeric inorganic hybrid bulk hetero-junction solar cells

This chapter describes the use of solution processable ZnO precursor for the single step fabrication of P3HT/ZnO polymeric hybrid bulk hetero-junction (PHSC) solar cells. The aim of using solution processsable precursor is to do in situ generation of ZnO nanoparticle inside the polymer matrix, and thus fabricating PHSC in single step. For further improving performance of solution processed P3HT/ZnO PHSC efforts are also done for improvement of P3HT interface by modifying it with ester functionality.

4.1 Introduction

PHSC are recently emerging as an alternative to fully, organic solar cells [1]. These devices combine the solution processability of organic compounds with potential advantages of the inorganic semiconductors such as high dielectric constant which facilitates carrier generation processes, a high carrier mobility and thermal morphological stability of the blended materials. Additionally they may offer control over BHJ morphology, by carefully using tunable nanostructures of inorganic semiconductors. Many PHSC have been reported using CdSe [2], CdTe [3], PbS [4], TiO_2 [5-8] and ZnO [9-14]. Metal oxide semiconductors like TiO_2 and ZnO are of particular interest due to non-toxicity and abundance in nature. Currently, the most heavily investigated of these materials is TiO_2, as it has been extensively used in dye sensitized solar cells due to the high surface area of the semiconductor [15–17]. Recently much research interest has been focused on ZnO, because it has a very similar electronic structure to that of TiO_2, however, it has some advantages in comparison. First, it tends to have higher electron mobility than TiO_2. Additionally, it can be synthesized using a variety of relatively low temperature, low cost fabrication techniques. This makes it attractive for low cost scalable solar cell fabrication.

For high efficient PHSC it is desired to control the complete morphology of bulk hetero-junctions using carefully nanostructured metal oxide. But until now highest efficiencies have been reached with random mixtures of conjugated polymers and metal oxide nanoparticles. However, it's difficult to find the common solvent for conjugated polymer and nanoparticles, thus the processing window for such combinations of material is often quiet narrow. These drawbacks could be overcome via in situ generation of ZnO nanoparticles in the organic matrix. It could be achieved via organometallic precursor like diethyl zinc (DEZ). Here, DEZ is coated together with semiconducting polymer from solution in controlled humid conditions [18]. During and after deposition, DEZ is converted to $Zn(OH)_2$ by reacting with ambient moisture, and after annealing, interpenetrating ZnO nanoparticles are formed in polymer matrix, leaving no residual byproduct.

Oosterhout et al. has achieved photovoltaic efficiency of 2% by using DEZ as the ZnO precursor and regioregular poly(3-hexylthiophene) (P3HT) as the semiconducting polymer [19]. They further demonstrated that adding ester functionality in P3HT backbone (7:3 ratio), improves photovoltaic performance for very thin film of the active layers (~50nm) [20]. Addition of ester functionality in P3HT causes reduced polarity difference between ester functionalized copolymer and hydrophilic ZnO. This leads to the much finer phase separation, leading to increased surface area, thus facilitating better charge separation in very thin film of active layer (~ 50 nm). However the effect of ester incorporation vanished for relatively thicker films (~130nm) as the more intimate mixing in ZnO: P3HT-E reduced the ZnO connectivity and thus loss percolation pathways, therefore, only in thin devices, the current and power conversion efficiency were enhanced.

This chapter presents the experiments and results due to the effect of incorporation of ester functionality in the regioregular P3HT backbone in the 9:1 feed ratio (P3HT-E1), on photovoltaic performance of ZnO PHSC using the DEZ precursor. It also describes the comparative performance analysis has been done with ZnO PHSC of pure P3HT and ester modified P3HT backbone of 7:3 feed ratio (P3HT-E3). In experiments first efforts are being made to find optimum weight/weight (w/w) ratio of P3HT w.r.t. ZnO for the fabrication of thin film P3HT/ZnO PHSC. Thereafter all experiments were followed carrying that optimum weight/weight (w/w) ratio of P3HT w.r.t. ZnO.

4.2 Experimental section

The structures of polymers employed in the present investigation are shown in the Fig.4.1. Regioregular P3HT (Rieke Metals, Mn = 45-50 kg/mol) was purchased from the Sigma-Aldrich USA and used as received without further purification. Diethyl Zinc (0.4 M solution in toluene-tetrahydrofuran) was supplied by Tosho Fine Chemicals, Japan.

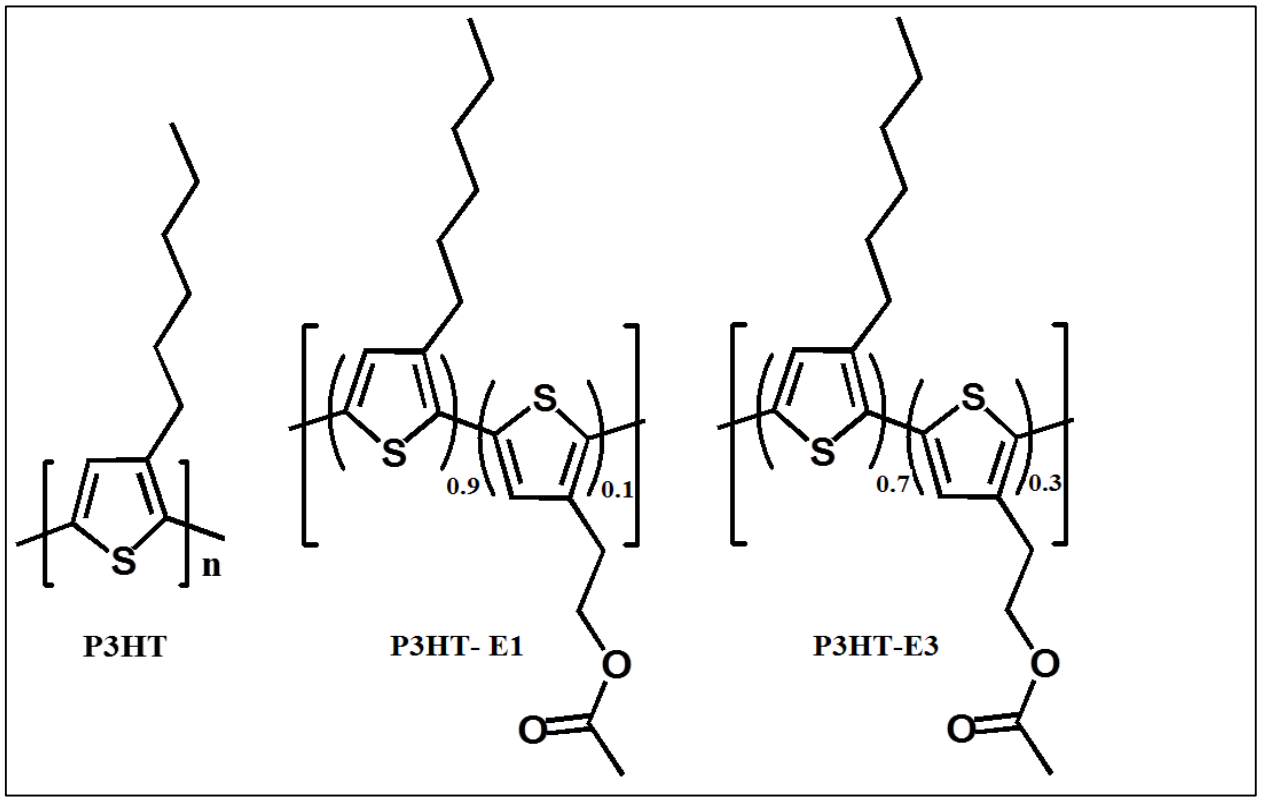

Figure 4.1 Schematic structure of P3HT, P3HT-E1 and P3HT-E3

4.2.1 Addition of ester functionality in P3HT backbone

This section describes the modification of P3HT regioregular backbone with ester functionality in the feed ratio of 9:1 (P3HT-E1). Ester functionalized regioregular polythiophene derivative (P3HT-E1) was synthesized by Grignard Metathesis (GRIM) method utilizing

respective 2,5-dibromo derivatives in 9:1 feed ratio as shown in Scheme-1(Figure 4.2). The alike process and experimental conditions were also used for getting P3HT-E3.

Starting materials 3-thiopheneethanol, 3-hexylthiophene, 4-dimethylaminopyridine (DMAP) and Bis(diphenylphosphino)propane Nickel chloride [Ni(dppp)Cl_2] were purchased from Sigma-Aldrich, USA and used as received. Ester functionalized polythiophene copolymer, P3HT-E1, was synthesized as per scheme-1 shown in Fig. 4.2. Synthesized materials were confirmed by fast ion bombardment (FAB) mass in the positive ion monitoring mode. Nuclear magnetic resonance (NMR) spectra were recorded on a JEOL (JNM A 500 MHz) spectrometer in $CDCl_3$ or d_6-DMSO with reference to tetramethylsilane. Electronic absorption spectra were measured using UV-visible spectrophotometer (JASCO, V550). Highest occupied molecular orbital (HOMO) energy level was measured using photoelectron spectroscopy in air (AC3, Riken). The lowest unoccupied molecular orbital (LUMO) energy level was determined from the edge of the optical absorption using the following relation LUMO = HOMO + E_g, where, E_g stands for energy band gap estimated from the optical absorption edge.

4.2.1.1 Synthesis of 2-(3-thienyl) ethyl acetate [2]

In a round bottom flask fitted with septum, 2.61 gm of 3-thiophene ethanol (20 mmol), 2.84 ml of triethylamine (20 mmol) and catalytic amount of 4-dimethylamino pyridine was added and the solution was stirred at 0^oC under N_2 atmosphere. 3.2 gm of acetic anhydride (30 mmol) was then slowly added by a syringe. The reaction was carried out at room temperature and reaction was continued for 6 hours under stirring. After the completion of the reaction, 20 ml ether and 7 ml of 2M HCl was added and solution was stirred. Organic layer was washed with 10 % sodium carbonate aqueous solution. Organic solvent was evaporated and product was purified by silica gel column using hexane-ethyl acetate solvent system to obtain compound **2** as white solid in the yield of 93 %. Purity of the compound was confirmed by HPLC and LC-MS (observed 174.70 and calculated 173.23). ^{1}H-NMR, (δ ppm in $CDCl_3$): 7.26 (m, 1H, thiophene ring, H (5 position)), 7.03 (m, 1H, thiophene ring, H (2 position)), 6.97 (dd, J=1,1 Hz, 1H, thiophene ring, H (4 position)), 4.27 (t, 2H, -CH_2-CH^*_2-O-), 2.97 (t, 2H, -CH^*_2-CH_2-O-), 2.05 (s, 3H, Me).

4.2.1.2 Synthesis of 2, 5-dibromo-3-ethylacetyl thiophene [3]

In a round bottom flask fitted with septum, 3.42 gm of compound 2 (20 mmol) was dissolved in the 70 ml dichloromethane. Solution was cooled at 0^{o}C and stirred under N_2 atmosphere. 10.8 gm of N-bromosuccinimide (NBS, 60 mmol) was slowly added after stirring at this temperature for 30 min, it was brought at room temperature reaction was continued for 24 hours. After the completion of the reaction, water was added and organic layer was washed with 10 % sodium carbonate aqueous solution. Finally crude product after solvent evaporation was purified by silica gel column using hexane-ethyl acetate to obtain the pure compound **3** in the 48 % yield and 98 % purity (confirmed by HPLC). The structure of the compound was confirmed by LC-MS (Observed: 329.3 (M+H), calculated 328.02 (M^+)). ^{1}H-NMR (δ value in $CDCl_3$); 6.83 (s, 1H, thiophene ring), 4.22 (t, 2H, CH_2-CH*$_2$-O-), 2.86 (t, 2H, CH*$_2$-CH_2-O-), 2.05 (s, 3H, Me).

4.2.1.3 Synthesis of 2, 5-dibromo-3-hexythiophene [5]

Compound 5 was synthesized using similar methods discussed in the section 2.2.2 and 3-hexylthiophene and the product was obtained in 33 % yield with 98 % purity as confirmed by HPLC. LC-MS data (observed 327.4 (M+H), calculated (326.09 for M^+)).

4.2.1.4 Synthesis of P3HT-E1 [6]

A dry 500-mL three neck flask was flushed with Argon and charged with compound 3 (18 mmol) and compound 5 (2 mmol). Anhydrous tetrahydrofuran (40 mL) and tert-butyl magnesium chloride (10 mL, 20 mmol) were added via syringe. Reaction mixture was allowed to stir for 30 minutes at ambient temperature followed by addition of Ni(dppp)Cl_2 (108 mg, 0.2 mmol) previously dissolved in anhydrous dichloromethane (10 mL) via syringe. Polymerization was allowed to proceed for 12 hours under reflux. It was then allowed to cool at room temperature and precipitated in a mixture of methanol and HCl. Polymer was filtered and purified by Soxhlet extraction in a sequence with methanol, hexane and finally chloroform. Chloroform was finally evaporated under reduced pressure and residue was dried to give the final target polymer P3HT-

E1 in 46 % yield. Structure and regioregularity of the P3HT-E1 was confirmed by ^{1}H-NMR (δ value in $CDCl_3$). 7.02 (s, 1H, hexyl thiophene ring), 4.37 (t, 2H, CH_2-CH^*_2-O-), 3.16 (t, 2H, CH^*_2-CH_2-O-), 2.81 (t, 2H, α-CH_2, hexylthiophene), 2.56 (t, 2H, α-CH_2, hexylthiophene), 2.08 (s, 3H, thiophene-ester), 1.56 (m, 2H, CH_2), 1.40 (bm, 6H, CH_2), 0.93 (t, 3H, CH_3, hexylthiophene). The set of NMR signals appearing around δ = 2.80 and 2.57 are in regioregular P3HT are associated to the protons of the α-methylene group of the alkyl substituent and correspond to two different diads arising from the head-to-tail (HT) and head-to-head (HH) coupling determines the regioregularity of polymer [**21]**. The integration of peak area for P3HT-E indicates that regioregularity of the synthesized P3HT-E1 is >95 %.

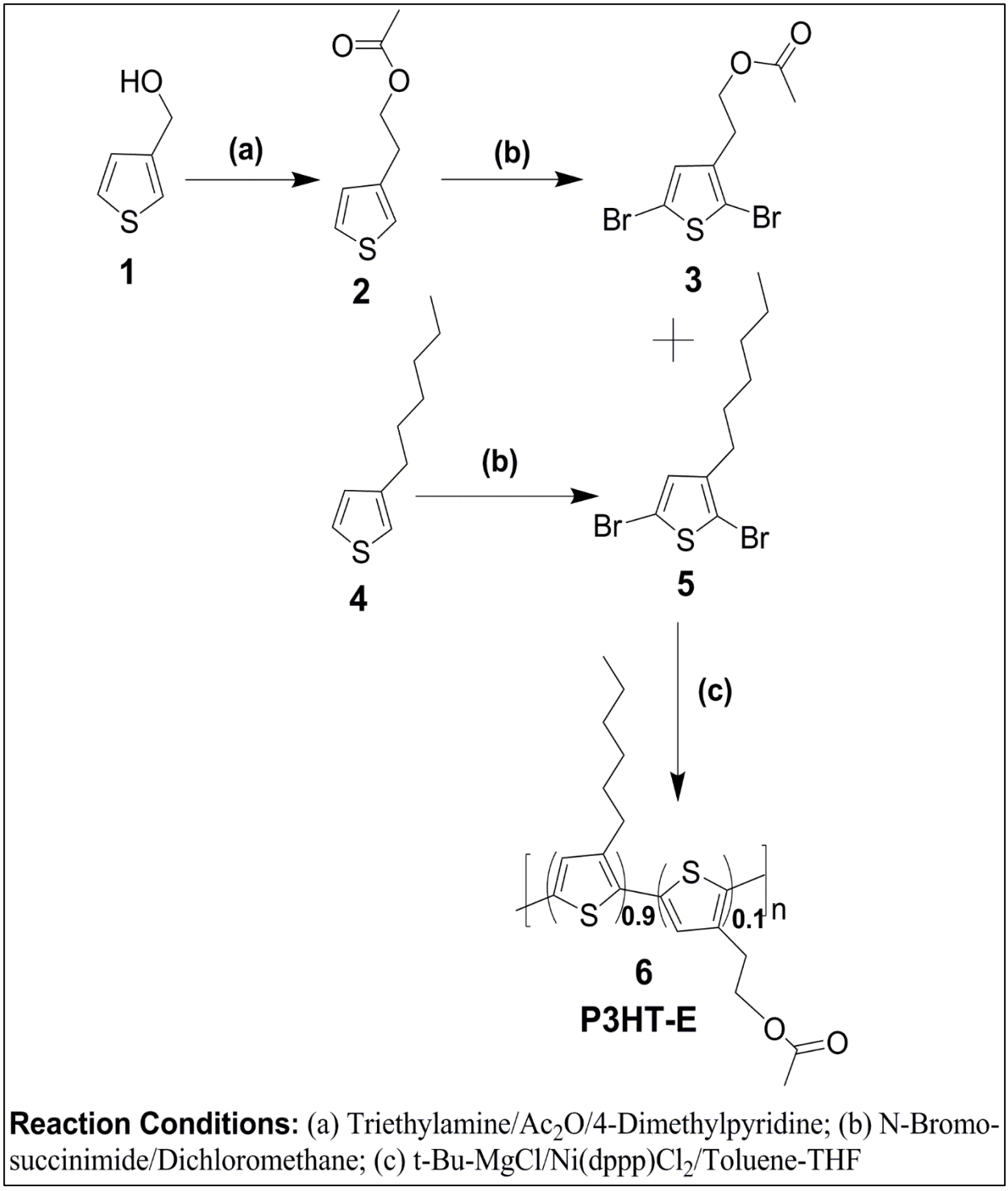

Figure 4.2 Scheme 1- Synthesis steps of P3HT-E1

4.2.2 Solar cell fabrication and characterization

For realizing the suitable donor acceptor ratio, first device performance were optimized for P3HT/ZnO PHSC solar cells. Devices were fabricated by varying weight ratios (1:1, 1:2, 1:3, 1:5) of the P3HT and ZnO. Typically, use of 150 µl of DEZ (0.4 M solution) mixed with 350 µl of P3HT (10 mg/ml) in chlorobenzene is expected to make the 1:1 (w/w) ratio of P3HT and ZnO assuming the 100 % conversion of DEZ to ZnO.

For the fabrication of DEZ/P3HT-E1 and P3HT-E3, solutions were prepared by mixing 300 µl of DEZ (0.4 M solution in toluene-tetrahydrofuran) with 350 µl of polymer in chlorobenzene (14.3 mg/ml). This gives 1:2 (w/w) ratio of ZnO to polymer in the thin film provided that DEZ is fully converted into ZnO.

All the solutions were prepared inside the glove box with inert nitrogen atmosphere (<1 ppm H_2O and <1ppm O_2) for avoiding any pre-hydrolysis of DEZ solution. As DEZ solution is very reactive, so it reacts violently in ambient atmospheric conditions. During mixing, if there present any traces of moisture in atmosphere, it causes pre hydrolysis and formation of $Zn(OH)_2$ nanoparticles in the solution. Pre formation of $Zn(OH)_2$ defies the purpose of in situ generation of ZnO nanoparticles inside the polymeric matrix, and thus should be taken care of.

For device preparation, ITO patterned glass plates were cleaned through sonication in distilled water detergent wash, acetone, and isopropanol respectively. After ultraviolet ozone treatment, substrate was transferred to a nitrogen-filled glove box with a controlled humidity (relative humidity~ 40%). In all the devices, PEDOT:PSS(BAYTRON P, HC Starck, GMBH, Germany) having thickness of about 70 nm was spin coated followed by heating at 150^0C for 10 min on a hot plate . Then, photoactive layer (~110 ± 10 nm for all devices) was spin coated from the solution described above. After aging (15 min) and annealing (100^0C for 15 min.) to form the ZnO, the substrates were transferred to a glove box with an inert nitrogen atmosphere (<1 ppm H_2O and <1ppm O_2) using an air-tight container. Devices were then finally completed by thermal evaporation of Al (100 nm).

Thickness of the PEDOT: PSS and active layer as discussed above were measured using DEKTAK Stylus Profiler (6M, ULVAC Inc.). Electronic absorption spectroscopic investigations for thin films of P3HT, P3HT-E1, P3HT- E3, P3HT/ZnO, P3HT-E1/ZnO and P3HT-E3/ZnO blend films on glass substrate were conducted using JASCO V 530 spectrometer. Photovoltaic measurements of the devices were performed under irradiation of 100 mW/cm^2 simulated solar light at global AM 1.5 condition using a solar simulator (Bunko Keiki, KHP-1). Irradiated active area of (0.06 cm^2) was precisely controlled using a black metal mask. Photocurrent action spectrum also known as Incident photon-to-current efficiencies (IPCE) as a function of wavelength was measured with a constant photon flux of $1x10^{16}$ photon/cm^2 at each wavelength in DC mode using an action spectrum measurement system connected to a solar simulator (model CEP- 2000, Bunko-Keiki, Japan).

4.3 Results and Discussion

Normalized electronic absorption spectra of thin films of polymers and polymeric ZnO blends used in the present investigation are shown in the Figure 4.3. The absorption spectra of pure P3HT and P3HT-E3 indicates absorption maximum at 520 nm associated with π-π* electronic transition along with appearance of vibronic shoulders at 550 nm and 610 nm. These clear vibronic shoulders are associated with polymer crystallization [21, 22]. UV/visible absorption spectra of pure films of P3HT and P3HT-E3 are virtually identical, indicating a similar degree of crystallization and a comparable optical band gap. However, in the case of P3HT-E1, the 525 nm and 550 nm peak was the main peak, indicating more rod like conformation with extended π-conjugation in the condensed state. The electronic absorption behavior is interestingly different for both of the polymer in the presence of the ZnO acceptor. The presence of ZnO makes nearly no change in the case of P3HT while 520 nm peak became the main peak for P3HT-E1 and 495 nm peak becomes main peak for P3HT-E3 (Figure 4.4). This indicates that the interaction between the P3HT-E and ZnO hindered polymer crystallization. This difference can be explained by an increased interaction between this polymer and ZnO and by smaller polymer domains, impeding effective aggregation. Figure 4.5 shows the photoelectron emission spectra of P3HT-E3 (for example) used for calculation of HUMO energy level for different polymers. The LUMO energy

level was determined from the edge of the optical absorption using the following relation LUMO = HOMO + E_g, where, E_g stands for energy band gap estimated from the optical absorption edge.

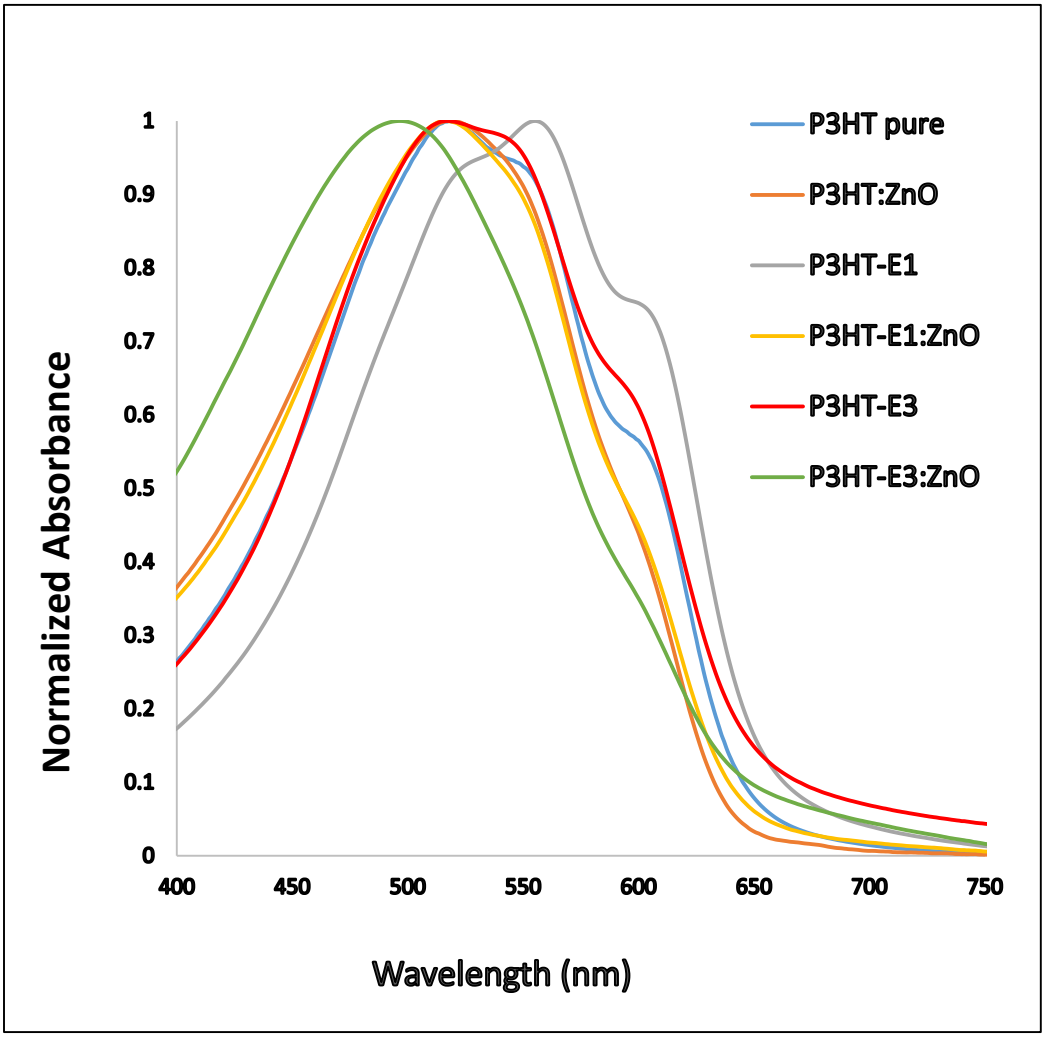

Figure 4.3 Normalized absorption spectra of thin films of polymers and polymeric/ZnO blends

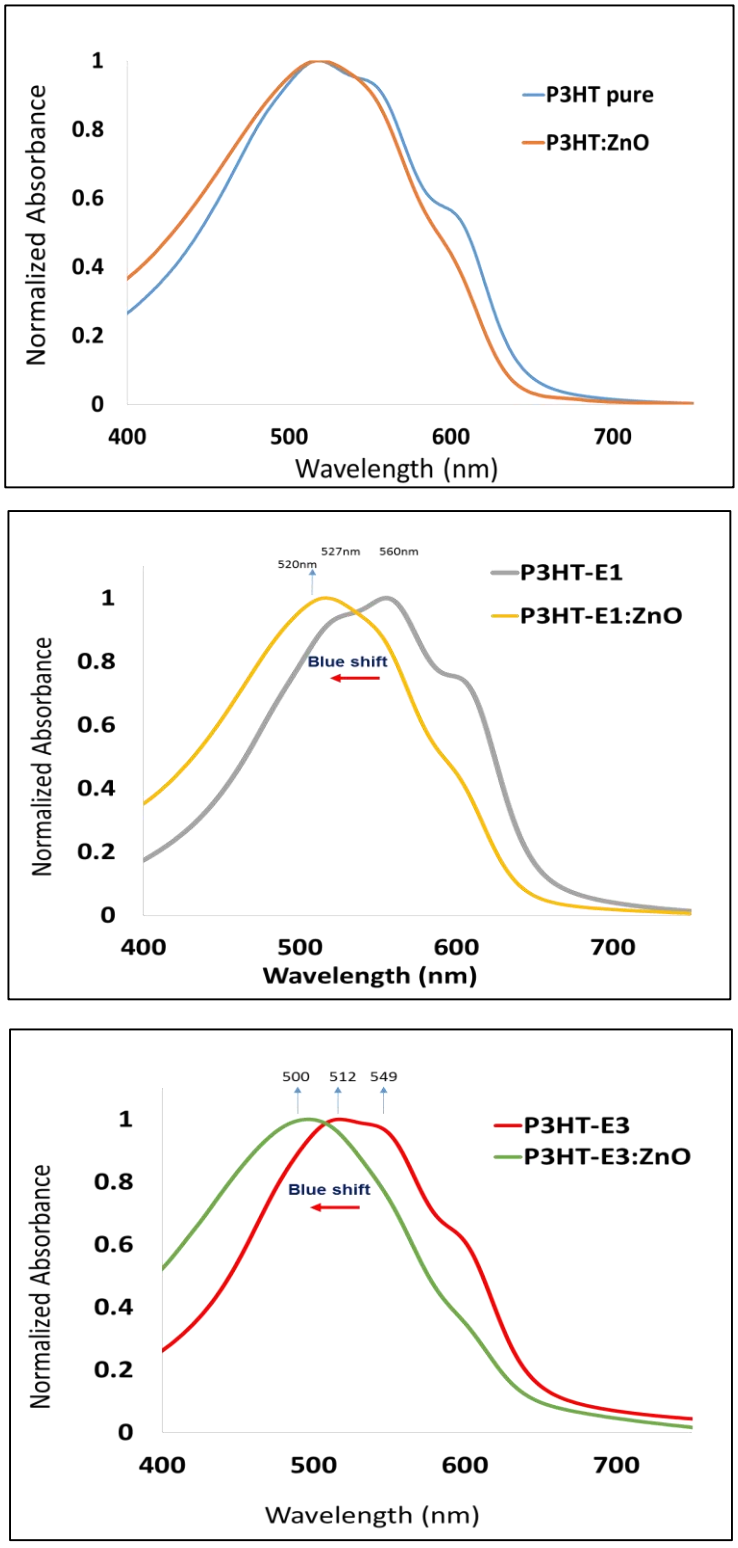

Figure 4.4 Blue shift in absorption spectra in presence of ZnO for P3HT-E1 and P3HT-E3

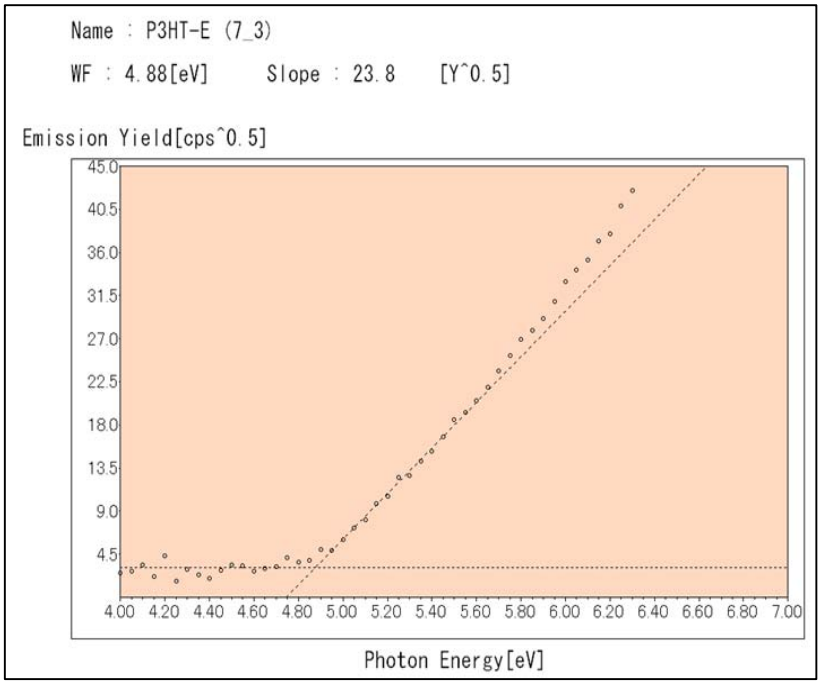

Figure 4.5 Photoelectron emission spectra for P3HT-E3 used for calculating HUMO energetic level

Figure 4.6 (a) shows the FTIR spectra of regioregular P3HT-E1, P3HT-E3 and P3HT exhibiting principal vibration bands at 725, 820, 1020, 1100, 1260, 1377, 1450, 1510, 2855, 2925 and 3057cm^{-1}. These bands are consistent with typical IR vibration bands of poly (3-alkyl) thiophene [23]. In addition to these bands P3HT-E1 and P3HT-E3 also shows vibration band at 1750 cm^{-1} associated with C=O stretching vibration of ester group verifying the presence of ester group. In an interesting report Furukawa et al. [24] emphasized that vibration bands appearing at 1450 cm^{-1} and 1510 cm^{-1} are associated with symmetric and asymmetric C=C ring stretching vibrations, respectively and their ratio is indicative of the conjugation length of the polymeric backbone. Peak area integration of these vibration bands exhibit a ratio of 2.35, 2.28 and 2.24 for P3HT, P3HT-E1 and P3HT-E3 respectively indicates nearly similar conjugation length of polymeric backbone (Figure 4.5 (b)).

Based on NMR peak area integration (Figure 4.7) as discussed previously, the regioregularity of P3HT-E1 (> 95 %) and P3HT-E3 are also nearly the same as compared to that of commercial P3HT also supporting this fact. The introduction of the ester group was estimated to be 6.5 % for P3HT-E1 and 22.4 % for P3HT-E3 by the NMR peak area integration associated

with NMR signals at δ=7.02 ppm for (hexyl thiophene ring C-H) and 3.16 ppm (ester methylene 2H).

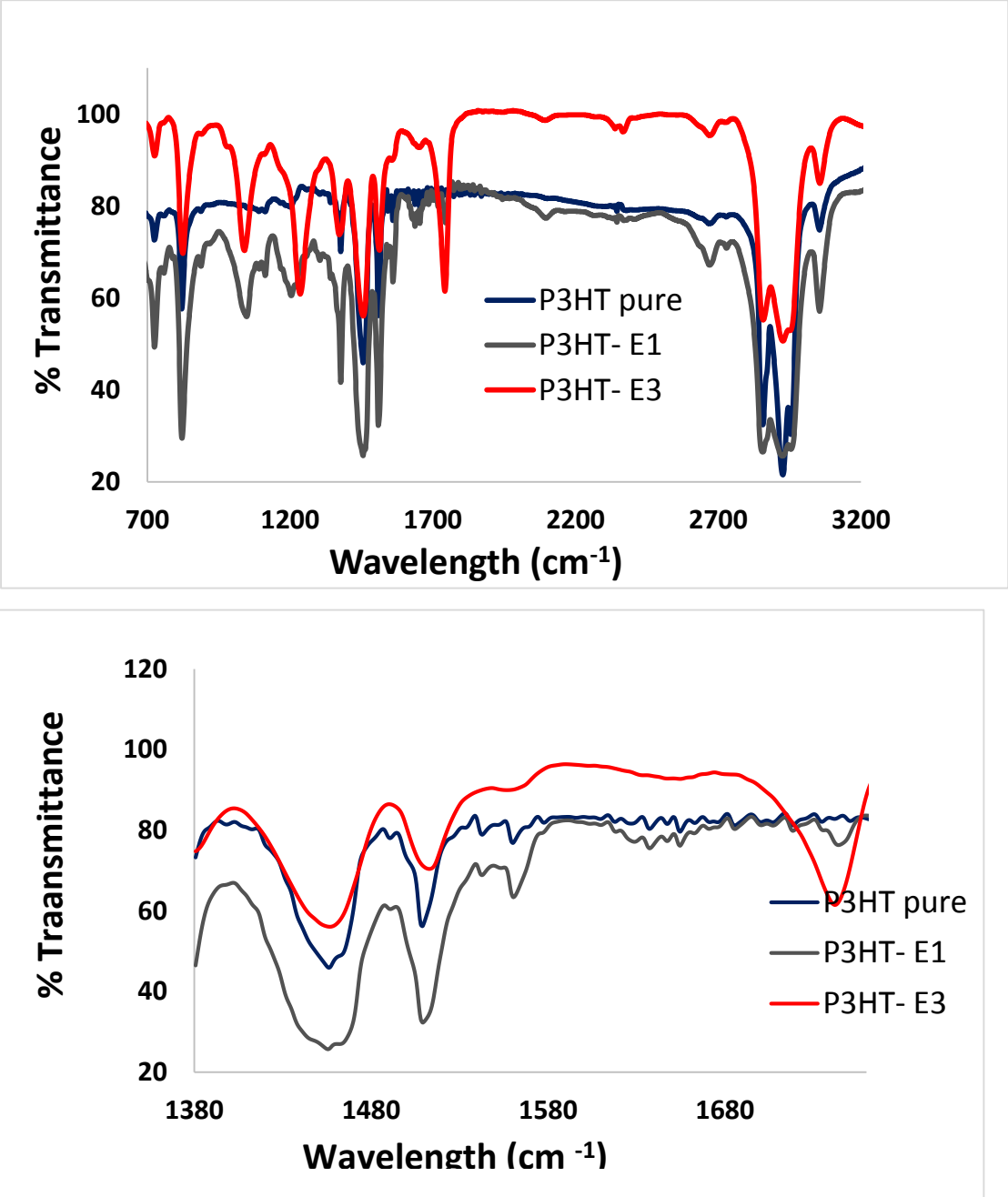

Figure 4.6 (a) FTIR spectra of different polymers (b) Enlarged FTIR spectra from Wavelength (cm^{-1}) of 1380 to 1760 showing presence of ester group for P3HT- E1 and P3HT-E3

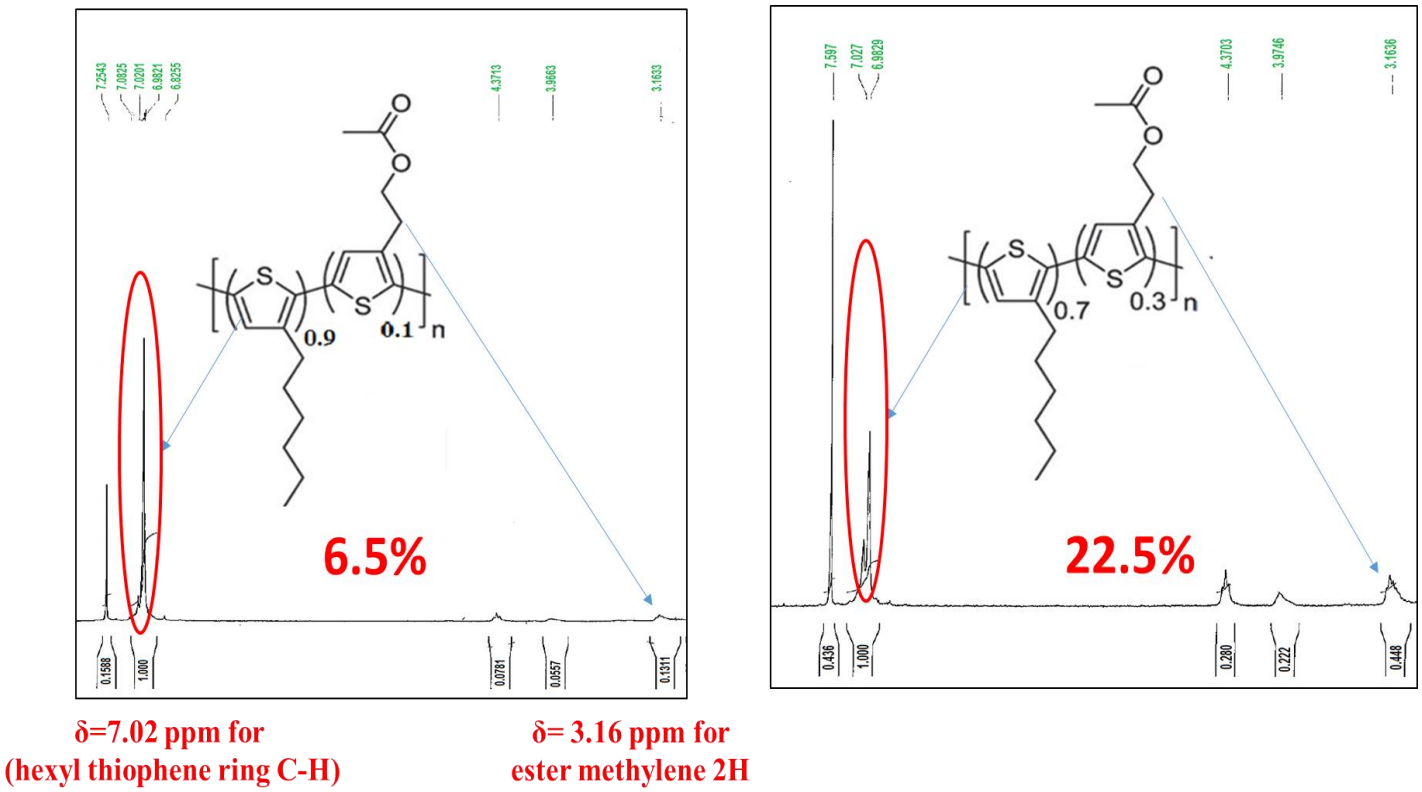

Figure 4.7 NMR spectra of P3HT-E 1 (a) and P3HT-E3 (b) showing NMR signals at δ=7.02 ppm for (hexyl thiophene ring C-H) and 3.16 ppm (ester methylene 2H).

For the optimization of donor acceptor ratio for better performance of PHSC, devices of P3HT/ ZnO were fabricated with varying w/w ratios. Figure. 4.8 shows the IV characteristics of PHSCs with varying donor/acceptor ratios. Best performance was obtained for P3HT/ZnO w/w ratio of 1:2. The photo-action spectra reveals that the best performance was observed in case of utilization of 1:2 w/w ratio of P3HT/ZnO in our experimental conditions. Relatively good performance in case of 1:2 w/w ratio could be attributed to the formation of sufficient ZnO from DEZ with respect to P3HT in the binary blend. In case of higher w/w ratios (1:3, 1:5) although there might be sufficient ZnO formation, but relative percentage of P3HT becomes less compared to that of formed ZnO. This is expected to hamper the photon harvesting by P3HT ultimately leading to reduced performance. The different in amount of formation of ZnO with respect to P3HT is shown using schematic Figure 4.9. This assertion is also being reflected in IPCE (Figure

4.10), where for higher w/w ratios, one can see reduced P3HT peak value (around 520 nm), leading to conclusion that there is insufficient P3HT in the binary system.

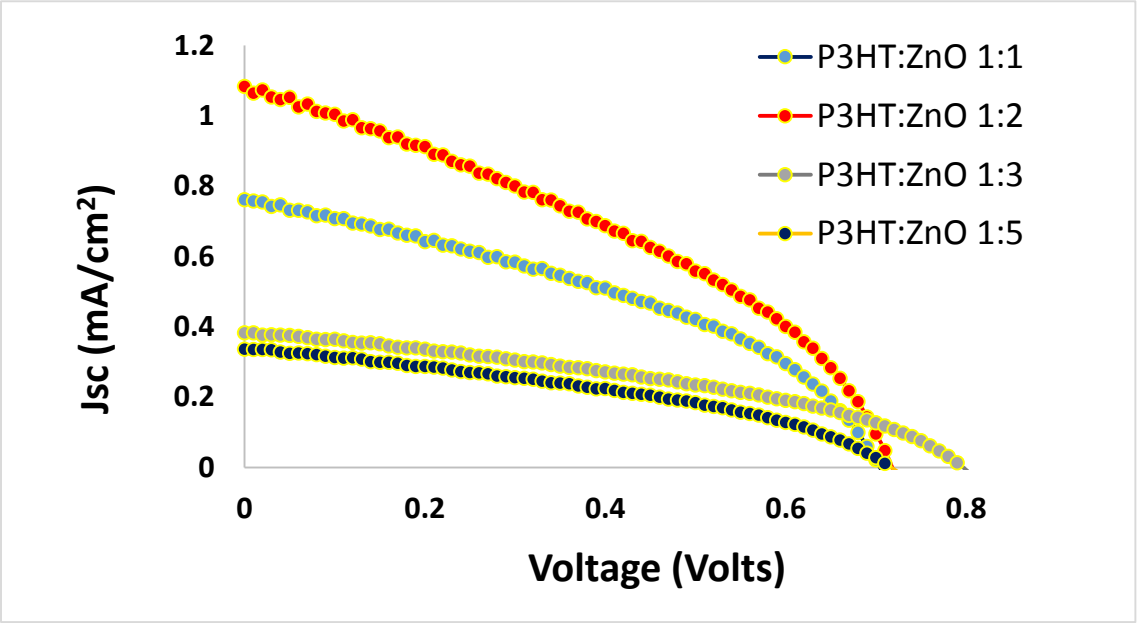

Figure 4.8 IV characteristics of P3HT/ZnO PHSC with varying donor/acceptor w/w ratios

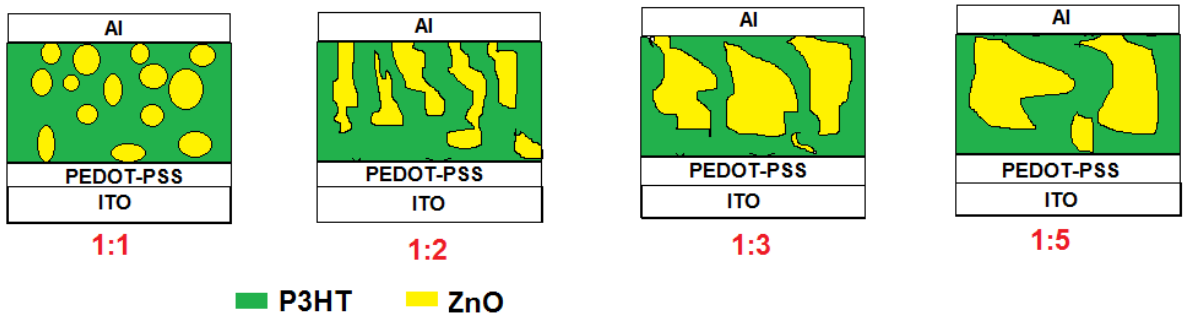

Figure 4.9 Schematics showing amount of formation of ZnO in respect to P3HT for different initial feed ratios

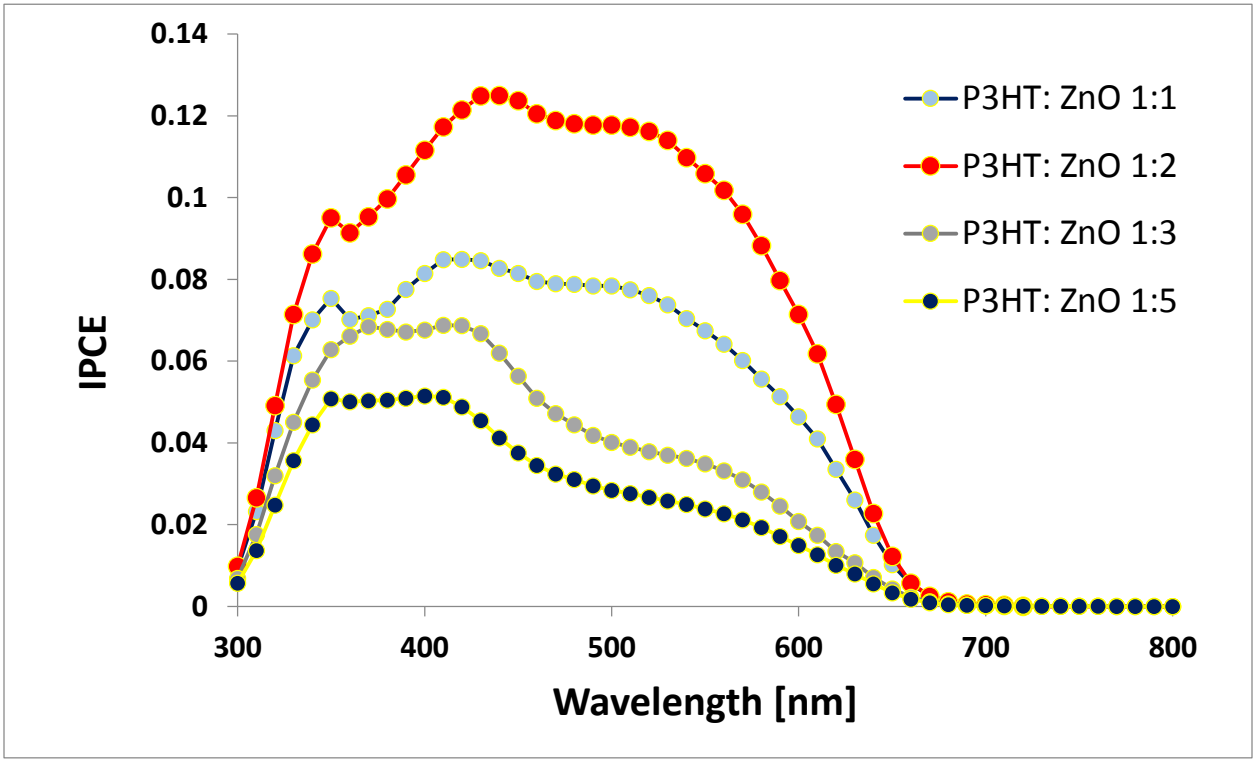

Figure 4.10 IPCE characteristics of P3HT/ZnO PHSC with varying donor/acceptor w/w ratios

Considering w/w ratio of 1:2 best for P3HT/ZnO system, all further experiments with different polymers systems were performed with polymer/ZnO w/w ratio of 1:2. Photovoltaic characteristics of processable polymer-ZnO PHSC are shown in the Figure 4.11. A perusal of this figure and photovoltaic parameters as shown in Table 4.1 exhibit that only slight (about 6 %) incorporation of ester functionality in the polymeric backbones leads to enhancement in the photoconversion efficiency from 0.8 % (P3HT) to about 1 % for P3HT-E1. The observed enhancement in the Jsc is also supported by enhanced IPCE as shown in Figure 4.12. The main factor for increase in the efficiency for P3HT-E1 is the enhanced Jsc and FF. The increase in the Jsc is due to increased charge carrier generation. As incorporation of hydrophilic ester moiety in P3HT lead to better interaction and phase separation with hydrophilic ZnO electron acceptor. The enhanced interaction between the ZnO and P3HT-E1 is also reflected in the electronic absorption spectra shown in Figure 4.3 which leads to slight blue shift in the absorption maximum upon the incorporation of

	Jsc (mA/cm2)	Voc (V)	Fill Factor	Efficiency (%)
P3HT : ZnO	1.88	0.88	0.48	0.80
P3HT-E1 : ZnO	2.34	0.76	0.55	0.98
P3HT-E3 : ZnO	1.51	0.85	0.41	0.53

Table 4.1 Photovoltaic characteristics of Polymer/ZnO PHSC with different ester functionalized polymer

ZnO. Although almost same amount of blue shift is also observed for P3HT-E3, but with increasing amount of added ester functionality (22% in case of P3HT-E3) causing reduction in Jsc. Interestingly, Oosterhout et al. [20] have observed reduced Jsc for similar kind of P3HT-E3 polymer. They observed the enhanced Jsc as well as efficiency as compared to P3HT only for lower thicknesses (about 50 nm) while for thicker films the trend is just reversed. In present investigation thickness of all devices were kept at nearly ~110 ± 10 nm.

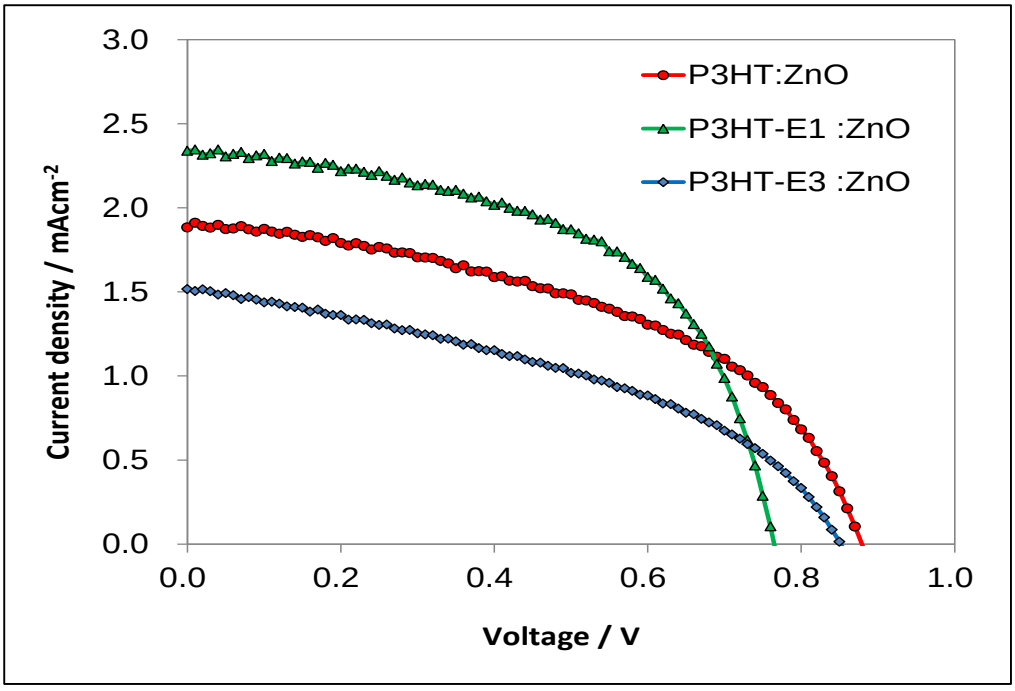

Figure 4.11 Photovoltaic IV characteristics of Polymer/ZnO PHSC with different ester functionalized polymer.

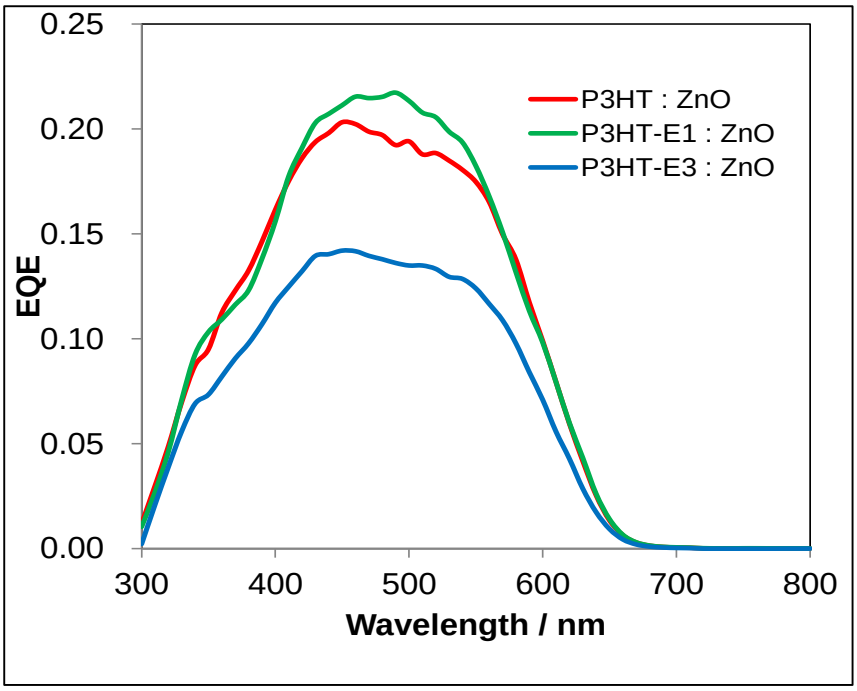

Figure 4.12 IPCE characteristics of Polymer/ZnO PHSC with different ester functionalized polymer.

Since for efficient light absorption, there should be sufficient film thickness so P3HT-E3 does not seems to be suitable for higher thickness devices. Increasing the amount of ester functionality causing enhanced phase separation, but for higher thickness this effect is subverted by the loss of percolation pathways which is required for efficient charge transport. The effect of higher esterification and its effect on polymer/ZnO BHJ is shown using schematic figure 4.13. So, although with increase ester functionality more charge carrier will be generated, but they will recombine before being collected at their respective electrodes.

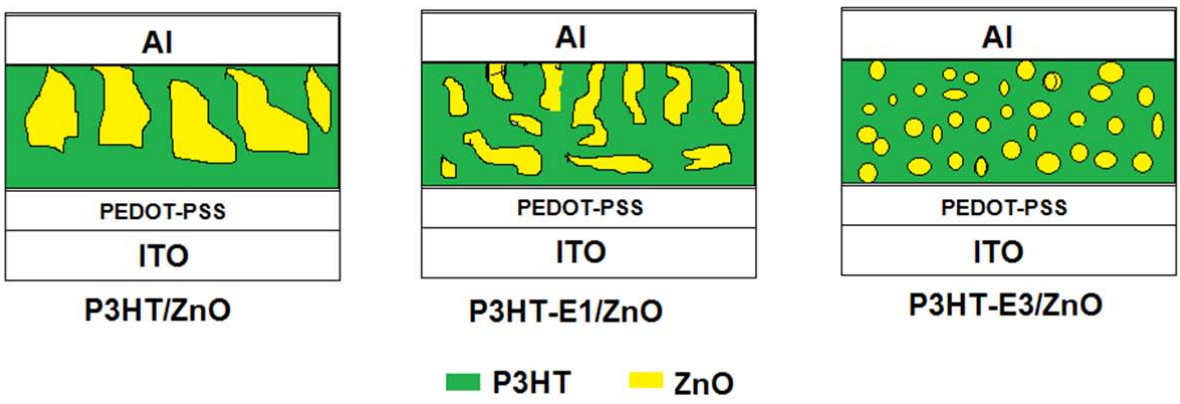

Figure 4.13 Schematic figure showing probable scenario of high esterification on polymer/ZnO BHJ

4.4 Conclusion

PHSC of P3HT/ZnO is successfully fabricated using solution processable DEZ precursor in single step. For further enhancement of performance ester functionalized regioregular polythiophene copolymer (P3HT-E1 and P3HT-E3) were synthesized and characterized. It is observed although addition of ester functionality improves the phase separation, but increasing the amount of ester extent leads to loss of percolation pathways in BHJ thin films. Thus a trade-off is needed for extents of addition of ester moiety for enhanced phase separation. In present investigation P3HT-E1/ZnO PHSC shows enhanced efficiency compared to P3HT/ZnO PHSC. Thus, in further investigation, P3HT-E1 are used for present thesis.

References

[1] J. Boucle, J. Ackermannb, Polym. Int. 61, 355 (2012).

[2] D. C. Olson, S. E. Shaheen, R. T. Collins, D. S. Ginley, J. Phys. Chem. C 111, 16640 (2007).

[3] I. Gur, N.A. Fromer, A.P. Alivisatos, J. Phys.Chem.B110, 25543 (2006).

[4] K.P. Fritz, S. Guenes, J. Luther, S. Kumar, N.S. Sariciftci, G.D. Scholes, J. Photochem Photobiol. A 195, 39 (2008).

[5] R. Zhu, C.Y. Jiang, S. Ramakrishna, Adv. Mater. 21, 994 (2009).

[6] W. J. E. Beek, L. H. Slooff, J. M. Kroon, M. M. Wienk, R. A. J. Janssen, Adv. Funct. Mater. 15, 1703 (2005).

[7] P. A. VanHal, M. M. Wienk, J. M. Kroon, W. J. H. Verhees, L. H. Slooff, W. J. H. VanGennip, P. Jonkheijm, R. A. J. Janssen, Adv. Mater. 15, 118 (2003).

[8] D. J. D. Moet, L. J. A. Koster, B. DeBoer, P. W. M. & Blom, Chem. Mater. 19, 5856 (2007).

[9] P. Schilinsky, C. Waldauf, C. J. Brabec, Appl. Phys. Lett. 81, 3885 (2002).

[10] P. A. Van Hal, M. P. T. Christiaans, M. M. Wienk, J. M. Kroon, R. A. J. Janssen, Phys. Chem. B 103, 4352 (1999).

[11] M. Shim, P.J. Guyot-Sionnest, Am. Chem. Soc. 123, 11651 (2001).

[12] F. C. Spano, J. Chem. Phys. 122, 234701 (2005).

[13] J. F. Chang, J. Clark, N. Zhao, H. Sirringhaus, D. W. Breiby, J. W. Andreasen, M. M. Nielsen, M. Giles, M. Heeney, and I. McCullochet, Phys. Rev.B. 74, 115318 (2006).

[14] J. K. J. vanDuren, X. Yang, J. Loos, C. W. T. Bulle-Lieuwma, A. B. Sieval, J. C. Hummelen, R. A. J. Janssen, Adv. Funct. Mater. 14, 425 (2004).

[15] B. O'Regan, M. Gratzel, Nature 353, 737–740 (1991).

[16] W. Jih-Jen, C. Guan-Ren, L. Chia-Chun, W. Wei-Ting, C. Jen-Sue , Nanotechnology 19, 105702 (2008).

[17] N. Tetreault, M. Gratzel, Energy & Environmental Science, 10.1039/ C2EE03242B (2012).

[18] J. D. Moet, L. J. A. Koster, B. de Boer, P. W. M. Blom, Chem. Mater 19, 5856 (2007).

[19] S. D. Oosterhout, M. M. Wienk, S. S. Van Bavel, R. Thiedmann, L. J. A. Koster, J. Gilot, J. Loos, V. Schmidt, R.A. J. Janssen. Nature Material 8, 818 (2009).

[20] S.D. Oosterhout, L. J. A. Koster, S. S. Van Bavel, J. Loos, O. Stenzel, R. Thiedmann, V. Schmidt, B. Campo, T. J. Cleij, L. Lutzen, D. Vanderzande, M. M. Wienk, R.A. J. Janssen. Advance Energy Materials 1, 90 (2011).

[22] S. S. Pandey, W. Takashima, S. Nagamatsu, T. Endo, M. Rikukawa, K. Kaneto, Jpn. J. Appl. Phys. 39, 94 (2000).

[22] M. Ahlskog, J. Paloheimo, H. Stubb, P. Dyrklev, M. Fahlman, O. Inganäs, M. R. Anderson, J. Appl. Phys. 76, 893 (1994).

[23] T-A. Chen, X. Wu, R. D. Rieke, J. Am. Chem. Soc. 117, 233 (1995).

[24] Y. Furukawa, M. Akimoto, I. Harada Synth. Met. 18, 151 (1987).

Chapter 5:

Single step fabrication of dye-sensitized polymeric hybrid bulk hetero-junction solar cells using solution processable precursor

This chapter describes the extension of concept of single step fabrication of P3HT/ZnO PHSC for fabrication of dye-sensitized polymeric hybrid bulk hetero-junction DSPHSC. Here dye is used as additional sensitizer along with ester modified P3HT for photon harvesting in near infra-red region of solar spectrum. Considering the analogous structure of DSPHSC and all solid state DSSC, a perspective for single step fabrication for solid state dye sensitized solar cells is also given with using solution processable precursor.

5.1 Introduction

As photon harvesting window of poly (3-hexylthiophene) (P3HT) and its ester derivatives were limited to 650 nm only. Employing narrow band gap polymers instead of P3HT is one of approaches to cover wide range of wavelengths including visible and near infrared regions (NIR) for effective polymeric hybrid BHJ solar cells (PHSC). Utilization of low band gap polymers for this purpose has been well documented in the recent past [1]. To avoid the cumbersome and multi-step synthesis, Peet et el. [2] and Honda et al. [3] suggested the incorporation of small molecule sensitizer in the P3HT-PCBM blend system to enhance the photon harvesting window. The same approach could be extended to PHSC. For the proper functioning of such ternary blend system, it is necessary not only to have energetic cascade between the donor-dye-acceptor, but also the location of the dye molecules on the donor-acceptor interface.

Apart from increasing photon harvesting window, the metal oxide acceptor based dye sensitized PHSC (DSPHSC) also provide interesting analogous structure and working principal with all-solid dye sensitized solar cells. Dye-sensitized solar cells (DSSCs) are one of the low cost solar cells, due to ease of their fabrication by printing processes under ambient conditions [4, 5].

Certified conversion efficiency for DSSCs consisting of a nanoporous TiO_2 layer as electron transport layer (ETL) stained with dyes and an liquid electrolyte have been reported to be 11.0% which is almost similar to that of amorphous Si solar cells [6]. Recently, solid DSSCs having solid hole transport layers (HTL) instead of the liquid electrolyte have been focused to avoid complicated encapsulation of DSSCs to protect the evaporation of the liquid electrolyte [7-9]. Solid DSSCs consisting of the inorganic ETL/dye/HTL are generally fabricated step by step: namely, fabrication of a nanoporous TiO_2 layer, sintering, dye adsorption and fabrication of a hole-transport layer (Figure 5.1). The step by step process is convenient way to control photoconversion interfaces, however, one of the undesirable items for this process is that many coating processes are needed to complete cells. In addition, thickness of hole transport layer is thicker than common hole diffusion length (> 100 nm), which disturbs the efficient hole collection by hole transport materials.

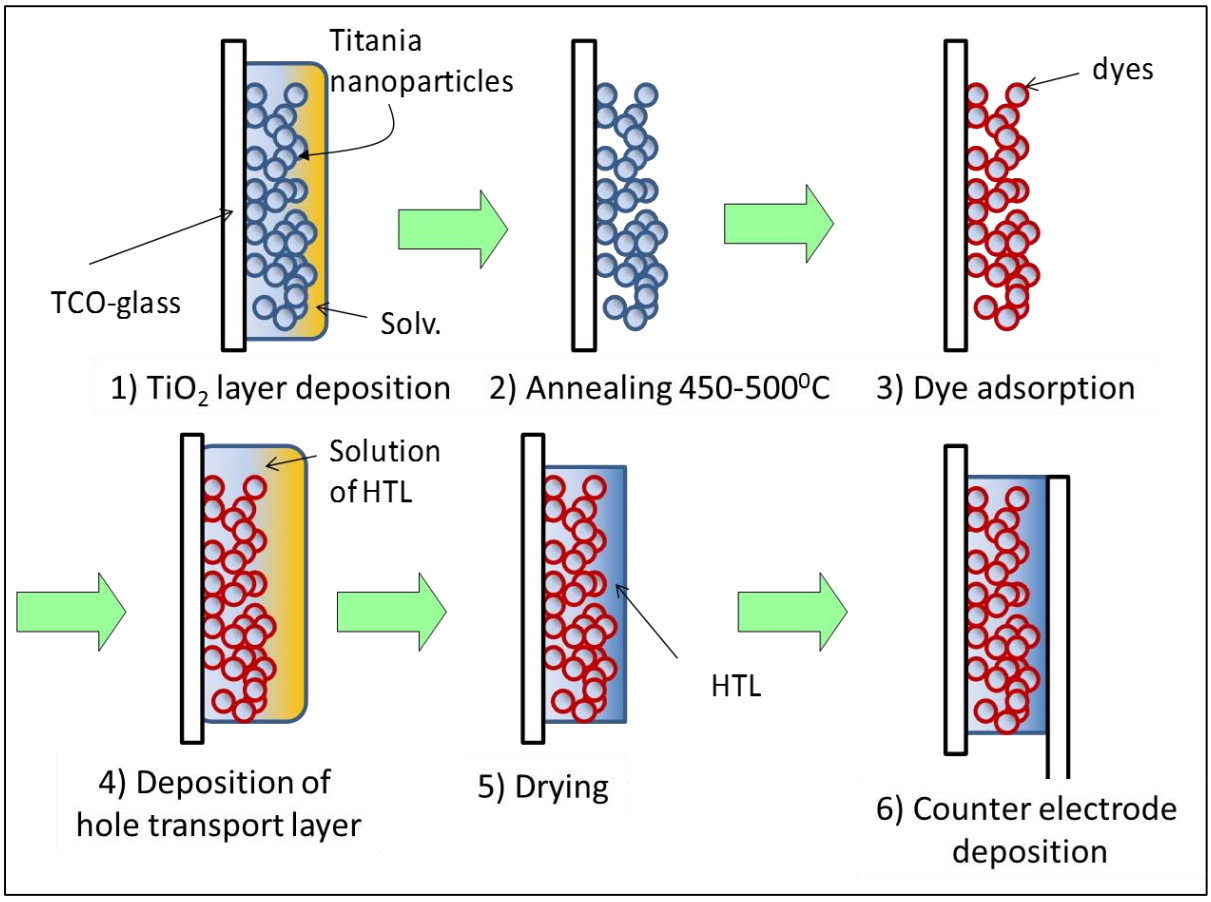

Figure 5.1 Multiple step process for fabrication of solid state DSSC

Considering analogous working principal and structure of DSPHSC and solid-state DSSCs, one could say both to be similar. In this chapter an alternate perspective for single pot fabrication process of solid-DSSCs using DSPHSC fabrication method are demonstrated. Hereafter the term all solid DSSC have been used to describe these analogous structures.

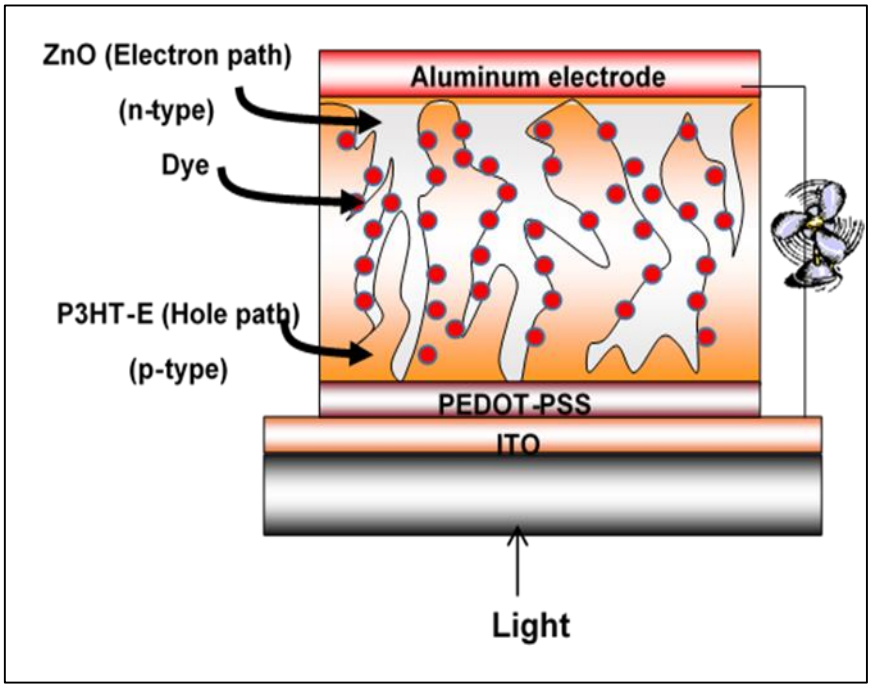

Figure 5.2 Schematics of all-solid DSSC

In the present work all-solid DSSCs consisting of inorganic/dye/organic bulk hetero-junction interfaces fabricated by single step coating process having capability of panchromatic photon harvesting are demonstrated. All-solid DSSCs are fabricated by incorporating an additional sensitizer (Squaraine dye) in the 1:2 w/w ratio of P3HT ester derivative and ZnO. P3HT ester derivative and dye harvest light from the visible and far-red wavelength region, respectively, resulting in to the panchromatic light absorption and photon harvesting. Squaraine dyes are a class of organic sensitizers having donor-acceptor-donor zwitter ionic structure. They possess sharp and intense light absorption with narrow full width at half maximum. Their wavelength can be tailored from visible to NIR region by judicious selection of suitable donor moieties with extended π-conjugation. In this chapter squaraine dye (SQ-36) having sharp, intense and far-red light absorption were added with varying proportion with respect to P3HT-E1 for finding optimized ratio. Considering better performance of P3HT-E1 with ZnO, it is used for all solid DSSC. P3HT-

E1 covers 400-650 nm and a dye covers the wavelength in the far-red region (> 650 nm).

5.2 Experimental detail

5.2.1 Materials and methods

The structures of functional materials such as ester functionalized poly (3-heylthiophene) (P3HT-E1), processable n-type ZnO precursor DEZ and far-red sensitive squaraine dye SQ-36 used in the present work are shown in the Figure 5.3.

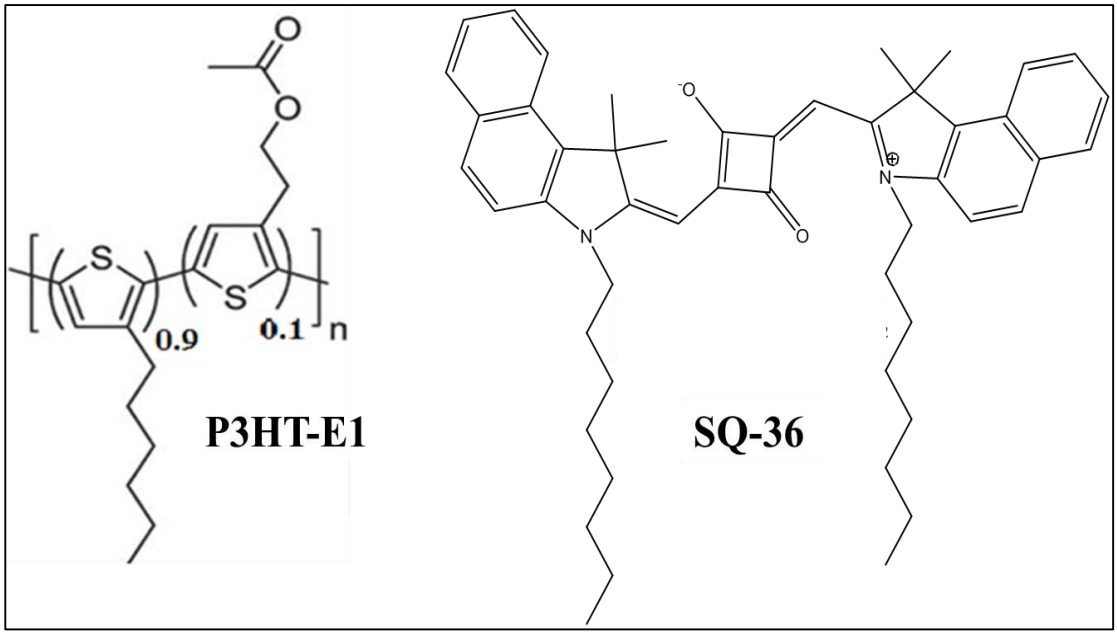

Figure 5.3 Structure of polymer and dye molecule used for the fabrication of all Solid DSSC.

P3HT-E1 was synthesized as per scheme-1 discussed in chapter 4. Symmetrical squaraine dye (SQ-36) was synthesized from 1-Octyl-2, 3, 3-trimethyl-benzoindole and squaric acid by the methods reported by Pandey et al. [10], the dye was synthesized in 83 % yield with >98 % purity as confirmed by HPLC. HR-FAB-MS, observed 720.4700 and calculated 720.4650 (M^+) confirms the synthesis of the compound. ^{1}H NMR (d_6-DMSO). δ_H 8.23 (d, J=8.5 Hz, 1H), 8.02 (d, J=8.5Hz, 2H), 7.70 (d, J=8.5 Hz, 1H), 7.62 (m, 1 H), 7.45 (m, 1H), 5.87 (s, 1H), 4.23 (t. 2H), 1.96 (s, 6H), 1.77 (m, 2H), 1.32-1.42 (bm, 2H), 1.23 (bm, 6H) and 0.83 (t, 3H).

Product was finally purified by silica-gel column chromatography and characterized by high performance liquid chromatography (for purity), fast ion bombardment mass spectroscopy and nuclear magnetic resonance spectroscopy. The energies of the highest occupied molecular orbital (HOMO) for the P3HT-E1 and SQ-36 was estimated from photoelectron spectroscopy in air (model AC3, Riken, Japan) while the energy of lowest unoccupied molecular orbital (LUMO) was calculated using the relation LUMO = HOMO + Eg, where, Eg is energy band gap estimated from the onset of the optical absorption.

5.2.2 Device fabrication

For the fabrication of all solid DSSC, different weight % of SQ-36 dye (5wt%, 10wt%, 20wt%, and 40wt %) were mixed against P3HT-E1 in chlorobenzene. Considering P3HT-E1/ ZnO w/w ratio of 1:2 best for these PHSC (as discussed in chapter 4) 300 µl of DEZ was mixed with 350 µl of P3HT-E1/SQ-36 solution. Assuming full conversion of DEZ to ZnO, thin film layer would have a 2:1 (w/w) ratio of P3HT-E1/ZnO against varied ratio of SQ-36 in ZnO/SQ-36/P3HT-E1 thin films.

For all the devices, Indium tin-oxide (ITO) patterned glass plates were cleaned by sonication in distilled water including detergent, acetone and isopropanol, respectively. After ultraviolet ozone treatment, substrate was transferred to a nitrogen-filled glove box with a controlled humidity (relative humidity~ 40%). In all the devices, Poly(3,4-ethylenedioxy-thiophene) poly (styrenesulfonate) (PEDOT:PSS(BAYTRON P, HC Starck, GMBH, Germany) having thickness of about 70 nm was spin coated followed by heating at 150°C for 10 min on a hot plate. Photoactive layer (~110 ± 10 nm for all devices) was then spin coated from the mixed solution described above (P3HT-E1-dye). After aging (15 min) and annealing (100 °C for 15 min.) to grow bicontinuous ZnO nanostructure in P3HT-E1 layer and make ZnO/dye/P3HT-E1 bulk hetero-junction interface, the substrates were transferred to a glove box with an inert nitrogen atmosphere (H_2O and O_2 <1ppm) using an air-tight container. Devices were then finally completed by thermal evaporation of Al (100 nm) top contact. The area of all fabricated devices were 0.15 $cm^{2.}$

5.2.3 Device characterization

Thickness of the PEDOT: PSS and active layers discussed above were measured using DEKTAK Stylus Profiler (6M, ULVAC Inc.). Electronic absorption spectroscopic investigations for thin films of pure P3HT,SQ-36 and P3HT/SQ 36/ZnO ternary blend films on glass substrate were conducted using JASCO V 530 spectrophotometer. After device fabrication, photovoltaic performance was measured with a Bunko-Keiki solar simulator KHP-1 equipped with a Xenon lamp (XLS-150A). The exposure light was adjusted to be AM 1.5 (100 mW/cm^2). The power and spectra of the solar simulator were adjusted using an Eiko Seiki solar simulator spectro-radiometer (LS-100).

5.3. Result and Discussion

Formation of an energy cascade among the donor, sensitizer and acceptor is required along with the location of sensitizer molecules on the donor/acceptor interface for the functioning all solid DSSC. Figure 5.4 exhibits the energy band diagram for all solid DSSC fabricated in this work. This figure clearly corroborates the formation of suitable energy cascade amongst the active components used for the device fabrication. Utilization of such a ternary blend is expected to exhibit panchromatic photon harvesting making the use of complementary electronic absorption of both of the polymer as well the dye-sensitizer.

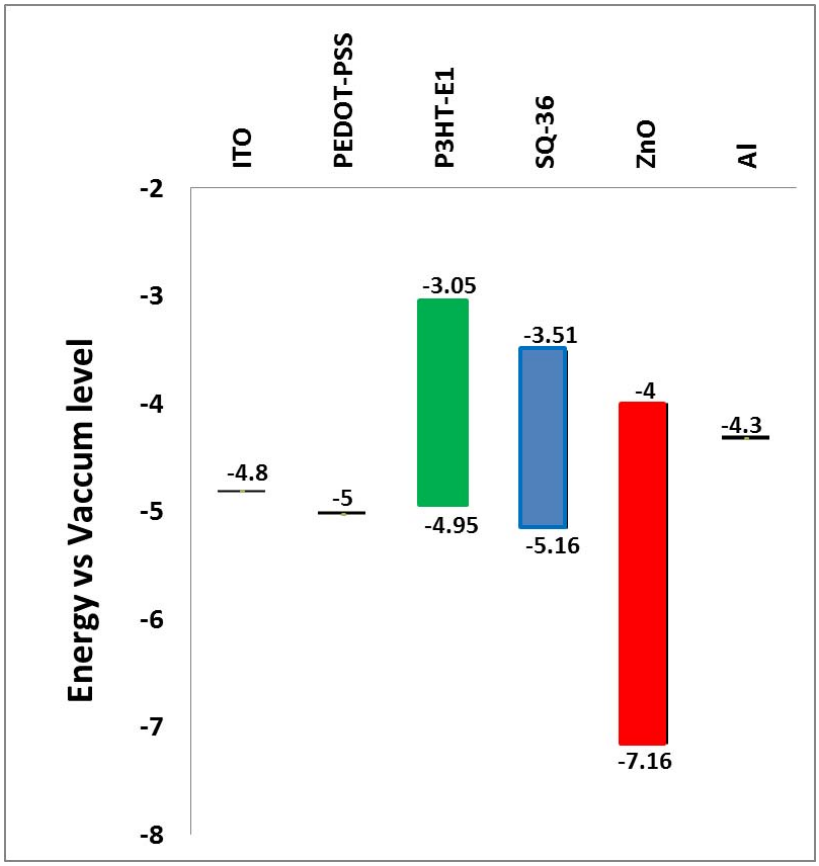

Figure 5.4 Energy band diagram of all solid DSSC fabricated using the ternary blend of P3HT-E1, SQ-36 and ZnO.

Electronic absorption spectra of thin films of P3HT-E1 and dye (SQ-36) used in the present investigation are shown in the Figure 5.5. The absorption spectra of pure P3HT-E1 indicates absorption maximum at 550 nm associated with π-π* electronic transition along with appearance of vibronic shoulders at 610 nm. These clear vibronic shoulders are associated with polymer crystallization. On the other hand, thin film absorption spectrum of SQ-36 exhibits the electronic absorption maximum at 703 nm with far-red light absorption in the range of 550-750 nm. The electronic absorption of the polymers and dye clearly indicates that one can expect the wide wavelength photon harvesting using this dye as additional sensitizer with polymer and ZnO ternary blend system.

The photo-action spectra of thin film ternary blend of P3HT-E1/SQ-36/ZnO with varying SQ-36 ratio against P3HT-E1 system have been shown in Figure 5.6. The action spectra reveal that

the introduction of the dye leads to the observation of photon harvesting in the range of 650 nm – 750 nm which is the signature of the dye incorporation between ZnO and P3HT-E1 layers.

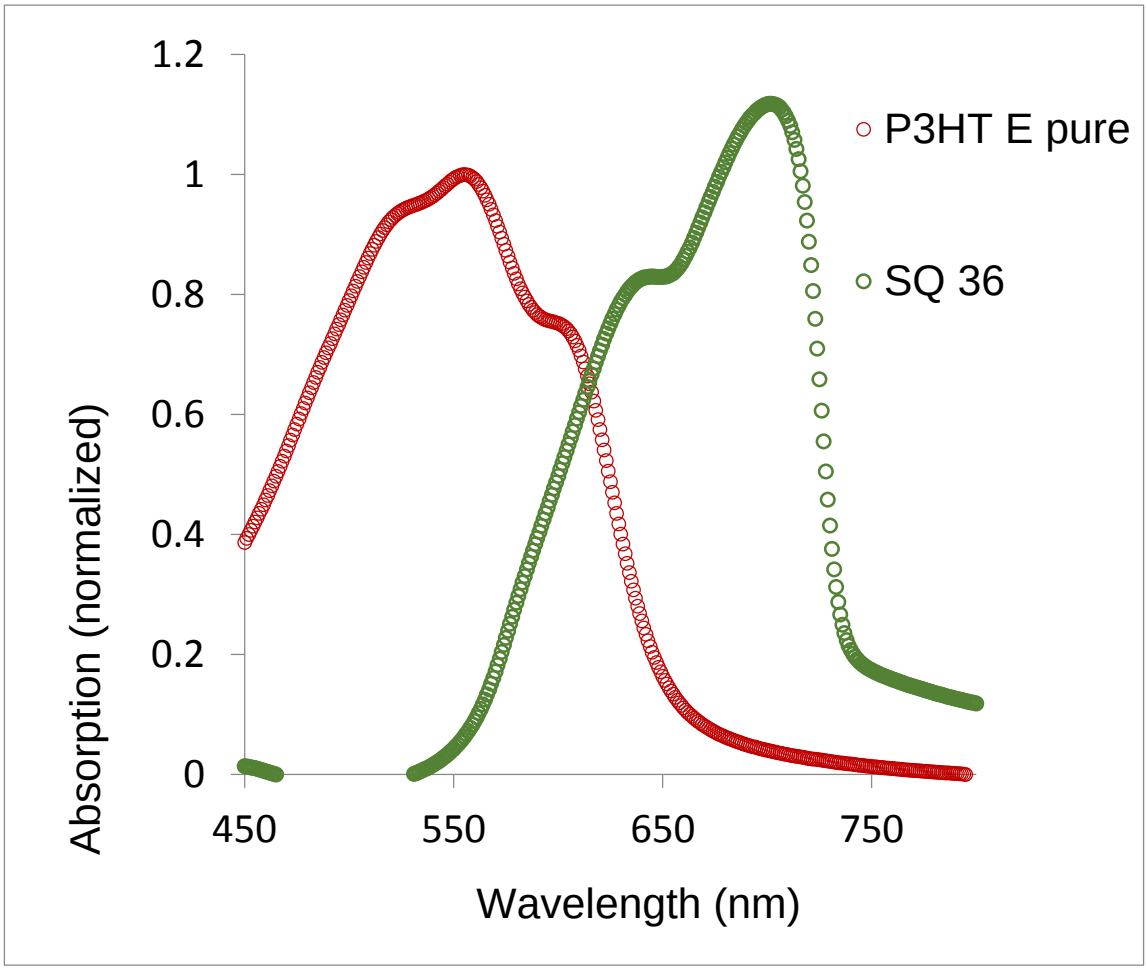

Figure 5.5 Normalized UV-visible electronic absorption spectra of thin films of P3HT-E1 and SQ-36

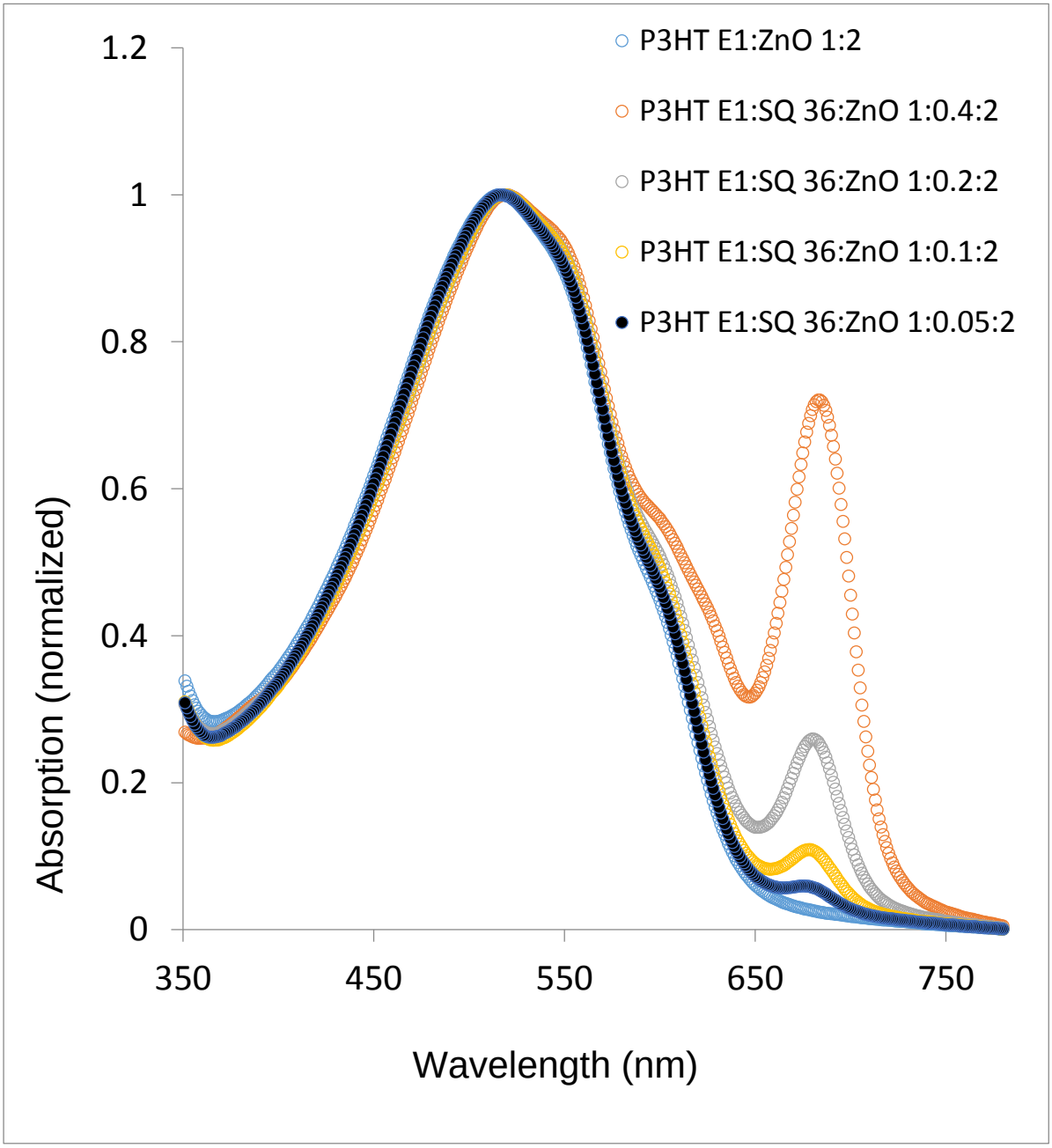

Figure 5.6 Normalized absorption spectra of the ternary blend of P3HT-E1/SQ-36/ZnO with varied SQ-36 ratio against the P3HT-E1.

The IPCE curves of the P3HT-E1/ZnO PHSC and all solid DSSCs are shown in Figure 5.7. Observation of the IPCE reveals that PHSC solar cell harvested photons only up to about 650 nm. At the same time, the IPCE corroborates that the introduction of the SQ-36 leads to extension of photon harvesting window up to 750 nm which is the signature of the dye incorporation between ZnO and P3HT-E1 layers due to maintenance of the energy cascade as shown in the Figure 5.4. An increase in the volume fraction of the dye in the ternary blend although results in to the enhanced photon harvesting in the far-red wavelength region but leads to decrease in the photon harvesting of the polymer. Therefore, use of an optimum extent of the small molecule sensitizer is highly required to harvest the photon in the entire visible to far-red region. Peet et al. [2] have demonstrated that there is need of optimum amount of sensitizer since increasing the amount dye from 20 % to 60 % led to drastic decrease in the efficiency in the case of their P3HT-fullerene-dye ternary solar cells.

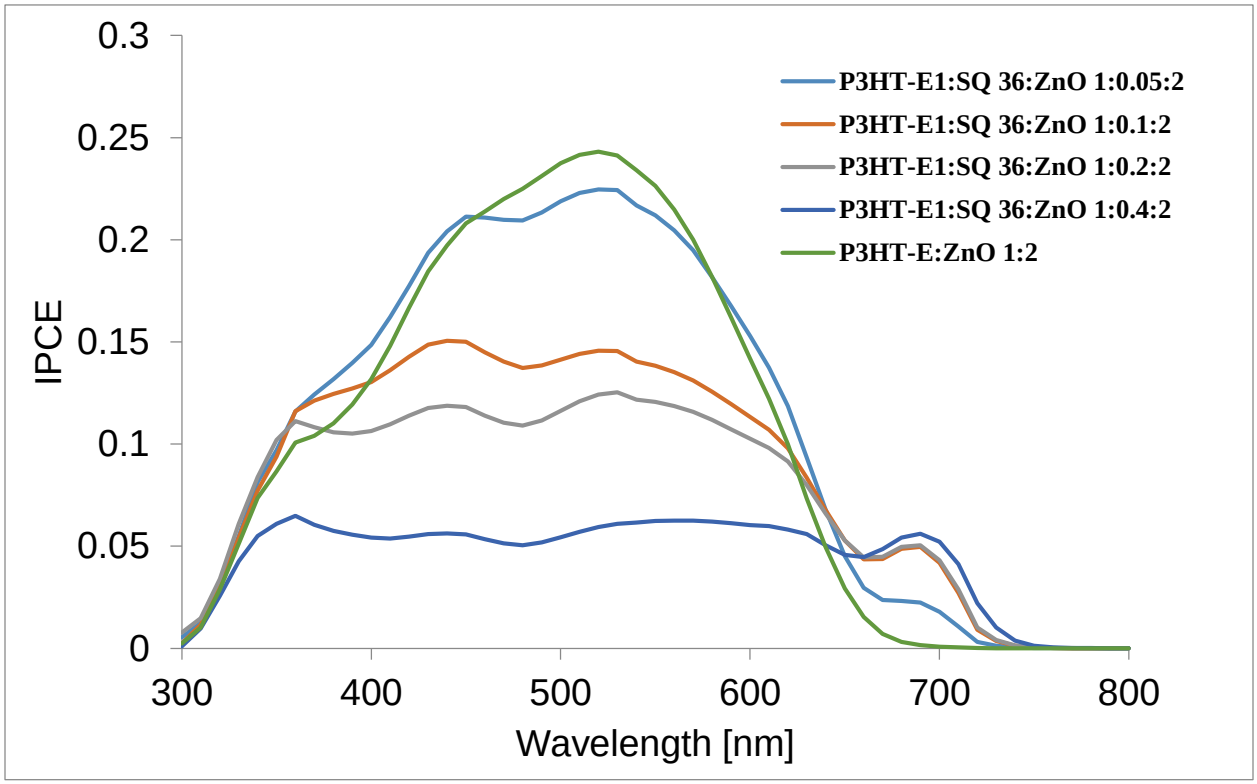

Figure 5.7 IPCE of PHSC and all-solid DSSC of P3HT-E1/SQ-36/ZnO with varied SQ-36 ratio against the P3HT-E1.

There might be two possible reasons for decrease in the photon harvesting as a function of increasing amount of sensitizing dye molecules in the all solid DSSC. Firstly, increase in the volume fraction of dye molecule leads to decrease in the fraction of P3HT-E1/ZnO leading to decreased photon harvesting in the visible wavelength region. Second possibility is the migration of dye molecules from P3HT-E1 /ZnO interfaces to the P3H-E1T domains. Considering the the associative interactions between the hexyl side chain of P3HT-E1 and long alkyl (octyl) chain of the dye SQ-36, there is higher probablity of the migration of dye molecules from P3HT-E1/ZnO interfaces to the P3HT-E1 domains. In general, squaraine dyes have much lower hole mobility as compared to regioregular polythiophenes [11]. Therefore, the migration of dye molecules in P3HT-E1 domains are expected to hamper the hole transport within the polymeric domains affecting charge collection of the polymer. This implies that design of the dye molecules in terms of the high hole mobility with moderate alkyl chain length are highly required to develop efficient all solid DSSC.

The interfacial location of the sensitizing dye moleclues and their implication on the photon harvesting has been schematically shown in the Figure 5.8. Fig. 5.8(a) exhibits the situation where, SQ-36 dye molecules are located at the interface of P3HT-E1/ZnO. In this case, photoexcited electrons form SQ-36 can be easily injected into ZnO and a hole into P3HT-E1, because of presence of suitable energetic casacade. On the contrary, when SQ-36 molecules are located in ZnO domain (Fig. 5.8 b), it can have facile electron injection from the dye to ZnO but at the same time hole injection is hampered. Similarly presence of the SQ-36 dye molecule in the P3HT-E1 domain (Fig.5.8 c), favors only the hole injection while electron injection is hampered. So, considering the energetic cascade of P3HT-E1/SQ-36/ZnO, all solid DSSC can only work if dye SQ-36 is located at interfacial postion of P3HT-E1/ZnO bulk hetrojunction.

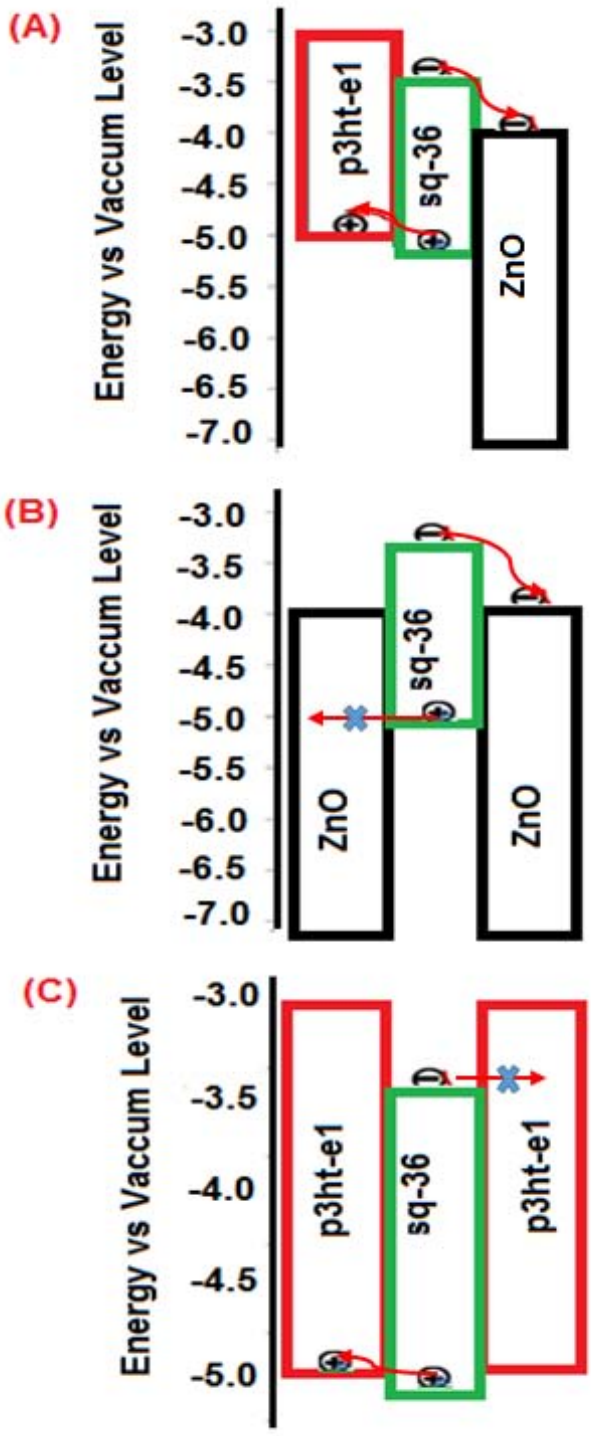

Figure 5.8 Energy diagram of SQ-36 molecules and surrounding materials (a) SQ-36 located at interface between P3HT-E1 and ZnO (b) SQ-36 in ZnO domain (c) SQ-36 in P3HT-E1 domain

5.4. Conclusion

Present experiments demonstrated fabrication of all solid DSSCs consisting of ZnO/dye/P3HT from a solution processable precursor solution consisting of DEZ, dye and P3HT in single step coating process. The absolute efficiency although is lower at present stage but is expected to be improved by judicious selection of the dye molecular structures and optimization of the film fabrication conditions.

Present investigation exploits the analogous working principal and structure of DSPHSC and solid-state DSSCs for the single step solution processable fabrication of all solid DSSC. Thus this trend to be a very promising strategy towards the demonstration of efficient and competitive hybrid solar cells.

References

[1] C. L. Chochos, S. A. Choulis, Prog. Polym. Sci. 36, 1326, (2011).

[2] J. Peet, A. B. Tamayo, X. D. Dang, J. H. Seo and T. Q. Nguyen, Appl. Phys. Lett. 93, 163306 (2008).

[3] S. Honda, T. Nogami, H. Ohkita, H. Benten, and S. Ito, Appl. Mater. Interfaces; 1, 804, (2009).

[4] B. O'Regan and M. Grätzel, Nature, 353, 737 (1991).

[5] Grätzel M, *MRS Bull,* 30, 23 (2005).

[6] M. A. Green, K. Emery, Y. Hishikawa, W. Warta and E. D. Dunlop, Prog. Photovolt: Res. Appl, 20, 12 (2012).

[7] U. Bach, D. Lupo, P. Comte, J. E. Moser, F. Weissörtel, J. Salbeck, H. Spreitzer and M. Grätzel, Nature, 395, 583 (1998).

[8] P. Wang, S. M. Zakeeruddin, J. E. Moser, M. K. Nazeeruddin, T. Sekiguchi and M. Grätzel, Nature Materials, 2, 402 (2003).

[9] B. Li, L. Wang, , B. Kang, P. Wang and Y. Qiu, Solar Energy Materials and Solar Cells, 90, 549 (2006).

[10] S. S. Pandey, T. Inoue, N. Fujikawa, Y. Yamaguchi and S. Hayase, J. Photochem Photobiol. A 214, 269 (2010).

[11] D. Bagnis, L. Beverina, H. Huang , F. Silvestri , Y. Yao, H. Yan, G. A. Pagani, T. J. Marks , A. Facchetti Journal of American Chem. Society, 132, 4074 (2010).

Chapter 6: Conclusion

The work described in present thesis provides the first element of investigation concerning the fabrication of all solid DSSC using solution processable n-ZnO precursor in single step with DSPHSC fabrication method.

The first part of the present thesis provides insight into the theory relevant for solar cells, especially of polymeric bulk hetero-junction (PSC) and polymeric hybrid bulk hetero-junction solar cells (PHSC). The purpose of this part is to furnish the basic knowledge required to understand the experiments and results proposed in this study.

A brief introduction of the materials and experimental methods used in this study is given in the second part of this thesis. It presents a general background of the properties and applications of the materials used in this work. The fabrication and characterization method for the materials and thin films devices are also briefly described.

The third part provides the brief study about the various compatible roll to roll fabrication process, for the deposition of organic bulk hetero-junction solar cells. The study also provide the first elements of investigation for the fabrication of P3HT/PCBM PSC using circular nano vapor spray deposition (NVD) process. The study successfully demonstrated that NVD spray deposition technique is a promising deposition process for the fabrication of active layers in solution processed organic solar cells. Strong solvent effect was observed with 40 % increase in efficiency when using chlorobenzene/dichlorobenzene/ solvent of 7/3 ratio is used in comparison to pure chlorobenzene solution, which is due to better phase separation of donor /acceptor interfaces. The study also shows that performance of NVD spray coated system is at par with the spin coating technique, which is widely used laboratory technique.

In the fourth part, first P3HT/ZnO PHSC was fabricated using solution processable diethyl zinc precursor (DEZ) in single step. In this method, during and after deposition, DEZ is converted to $Zn(OH)_2$ by reacting with ambient moisture, and after annealing, interpenetrating ZnO nanoparticles are formed in polymer matrix, leaving no residual byproduct. For enhancing the BHJ nanomorphology ester functionalized regioregular polythiophene copolymer (P3HT-E1 and P3HT-E3) were synthesized and characterized towards their application for the fabrication of thin

film PHSC. It was observed that addition of 6% of ester functionality (P3HT-E1) leads to enhanced efficiency by 25% for P3HT-E1/ZnO PHSC compared to P3HT/ZnO PHSC. Addition of ester functionality leads to better phase separation thus enhanced Jsc for P3HT-E1/ZnO PHSC. Although addition of ester functionality improves the phase separation, but increasing the amount of ester extent to 22% (P3HT-E3) leads to loss of percolation pathways in BHJ thin films. Thus a trade-off is needed for extents of addition of ester moiety for enhanced phase separation.

In fifth part of this thesis concept of single step fabrication of P3HT/ZnO PHSC is extended for fabrication of all solid DSSC in single pot process. Squaraine dye (SQ-36) having sharp, intense and far-red light absorption were added with varying proportion(5%, 10%, 20% and 40%) with respect to P3HT-E1 for finding optimized ratio. Dye was used as additional sensitizer beside ester modified P3HT for photon harvesting. Although the absolute efficiency is lower at present stage but is expected to be improved by judicious selection of the dye molecular structures and optimization of the film fabrication conditions. This novel borderline strategy exploit the specificities and advantages of both DSSC and PHSC approaches thus this trend to be a very promising strategy towards the demonstration of efficient and competitive hybrid solar cells.

I believe that our results can open a new direction for single step fabrication of all solid DSSCs using inorganic oxide precursor.

Future possibilities

For the future, efforts are needed to control the nano-morphology and interface of polymer and inorganic semiconductors. Although this is difficult, but it is very crucial for enhancing the performance of PHSC. Also the optimization of devices by changing the active layer thickness is needed. Another crucial area that need to be researched is the role of blocking layers on the performance of PHSC. For enhancing performances, there is need of logically designing the additional sensitizers (dyes) molecules, which along with having energetics match should have excellent charge transporting properties. An interesting challenge would be the realization of dye molecules on donor acceptor interface in all solid DSSC. Finally, studying and exploring the use of other different kind of solution processable inorganic material precursor for the fabrication of PHSC and all solid DSSCs will obviously be one of next step of present work.

Achievements

(A) Publications

1. "Controlling the processable ZnO and polythiophene interface for dye-sensitized thin film organic solar cells" , **Sandeep K Das ***, Katsunori Abe, Kenji Yoshino, Yuhei Ogomi, Shyam S. Pandey and Shuzi Hayase, **Thin Solid Films, Vol 536 , 302-307 (2013)**.

2. "Single step fabrication of all solid dye-sensitized solar cells using solution processable precursor" , **Sandeep K Das *** , Daiki Yamashita , Yuhei Ogomi , Shyam S. Pandey , Kenji Yoshino and Shuzi Hayase , **Physica Status Solidi –A, Vol. 210, 846–1850 (2013).**

3. "Solution processable thin film organic photovoltaic cells based on far red sensitive soluble squaraine dye" , Shyam S. Pandey, Takafumi Mizuno, **Sandeep K. Das**, Yuhei Ogomi and Shuzi Hayase, **Thin Solid Films, Vol. 522, 401-406 (2012).**

4. "Huge suppression of charge recombination in P3HT–ZnO organic–inorganic hybrid solar cells by locating dyes at the ZnO/P3HT interfaces" , Qing Shen* , Yuhei Ogomi, **Sandeep K. Das**, Shyam S. Pandey, Kenji Yoshino, Kenji Katayama, Hisayo Momose,Taro Toyoda and Shuzi Hayase*, **Phys. Chem. Chem. Phys**. (**Published online in July 2013).**

5. Fabrication of thin film polymer bulk heterojunction solar cells by circular nano-vapour spray deposition technique" ,**Sandeep K Das ***, Hiroki Tanaka, Shyam S. Pandey, Takafumi Mizuno, Yuhei Ogomi and Shuzi Hayase, **(Manuscript under preparation).**

(B) Conferences

1. **Oral:** Charge sepration and recombination at nano interfacace of ZnO/dye/P3HT hybrid solar cells; Qing Shen, Yuhei Ogomi, **Sandeep K Das**, Shyam S. Pandey, Kenji Yoshino, Taro Toyoda and Shuji Hayase**; The 60th Spring Conference of Japan Society of Applied Physics, March 27-30, 2013 , Kanagawa , Japan.**

2. **Oral:** Controlling the charge sepration interface in organic inorganic hybrid solar cells; **Das Sandeep K**, Kukihara Kenji, Yamashita Daiki, Morita Atushi, Kimura Syota, Tsukamoto Syota, Ogomi Yuhei, Shen Qing, Yoshino Kenji, Pandey Shyam S, Hayase Shuzi, **The 93rd Spring Conference of Japan Chemical Society,March 22-25, 2013, Shiga, Japan.**

3. **Oral:** Fullerene free sensitized bulk heterojunction solar cells using solution processable ZnO ; **Sandeep K Das**, Daisuke Yamashita, Yuhei Ogomi, Shyam S. Pandey, Kenji Yoshino and Shuzi Hayase; **International Union of Materials Research Society-International Conference on Electronic Materials (IUMRS-ICEM-2012), Sept. 23-28, 2012 , Yokohama, Japan.**

4. **Poster**: Utilization of solution processable ZnO for dye sensitized thin film organic Solar cells **; Sandeep. K. Das**, D.Yamashita, Y. Ogomi, Shyam. S. Pandey, K.Yoshino and Shuzi Hayase**; The 48th Kyushu Branch Chemical Society Meeting, June 30, 2012 , Kitakyushu, Japan.**

5. **Oral**: Organic-inorganic hybrid thin film solar cells using solution processable zinc oxide; **Sandeep K Das,** Daiki Yamashita, Hiroki Tanaka, Yuhei Ogomi, Shyam S Pandey, Kenji Yoshino and Shuzi Hayase; The **59th Spring Conference of Japan Society of Applied Physics, March 15-18, 2012 , Tokyo, Japan.**

6. **Oral:** Parametric optimizations for circular spray nano vapor deposition to fabricate thin film organic polymer solar cells; **Sandeep K. Das,** Hiroki Tanaka, Shyam S. Pandey, Takafumi Mizuno, Yuhei Ogomi and Shuzi Hayase; **The 72nd Autumn Japan Society of Applied Physics, Aug. 29-Sept. 2, 2011 , Yamagata, Japan.**

Acknowledgement

I would like to thank **Prof. Hayase** for welcoming me in laboratory and giving me chance to work under his guidance. His vast technical knowledge and insight have given me an excellent background in this field. I also thanks **Prof. Pandey** for his valuable support and constant encouragement. His enthusiasm and faith in me have inspired a true passion for work in this field and enabled me to see through all the setbacks I encountered along the way.

My sincere thanks to **Prof. W. Takashima**, for his excellent support and proving his valuable laboratory facilities which was crucial for this work. I would also like to thank **Prof. Ma** for her valuable suggestion for improving the quality of thesis work.

I would also like to thank **Dr. Gururaj Shivashimpi, Dr. Park, Dr. Nishimura** and **Dr. Usagawa** who made it possible to spend these precious three years in Hayase laboratory. I would also like to thanks **Mr. Gaurav Kapil, Mr. Zaman, Mr. Nakayashiki** and **all Hayase lab members** for making my stay memorable in Japan.

I am also grateful to Kyushu Institute of Technology for all kind supports such as travelling to conferences, excellent lectures and research facilities, which helped me to learn not only science but also the Japanese culture. Especially I would like to thanks **Miss Yasuko Nagamatsu** for her constant help during my stay in Japan.

Moreover, I thank my parents **(Mr. A.K. Das and Mrs. Ranjana Das)**, my wife **(Priyanka)**, my brother **(Mr. Ashwani)**, my sister in law **(Mrs. Piyusha)** and my dear friends **(Sumantu, Piyush, Saujanya)** for their love, cooperation and encouragement which was a constant source of inspiration for me.